General Disclaimer

One or more of the Following Statements may affect this Document

- This document has been reproduced from the best copy furnished by the organizational source. It is being released in the interest of making available as much information as possible.

- This document may contain data, which exceeds the sheet parameters. It was furnished in this condition by the organizational source and is the best copy available.

- This document may contain tone-on-tone or color graphs, charts and/or pictures, which have been reproduced in black and white.

- This document is paginated as submitted by the original source.

- Portions of this document are not fully legible due to the historical nature of some of the material. However, it is the best reproduction available from the original submission.

N.I

Technical Report

to

National Aeronautics and Space Administration

CATHODOLUMINESCENCE OF ENSTATITE FROM CHONDRITIC AND ACHONDRITIC METEORITES AND ITS SELENOLOGICAL IMPLICATIONS

September 1, 1967 - July 1, 1968

Grant No. NGR-39-009-015

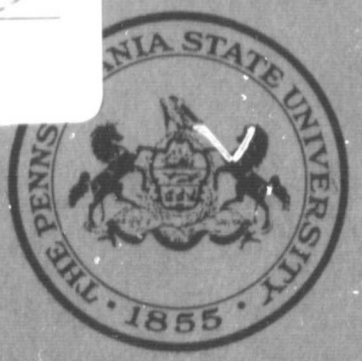

SPACE SCIENCE AND ENGINEERING LABORATORY
Institute for Science and Engineering
The Pennsylvania State University
University Park, Pennsylvania

Technical Report

Grant No. NGR-39-009-015

(SSEL-16)

National Aeronautics and Space Administration

Cathodoluminescence of Enstatite From Chondritic and Achondritic Meteorites and its Selenological Implications

by

Raymond T. Greer and Jon N. Weber

September 1, 1967 - July 1, 1968

The Pennsylvania State University

University Park, Pennsylvania

ABSTRACT

In conjunction with the use of luminescence for the identification of lunar materials, a basic laboratory study has demonstrated the feasibility of obtaining useful correlations of mineral luminescent phenomena. Two monochromator-photomultiplier attachments to an electron microprobe have been developed which permit the study of cathodoluminescence phenomena on a micron scale. The attachments extend the analytical capabilities of the instrument and facilitate: 1. recording of luminescence spectra; 2. obtaining the distribution of luminescent phases in micro- and bulk specimens; 3. evaluating and recording the relationships between optical fluorescence patterns and conventional X-ray analyses of an area scan; 4. studying the effects of electron beam dosages on cathodoluminescence intensity; and 5. relating luminescence intensity to composition within a phase. This information provides a more reasonable basis for interpreting recent observations of lunar luminescence.

Under 30 keV electron bombardment, enstatite chondritic and achondritic meteorite specimens were found to display large variation in fluorescence characteristics within what appeared to be homogeneous, single phase material. Enstatite subsamples, 10 to 200 μ in diameter,

were selected from 13 different meteorite specimens for examination by electron microprobe techniques and new oscillographic luminescence display systems, and relationships between fluorescence spectral data and elemental composition were sought.

High concentrations of iron and calcium tend to suppress optical fluorescence whereas manganese acts as an activator. The concentrations of both iron and calcium, however, are positively correlated with the concentrations of manganese, and the quenching effect of iron and calcium is in some cases sufficiently large to cancel the contribution of manganese to the visible emission spectrum. These observations are consistent with the influence of differences in crystal structure, host, activator concentration, impurity level, and history of the meteorite specimen.

Relationships between minor and trace element chemical composition and both the intensity and wavelength of the optical fluorescence are shown by comparing photographs of the optical fluorescence color patterns generated by the microprobe electron beam raster and photographs of the cation oscillographic displays of the same sample area (200 x 200 μ). These relationships, however, are much more apparent from elemental and fluorescence data obtained from a series of points, each one micron in diameter, because the element concentration detection limit is lowered by two orders of magnitude.

ACKNOWLEDGMENTS

The authors are indebted to Professor Rustum Roy, in whose laboratories this investigation was made, for stimulating discussion.

Dr. Eugene W. White is gratefully acknowledged for his assistance, design of a wedge interference filter monochromator unit, and valuable discussions throughout this investigation.

Dr. Brian Mason, Curator of Meteorites, Smithsonian Institution, Washington, D. C., generously provided the meteorite specimens utilized in this investigation.

Financial support for this research was supplied by the National Aeronautics and Space Administration under contract number NGR-39-009-015.

TABLE OF CONTENTS

LIST OF TABLES

LIST OF FIGURES

Figure Page

Figure Page

I. INTRODUCTION

A. Introduction

Optical fluorescence spectra from many of the rock-forming minerals contain information of value to a variety of investigations of both macroscopic and microscopic polymineralic assemblages. Spectral analysis is nondestructive and can be used along with other techniques to study valuable extraterrestrial samples. Specific applications to the types and sizes of lunar and planetary materials anticipated, both on the surface and eventually available to the terrestrial laboratory, have been chosen to represent and to demonstrate how the complexities of the luminescent phenomena can be beneficial. The variations in color and intensity of the luminescent response can facilitate positive identification of mineral grains, singly or in bulk rock specimens, when a particular color (single or multiple emission band) is associated with the mineral or phase whose luminescent properties have been evaluated.

The sensitivity of a luminescent inorganic solid to changes of composition, structure and atomic interactions can be an advantage in preliminary surveys for lunar resources.

B. Experimental Relations Concerned With Predicting the Nature of Luminescent Emission

The criteria for the effective utilization of optical fluorescence are based on laboratory research on both natural

and synthetic inorganic solids. The majority of natural minerals exhibit luminescent response that has been highly characterized by synthetic materials; the exceptions are few, and of minor importance here. Luminescent minerals can be considered natural phosphors, their analogues being the synthetic luminescent preparations utilized in the lamp industry. However, the natural solids usually exhibit zone fluorescence instead of the uriform fluorescence displayed by the synthetics, which is the effect of nonuniformity of the crystallization environment and of the trace element distribution. This color distribution and emission intensity variation constitutes an immediate analytical application for demonstrating compositional zoning, studying exsolution phenomena, or allowing the investigation of very small specimens. Conventional separation in such cases and analysis by other techniques is difficult, and in many cases, not possible. Other potentialities of the technique include the qualitative identification of inclusions and the study of the segregation of impurities; the precise determination of phase equilibria and diffusion mechanisms; or the alteration by oxidation or reduction, and vacancy formation.

Correspondingly, investigating the luminescent response of phase assemblages comprising meteorites, establishes a representative basis to extrapolate present laboratory analyses, and the demonstrated interrelations of crystal hosts and luminescence activators, to the

observations that can be recorded for other extraterrestrial specimens.

Although the nature of the activating electromagnetic or charged particle radiation necessary to stimulate luminescent emission can be critical (Blair and Edgington, 1968; DeMent, 1945; Leverenz, 1940; Meadows, 1967; Nash, 1966) (for example, silicates are efficiently excited by 2537 Å radiation since the major absorption band for a silicate is near 3000 Å, whereas sulfides are responsive to 3650 Å radiation), moderate energy electron beams are preferred as proving more efficient and less damaging to sensitive specimens, than for example proton bombardment. In addition, many of the unique applications and experimental techniques described conveniently provide quantitative analytical information when the specimens are bombarded by electrons.

Photons and charged particles excite phosphors to different degrees of luminescence because of differences in penetration ranges, available energy per particle and particle densities, and excitation intensities. Photons transfer energy immediately, and charged particles transfer energy in small quantities. When the predominant anions in a crystal are oxygen, both the specific host crystal and the activator can be important in determining if optical fluorescence will be excited by X-rays or by photons of lower energy.

It is also important to emphasize a general concept that the simple emission band locations and shapes of luminescent materials are determined by chemical composition

and crystal structure, and are essentially invariant concerning the type or intensity of excitation. The spectral emission of both natural and synthetic phosphors is a function of the system parameters (Garlick, 1949; Klick, 1955; Klick and Schulman, 1957; Johnson, 1939; Leverenz, 1950; Williams, 1966) listed in Table I.

Table I. Factors Influencing Spectral Distribution in Natural and Synthetic Inorganic Luminescent Solids

1. Chemical composition, crystal structure, host crystal perfection
2. Impurity concentrations, bond types, effective valences, coordination numbers, and locations in the solid
3. Temperature of the solid during luminescence

These factors permit the effective use of luminescence as a diagnostic tool, in conjunction with other analytical methods, for purposes of identification as well as enhancing and contrasting small differences in such variables as composition.

A selection of typical silicates has demonstrated the potential lunar analytical applications; however, the principles and intricacies are valid for a large number of natural and synthetic phosphors. Correlations and contrasts will be indicated for the bulk specimens, powders and individual grains. All three forms of the specimens can be studied in detail utilizing a modified electron microprobe X-ray analyzer

as a precisely controlled source of moderate energy electrons (30 keV), as well as applying the inherent analytical capabilities of the instrument.

The emissions from luminescent solids that are of immediate interest are X-ray fluorescence, conventional luminescence, and thermal radiation. The source of X-ray fluorescence is the electronic transitions in inner completed shells of atoms, yielding X-ray line spectra which are utilized in conventional electron microprobe X-ray analysis. The phenomenon of primary interest for the lunar surface studies is conventional luminescence which arises from two sources: 1. electronic transitions in inner incompleted shells of atoms, yielding the visible and near-infrared line spectra (typically the result of rare earth impurities in the solid), and 2. electronic transitions in outer shells of atoms, yielding visible and near-infrared band spectra (typical for the silicates that will be discussed). The thermal radiation is of minor interest here; the source is the transitions of atoms vibrating and rotating, and electrons undergoing similar transitions mentioned above, yielding infrared band spectra.

Cathodoluminescence denotes the process of generating radiation during and after cathode ray excitation. Luminescent systems can have energy absorption and emission at the same center, energy transfer between an absorption center and an emission center without the movement of charge carriers, or energy transport by charge carriers between these centers.

The notation of atomic spectroscopy can be used to describe the specific sites in luminescent centers. For solids, the luminescence spectra consists of bands 0.1 to 1 eV wide (Klick and Schulman, 1957; Leverenz, 1950).

Most luminescent inorganic systems consist of a matrix or host material into which a small concentration of foreign atoms or ions is incorporated (Fonda and Seitz, 1948; Johnson, 1939; Kroger, 1948). In such cases, defect stoichiometry or the addition or deletion of 1 ppm of impurity can change luminescent properties considerably. The optimum concentration of the activator is not critical for visual observation of luminescence. Impurities, such as iron, can alter and quench luminescence both by occupying lattice sites suitable for activators and by absorbing energy and then emitting radiation beyond the visible region of the spectrum. When host absorption is in a convenient spectral range, pure, presumably unactivated, crystals luminesce. Under cathode ray bombardment, luminescence is observed in a wide variety of materials (Leverenz, 1940; Prizbram, 1956).

C. Crystal Host and Activator

Numerous references provide compilations of the influence of activator ions in a variety of host crystals (Fonda and Seitz, 1948; Kroger, 1948; Leverenz, 1950; Pringsheim, 1949). Of primary selenologic importance are the large number of oxygen-dominated host crystals,

such as the silicates of the Group II elements (Mg, Ca, Sr, Ba, Zn and Cd). These exhibit a characteristic ultraviolet and blue emission band of the complex host crystal anion (radical). This ultraviolet and blue host crystal emission originates in the anion radicals (for example, in the SiO_4 tetrahedra in such orthosilicates as Mg_2SiO_4). When the silicates crystallize with about 0.01 weight % Mn, the longer wavelength green-to-red emission band is produced. The Mn-produced emission originates in cation sites (for example, Mn substituting for Mg in magnesium silicate crystals).

Leverenz (1950) explains the host crystal luminescence process as an excitation transition involving electron transfer within an SiO_4 group from one of the four oxygen atoms to the central Si atom. The resultant electron deficiency (positive hole) may then be exchanged among tetrahedrally arranged oxygen atoms, until the excited electron on the Si atom makes a radiative return to one of the ligand oxygen atoms. By this model, the principal emitting atom would be oxygen, although the entire SiO_4 group should be involved in the excitation process.

Manganese in, for example, $MgSiO_3$ (the magnesium metasilicate, enstatite) produces new emission bands at the expense of the original bands of the host crystal. Incorporation of increasing proportions of Mn activator in $MgSiO_3$ steadily reduces the luminescence efficiency of the original 4200 Å band of the host crystal, and

produces a new emission band peaked near 6700 Å. Also, higher Mn concentrations (0.15 to 6.2 weight % Mn) shift the red band to slightly longer wavelengths. The 6700 Å (peak) emission band of $(Mg,Mn)SiO_3$ is attributed to transitions within Mn atoms (ions) in regular lattice sites. Similarly, the 6420 Å (peak) band arises in the orthosilicate, $(Mg,Mn)_2SiO_4$. The original host crystal emission band in Mn activated silicates can be restored by incorporating Group IVB dioxides (for example, TiO_2, ZrO_2, HfO_2 and ThO_2). The subsequent intensification of the original host crystal emission band represents an increase in cathodoluminescence efficiency. This intensification would be associated with about 1 weight % of the impurities mentioned; otherwise the SiO_4 groups ($(SiO_3)_n$ chains for the metasilicate mentioned) are adequate to explain the short wavelength band.

The broad emission bands can be affected by temperature. In general, above 297 °K, the emission band will broaden without displacing its peak. Below this temperature range, the emission band will broaden and the peak will be displaced to longer wavelengths. For example, the luminescence spectrum of Mn-activated magnesium metasilicate at -180 °C consists of diffuse bands at 4450 and 5250 Å amd a number of relatively narrow lines in the red between 6100 and 7000 Å, with a very strong line at 6410 Å. At room temperature $(Mg,Mn)SiO_3$

exhibits a red luminescence which peaks near 6700 Å (Pringsheim and Vogel, 1943). Low temperature studies of the spectra and magnetic properties of excited and unexcited luminescent solids can provide information on bond types, effective valencies, and coordination numbers of the emitting atoms and the symmetries of the perturbed crystal fields surrounding the emitting atoms.

When impurities such as Fe or Ca are substituted in part for Mg in $MgSiO_3$ the luminescence efficiency of the system decreases, and a larger portion of the energy of the incident excitant beam is manifested as heat, rather than optical fluorescence. In addition, the presence of impurity atoms can displace the original emission band.

All pyroxene structures link SiO_4 tetrahedra by sharing two of the four corners, forming continuous $(SiO_3)_n$ chains. The 5.3 Å repeat distance along the length of the chain defines the c parameter of the unit cell. The cations (Ca, Fe, Mg, etc.) link the chains laterally. The pyroxene subdivisions, clino- and orthopyroxene, depend on the arrangements of the chains. The clinopyroxenes are monoclinic, and the orthopyroxenes are orthorhombic. In enstatite ($MgSiO_3$), Mg or (Mg,Fe) atoms laterally link the (SiO_3) chains. The three polymorphs with the structure of enstatite (protoenstatite, rhombic enstatite, and clinoenstatite) contain less than 30 mol. % $FeSiO_3$ and less than 15 mol. % $CaSiO_3$ as defined by the structural grouping for pyroxenes in the field $CaMgSi_2O_6$-$CaFeSi_2O_6$-$MgSiO_3$-$FeSiO_3$. The majority

of pyroxenes can be considered to be members of this four component system.

The two cation sites, designated M_1 (coordinated by oxygens, each linked to one silicon) and M_2 (surrounded by oxygens shared by neighboring tetrahedra in the chains), in the clinoenstatite structure both have six-fold coordination and this causes some distortion of the (SiO_3) chains. Both sites are occupied by Mg.

Ions other than Mg and Fe can be present in orthopyroxenes and commonly include Ca, Mn, Ni, Cr, Al and Ti; usually the sum of these constituents is less than 10 mol. %. For orthopyroxenes, there is evidence to indicate the distribution of Fe^{2+} between the M_1 and M_2 sites; the Fe^{2+} is found on the M_1 site in six-fold coordination. Fe^{2+} substitution for Mg results in a regular increase in the a, b and c cell parameters. Ca^{2+} substitutes for Mg, and gives an increase in a and c but no effect on b. The temperature of crystallization and the Ca content in orthopyroxenes are generally related; the amount of Ca^{2+} that can be accomodated in the orthopyroxene structure decreases with decreasing temperature (Deer, et al., 1965).

Because of the high purity and low Fe content, rhombic enstatite from the Bishopville enstatite achondrite meteorite has become an X-ray diffraction standard, and has been listed in the X-ray Powder Data File for some time. For similar reasons, Morimoto and co-workers (1960) chose the same

meteorite to obtain subsamples of rhombic enstatite, to convert the rhombic enstatite to clinoenstatite by heating at 1400 °C for 24 hrs., and then to determine the crystal structure of the monoclinic pyroxene clinoenstatite. It was established that the metal atoms in the clinoenstatite occupy the M_1 sites preferentially, and that the coordination number of the M_1 and M_2 sites is six (the M_1 and M_2 sites in the rhombic enstatite structure both have six-fold coordination, also). Brown (1960) also confirmed that the common clinopyroxenes vary chiefly in the relative proportions of Ca^{2+}, Mg^{2+} and Fe^{2+}; that Mn^{2+} and Fe^{2+}, having almost identical ionic radii (0.80 Å and 0.74 Å, respectively), occupy the same structural site; and that the Mg^{2+} and Ca^{2+} (0.66 Å and 0.99 Å, respectively) are in six-fold coordination. As predicted from the crystal chemistry, for both the rhombic and clinoenstatite, the substitution of Fe^{2+} for Mg^{2+} increases the b cell dimension linearly, and a linear relationship is also indicated for the a dimension; his work indicates no similar pattern for the c dimension. The larger Ca^{2+} substituting for Mg^{2+} in clinoenstatite increases the b cell dimension and also the a dimension regularly.

These relationships are important in accounting for the observations obtained in the present study of meteorite fluorescence. In both the enstatite chondrite and achondrite specimens, many of the metals which commonly substitute for the Mg cation in the pyroxene structure are

present in low concentrations, or below detection limits, for reasons to be discussed. Therefore, the disposition of the Fe, Mn and Ca cations and their structural accomodation are of primary interest.

Meteorites can be classified into four groups: Chondrites, Achondrites, Stony-irons, and Irons. Within each group there are several classes. The specimens utilized in this investigation are representatives of the Enstatite class within the Chondrite group and the Aubrite class within the Achondrite group. The distinction between the two groups, the chondrites and the achondrites, is the common occurrence of chondrules (spherical to ovoid bodies comprised of either individual grains or polycrystalline and sometimes polymineralic) in the chondrite meteorites, as compared with the absence of chondrules in the achondrite meteorites. However, chondritic structure is usually not well developed in the enstatite chondrites, and many of the so-called enstatite chondrites actually contain no chondrules. Thus textural, mineralogical and chemical characteristics are required to clearly define the groups.

The chondrites are subdivided according to their mineralogy, and the achondrites are subdivided into Ca-poor (0 - 3% CaO) and Ca-rich (5 - 25% CaO) achondrites. The Ca-poor achondrites are representatives of the Aubrite class. In the enstatite chondrites the essential minerals include pyroxene (rhombic enstatite and/or clinoenstatite,

$MgSiO_3$), 40 - 60%; nickel-iron, 19 - 28%; troilite (FeS), 7 - 15%; plagioclase (in some meteorites; An_{14} to An_{20}, $CaAl_2Si_2O_8$ with some Na-plagioclase intergrowths), 5 - 10%. Accessory minerals (0.1 to 1%) include daubreelite ($FeCr_2S_4$), oldhamite (CaS), alabandite (MnS), schreibersite ($(Fe,Ni)_3P$), and graphite (C). In addition, cohenite (Fe_3C), sphalerite (ZnS), sinoite (Si_2N_2O), and cristobalite, tridymite or quartz (SiO_2) have been reported (Mason, 1962, 1966).

The enstatite achondrites consist largely of rhombic enstatite (with some clinoenstatite). Only minor amounts of other minerals are present. These include forsterite (Mg_2SiO_4), diopside ($CaMgSi_2O_6$), plagioclase, kamacite (Fe-Ni alloy, Ni: 5 - 6%), troilite, MgS, oldhamite, alabandite, osbornite (TiN), and schreibersite (Reid and Cohen, 1967).

For the Adhi Kot, Abee and Jajh deh Kot Lalu chondrites, where tridymite or cristobalite have been identified, the pressure at which crystallization occurred was low. These phases are thermodynamically stable at high temperature and low pressure (tridymite: 876 - 1470 °C, cristobalite: 1470 - 1715 °C; at 1 atm.), but can crystallize at a much lower temperature. By analogy with terrestrial rocks, the enstatite chondrites represent an assemblage in thermodynamic equilibrium in the range 500 - 1000 °C (Mason, 1966, 1967).

Seven of the eleven enstatite chondrites (Adhi Kot, Abee, Atlanta, Hvittis, Khairpur, Jajh deh Kot Lalu, and Blithfield)

and six of the nine enstatite achondrites (Bishopville, Cumberland Falls, Khor Temiki, Norton County, Pesyanoe, and Shallowater) which have been identified as meteorites are included in this work. The dominant mineral in the Adhi Kot and Abee chondrites is clinoenstatite, in the other 11 specimens the mineral is rhombic enstatite. Clinoenstatite is the dominant phase in the high iron enstatite chondrites, and rhombic enstatite is the dominant phase in the moderate to low Fe enstatite chondrites. Of the accessory minerals in the 7 chondrites, daubreelite has been identified in all but the Adhi Kot, oldhamite in all but the Atlanta, alabandite in all but the Blithfield, and schreibersite in all but the Adhi Kot and Blithfield. The common accessory minerals for the achondrites include daubreelite and alabandite identified in the Cumberland Falls and Norton County, schreibersite in the Bishopville and Norton County, forsterite in the Cumberland Falls, diopside in the Cumberland Falls and Norton County, plagioclase in the Cumberland Falls, osbornite in the Bishopville and Norton County, and troilite in the Norton County.

The enstatite chondrites are characterized by a high degree of reduction. Compared with the other stony and stony-iron meteorites, the enstatite chondrites appear to have crystallized under significantly higher reducing conditions, except for the enstatite achondrites which indicate even higher reducing conditions on the basis of

grain size, chemical composition, and partitioning of impurities. Numerous investigations have demonstrated that the total iron content of the enstatite chondrites (usually less than 0.5% FeO) is higher than that for other chondrite groups. The iron is partitioned among the metal, sulfide and silicate phases. Most of what Fe is present appears as the metal or in the sulfides. Sulfur is positively correlated with Fe. In addition, Ca, Mn and Cr may be present in the sulfides, and some Si has been identified in the metal phase.

The transition metal elements Ti, V, Cr and Mn are depleted in these meteorites as compared with members from other meteorite classes. The rare earths are associated with Ca, and presumably they occur in the Ca minerals of both chondrites and achondrites. The concentration of any rare earth element is usually less than 1 ppm in representative bulk enstatite meteorite analyses. The specific relations described for the chondrites hold for the achondrites as well, the achondrites being an even higher purity assemblage.

Increasing grain size of the enstatite is associated with the disappearance of chondrules in the chondrites. Thus the Adhi Kot and Abee exhibit obvious chondrules, the Hvittis to a lesser extent, and no recognizable chondrules for the remaining specimens. This is indicative of the degree of recrystallization and the concomitant minor chemical changes.

D. Crystal Field Theory

An abbreviated discussion of the influence of the presence of divalent manganese in the silicate host crystals will clarify the parameters which determine the wavelength of the emission maximum in the 6000 - 7000 Å range, and will indicate how this can be useful in contrasting the crystal structure and polymorphism of $MgSiO_3$. The emission spectral displacements represent a sensitive indicator of structural variations since easily detectable 10 Å displacements correspond to approximately 0.01 eV, or less than 1% of the energy difference between the typical excited and ground states involved in the radiative transitions. Crystal or ligand field theory (Ballhausen, 1962; Keester and White, 1968; McClure, 1959) can be productively applied to explain the observed absorption and emission spectra. For example, it has been indicated that Mn serves as the primary activator ion in many oxygen-dominated host crystals of selenologic importance. The characteristic variation in color emission from one phosphor to another depends upon the value of Dq (the crystal field splitting parameter), and the $^6S - {}^4G$ energy level separation surrounding the divalent Mn ion and the degree of distortion of the coordination polyhedron. The chief color changes are due to changes in Dq. The emitting level of divalent Mn is the $^4T_{1g}(^4G)$ state. When the space within the crystal available to the ion is decreased, the value of Dq increases, and the $^4T_{1g}$ state

moves to lower energy (McClure, 1959). Further modifications of the color of the emitted light are produced by the band width in absorption and emission.

White and Keester (1966) have concisely summarized the cogent terms and established concepts of crystal field theory as follows:

> The d-electrons of transition metal ions are subjected to two sets of forces when the ions are incorporated in a crystal. First there is an interelectronic repulsion between the various electrons in the orbital. This interaction is described by the Racah B-parameter. The interelectronic repulsion causes a splitting of the d-energy level into a sequence of levels in the gaseous free ion. Secondly, the ion in a lattice site is subjected to an electrostatic field from the coordinating anions. This electrostatic interaction, the "crystal field", causes a further splitting of the free ion levels. The number and arrangement of crystal field levels is determined by the electronic symmetry of the parent free-ion level and the geometrical site symmetry of the coordinating anions. The degree of splitting of the crystal field levels for each free-ion level is characterized by the crystal field splitting parameter, Dq. The observed electronic spectra of transition metal ions arise from transitions between the various crystal field levels, subject to certain selection rules.
>
> Since there are two forces on the d-electrons there exists the possibility for either the interelectronic repulsion or the crystal field to be the dominant force. Respectively, these are the weak field and strong field cases. In the weak field case, the ground state has the same electronic symmetry and spin multiplicity as the free ion while at the strong field boundary there is a cross-over of levels and a different level becomes the ground state usually accompanied by a change in spin multiplicity which results in different selection rules and thus a totally different spectrum. A weak field usually implies tightly bound d-electrons with relatively little interaction with the coordinating anions while strong fields imply a

high degree of interaction and thus covalent bonding. Ions of low charge coordinated by oxide anions are usually described by the weak field diagram. The energy level schemes described above can be computed in a general way for each d-electron configuration in terms of B and Dq. The calculated levels for octahedral coordination are known as Tanabe-Sugano diagrams (Tanabe and Sugano, 1954) and have been widely reprinted, being given in both general references cited above and in many other review articles.

E. Statement of the Research Investigation

The use of luminescence to characterize lunar surface materials was prompted by observations of lunar luminescence reported by Kopal (1965), Rackham (1967), and Cameron and Gilheany (1967). An investigation of terrestrial minerals, likely to occur on the moon, has demonstrated the feasibility of obtaining quantitative measurements of mineral luminescence. It has also indicated striking variations of spectral energy distributions and excitation efficiencies within the individual specimen grains, thus emphasizing the importance of precise localized investigation of phase assemblages and the within phase variations to provide an understanding of the bulk luminescent response of the material. Previous work has not achieved significant quantitative analytical advances due to the lack of systematic study, and the poor structural and compositional control of materials on which measurements had been made.

To achieve the level of precision and discrimination necessary for evaluating the interrelations of wavelength and

intensity with the minor and trace element content, chemical composition of the host crystal, crystal structure, and history of crystallization, two equipment modifications were developed for use with an electron microprobe X-ray analyzer. The work reported here describes the development and application of two basic cathodoluminescence detector units: 1. an electron microprobe interference filter attachment, and 2. an electron microprobe light-wire grating monochromator assembly. Although other equipment units are available for observing luminescence phenomena (Gallup, 1936; Greer, et al., 1967a; Hardy, 1947; Korda, et al., 1967; Lillicrap, 1967; Sippel and Glover, 1965; Wieblen, 1965), a microprobe with the proper cathodoluminescence detector units offers a comprehensive analytical system for detailed investigations.

Some of the electron-excited luminescence information obtained in this study may be used to predict the physical, and to some extent the chemical, properties of minerals which may be present on the lunar surface and which have been exposed to various forms of radiation. This may then lead to the determination of the spatial distribution or availability of specific indigenous lunar or planetary surface resources.

II. APPARATUS AND PROCEDURE

A. Luminescence Display Systems

During the research, emphasis has been on the design and assembly of specialized equipment for an investigation of luminescence of probable lunar surface mineral phase assemblages. The work reported here describes the development and application of three basic cathodoluminescence detector units: 1. a Tesla coil unit, 2. an electron microprobe interference filter attachment, and 3. a light-wire grating monochromator assembly for use with an electron microprobe (or optical microscope).

A simple cathodoluminescence unit, a Tesla coil unit, was constructed and used for rapid identification and distinction of phase assemblages, for the determination of the distribution of reaction products, and for the evaluation of the luminescence properties of bulk specimens prior to thin-sectioning of these specimens, thus permitting a rapid preliminary examination. The principle of operation is a cold cathode discharge whereby the specimen is irradiated with electrons and positive ions. The vacuum chamber will accomodate specimens up to approximately 50 mm in diameter.

This technique used in conjunction with other analytical methods provides a sensitive tool for studying reaction mechanisms at interfaces and in bulk material (Greer, et al., 1967a). In addition, this device obviates extensive sample preparation such as that necessary for microprobe analysis, and

provides a convenient and immediate source of information from an extremely portable analytical unit.

The cathodoluminescence specimen chamber shown in Figure 1 consists of a long, horizontally mounted glass vacuum chamber, covered with black tape except for a horizontal window running the length of the tube. One end of the tube is connected to a rotary oil pump; the other end is fitted with a removable cap with ground glass vacuum joint. The cap supports a glass tray on which specimens or thin-sections can be placed. Luminescence is effected by means of a Tesla coil of the type commonly used as a "vacuum tester". Many specimens can be positioned on the tray; the field of view is changed by moving the Tesla coil and binocular microscope along the length of the vacuum chamber.

For use with a petrographic microscope, preferably one with an objective having as long a working distance as possible, a change in the geometry of the vacuum chamber is required. This chamber, which replaces the stage of the microscope, consists of two pieces of plate glass or ¼ inch thick Lucite separated by an "O" ring. The vacuum pump is connected through one of the plates. The luminescence is excited by positioning the Tesla coil on one of the glass plates, or by placing the tip of the Tesla coil on a wire mesh or metal ring on the upper glass plate to obtain a more uniform discharge. The sandwich assembly is sufficiently

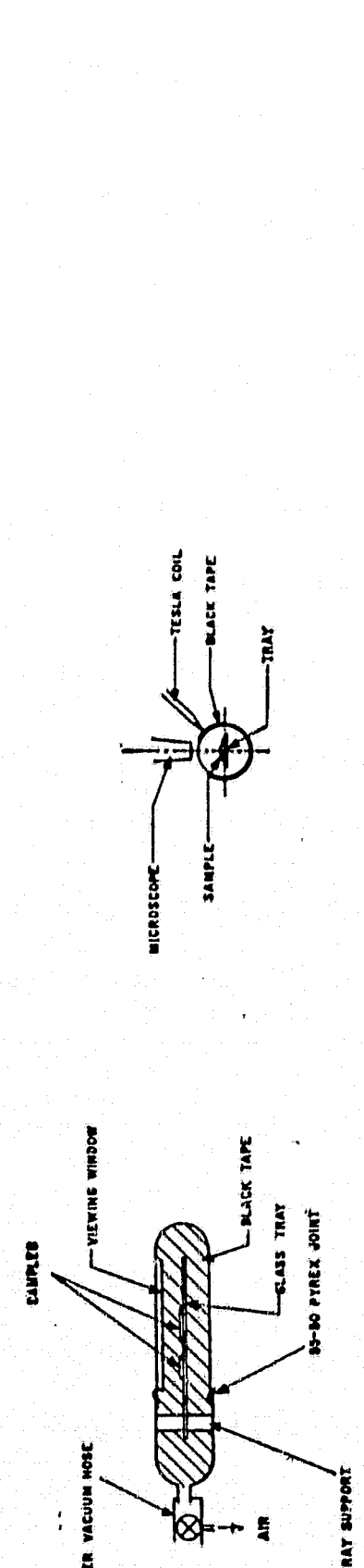

Figure 1. Tesla Coil Sample Chambers:
a. Side view of the cylindrical vacuum chamber,
b. End view of the cylindrical vacuum chamber,
c. Top view of the petrographic microscope vacuum
d. Side view of the petrographic microscope vacuum

thin to make movement of the thin-section in the vacuum chamber unnecessary; either the microscope or the vacuum chamber can be easily moved to change the field of view.

Luminescence begins within 10 to 30 seconds after the sample has been placed within the chamber and the pressure lowered by the rotary pump. The voltage applied to the Tesla coil is adjusted to provide optimum intensity of luminescence for a given specimen. Although prolonged excitation of a sample may result in a moderate temperature increase, this is not a problem for most applications. Should low temperatures be required, however, a coil of 1/8-inch copper or glass tubing in contact with the lower plate can be used to circulate water or other cooling fluid.

Color photographs can be obtained for example with Ektachrome X color film (ASA 64) using a 35 mm single lens reflex camera. The stray light is eliminated by taping a tube of black paper to the luminescence device. Typical exposure times can range from 1 to 30 seconds with an f/4.0 aperture setting.

The second and third cathodoluminescence units are used for the identification and distinction of phase assemblages, for the determination of the distribution of reaction products, and for the quantitative evaluation of the luminescence properties for specimens of microscopic size. The two units facilitate the study of cathodoluminescence phenomena on a μ scale of the specimen without disturbing

the normal function of the microprobe. Either detector unit replaces the ocular tube on the microscope of an Applied Research Laboratories Model EMX microprobe as indicated in Figure 2. Most nonmetallic materials luminesce in the visible region when bombarded by relatively high energy electrons (5 to 50 keV). Since the intensity and spectral distribution of the luminescence can vary even with small changes in impurity content, the luminescence characteristics give important information concerning the trace composition and growth characteristics of a given phase, and with these detection units quantitative measurements of the luminescence spectra are obtained without impeding the inherent use of the microprobe as an X-ray analytical tool.

The monochromator (interference filter) attachment consists of a housing, a monochromator, an ocular tube, a selection of interchangeable slits and interchangeable photomultiplier detectors. A diagram of this attachment is shown in Figure 3. The attachment replaces the ocular tube of the optical microscope on the microprobe. The interchangeable components are readily permuted so that the operator can perform a variety of experiments or use the microscope in the normal manner without having to remove the attachment. For visual microscopic examination, the ocular is inserted in the attachment. Then the specimen can be viewed either through the monochromator, in which case the specimen is seen in a given colored light, or alternatively, the monochromator can be bypassed for normal microscopic

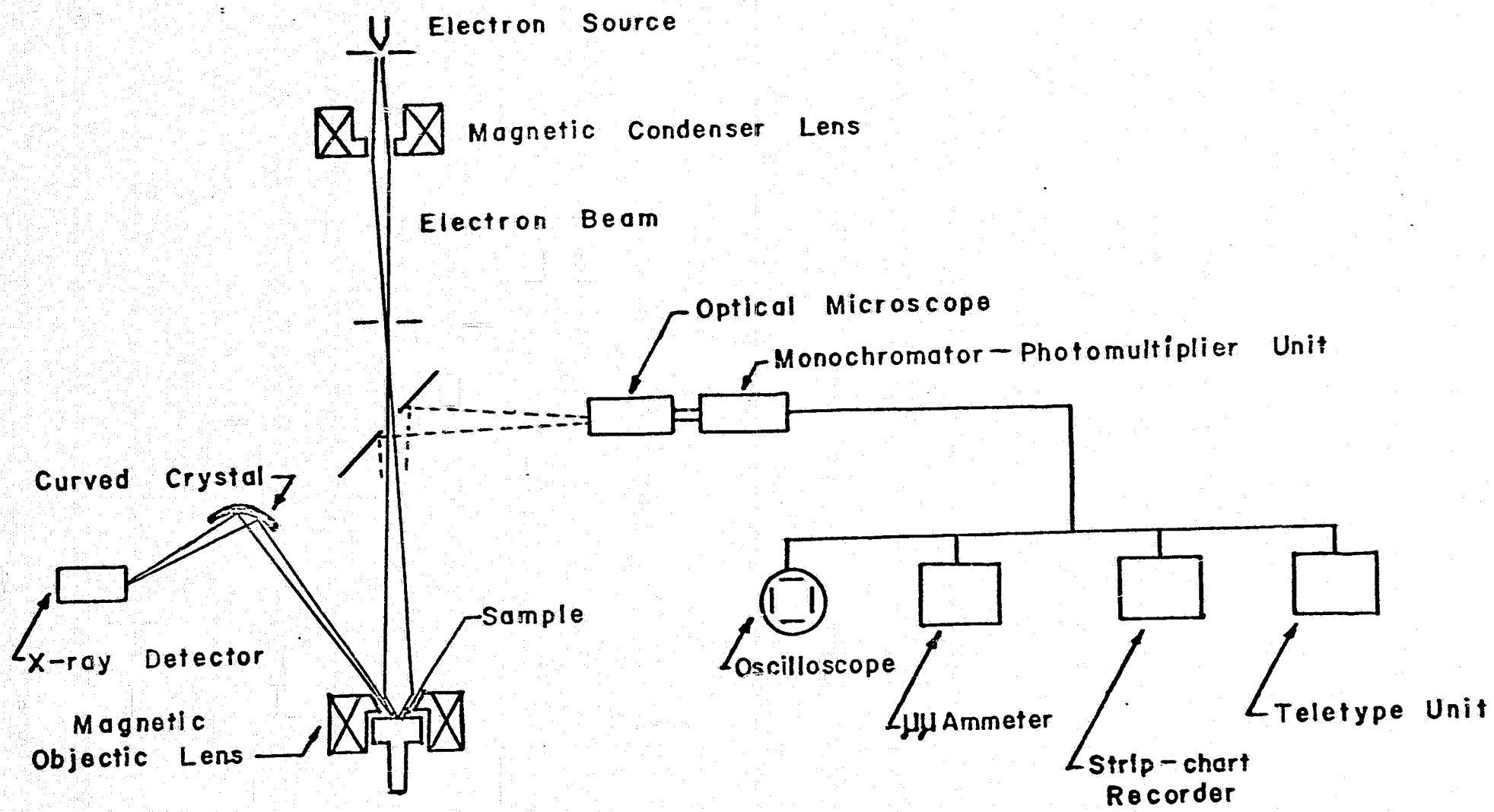

Figure 2. Cathodoluminescence Display System

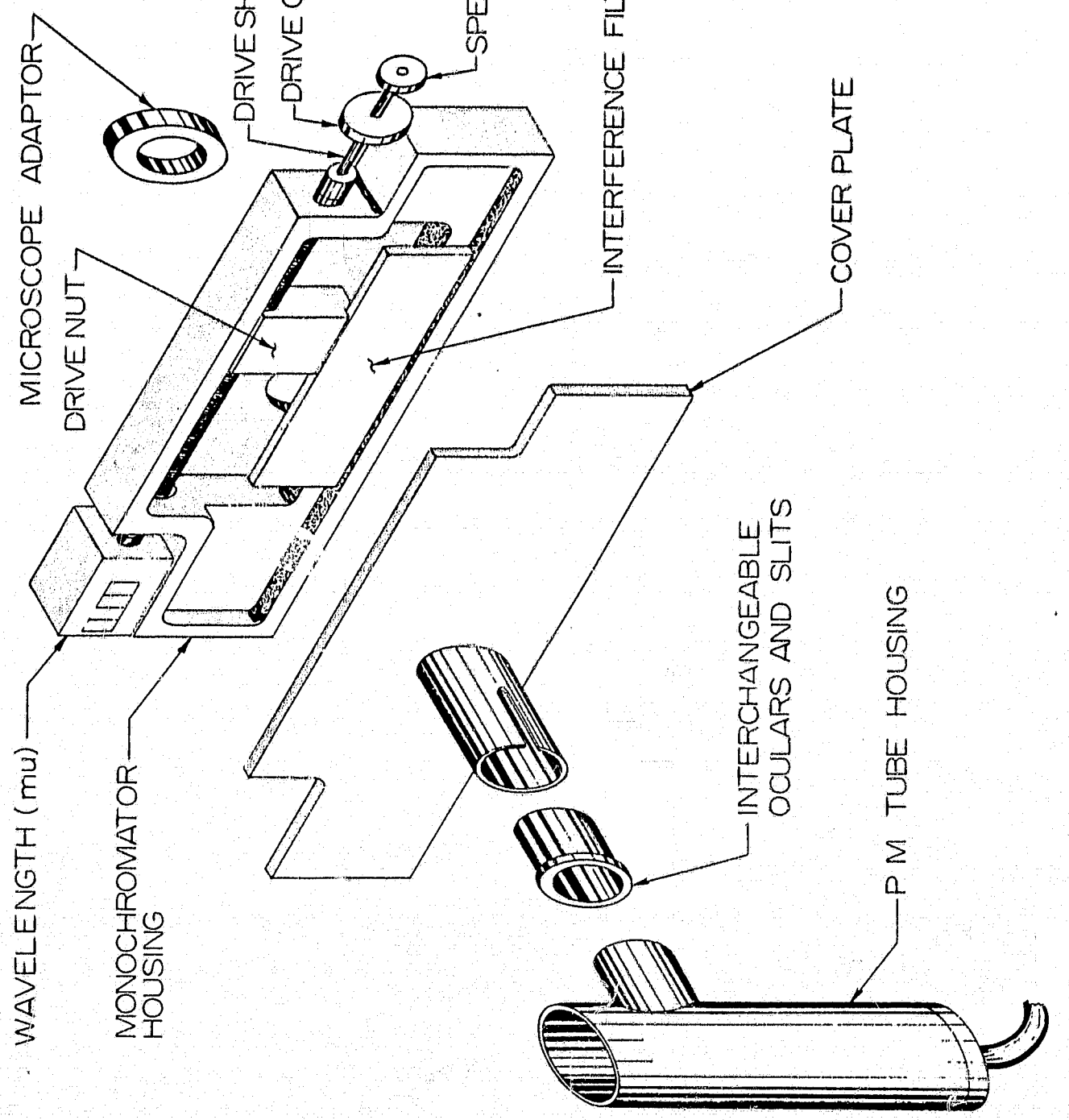

Figure 3. Cathodoluminescence Interference Filter Attachment.

observation. Defining slits for the monochromator are inserted in place of the ocular, and then photomultiplier tubes in light-tight housings are slipped onto the attachment for electronic detection of light intensities.

The monochromator within the attachment is a Bausch and Lomb wedge interference filter of narrow band width (10 nm) and 35% transmission. The linear dispersion is 5.5 nm per mm with a useful wavelength range of 400 to 700 nm. An odometer is used to read wavelength directly to the nearest 1.0 nm. The visible spectrum is scanned by use of a synchronous motor drive on the monochromator with strip chart recording of the signal. In this manner the complete visible emission spectrum of a luminescent area on the surface of the sample can be obtained. The amplified photomultiplier signal can also be displayed on an oscilloscope in a way analogous to the conventional electron backscatter image or X-ray images as described earlier by Heinrich (1967a, 1967b). Recently, infrared microprobe display capabilities (Kyser and Wittry, 1966; Wittry, 1966; Wittry and Kyser, 1964, 1965) have been developed; however, with this attachment light intensity displays at a particular wavelength in the visible can be photographically recorded.

The third cathodoluminescence detection unit is a light-wire and grating monochromator assembly. The light generated by the action of the electron beam (typically 30 keV, 0.03 μ amperes) on the specimen is collected by replacing the ocular of the electron microprobe optical microscope with a

flexible 1/8 inch Bausch and Lomb non-coherent light-wire. Typical incident light gathering efficiency of the fiber optic rod is 60% at the receiving end, with a light transmitting efficiency of 5% absorbance loss per foot and a transmittance capability in the visible and near infrared range. A variety of signal readouts is available such as teletype printout, strip chart recording, and oscillographic display.

A Bausch and Lomb 500 mm focal length monochromator with two interchangeable diffraction gratings, one blazed at 7500 Å with 600 grooves/mm and one blazed at 3000 Å with 1200 grooves/mm, permits narrow band spectra to be obtained when necessary.

By coupling the standard analytical capabilities of a microprobe (local X-ray emission spectrographic analysis), the associated electronic display and recording systems, and monochromator-photomultiplier units, several specific types of information can be obtained; these are listed in Table II.

Table II. Microprobe Optical Fluorescence Analytical Capabilities

1.	Recordings of optical fluorescence spectra; simultaneous monitoring of an element and the luminescence intensity with the monochromator set at a wavelength of interest
2.	Distribution of luminescent phases in specimens
3.	Relationships between fluorescence patterns and conventional X-ray representation of an area scan
4.	Relation of luminescence intensity to composition within a phase

B. Experimental Procedure for Specimen Phase Identification and Analysis

As one part of a systematic study of luminescence of natural materials likely to occur on lunar and planetary surfaces, a variety of meteorite specimens were examined under electron bombardment. Detailed examination of what appeared at first to be homogeneous material, free from obvious inclusions of extraneous phases, revealed striking variation in fluorescence and chemical composition. To characterize the extent of such variation, an electron microprobe was utilized to examine enstatite grains derived from the following meteorite specimens: 1. Enstatite Chondrites: Abee, Adhi Kot, Atlanta, Blithfield, Khairpur, Jajh deh Kot Lalu, and Hvittis; and 2. Enstatite Achondrites: Bishopville, Cumberland Falls, Khor Temiki, Norton County, Pesyanoe, and Shallowater.

Enstatite grains (less than 0.01 mm for the clinoenstatite specimens to greater than 1 mm for the rhombic enstatite achondrite specimens) were chosen for the study. They were shown to be of high quality and purity, and there was sufficient variability in the element concentrations, structure, and history exhibited by the specimens to permit an evaluation of the interrelations as they influence optical fluorescence emission, and to demonstrate the capabilities of the system for luminescence analysis of solids.

The enstatite subspecimens were examined by an optical microscope, X-ray diffraction, cathodoluminescence and an

electron microprobe. An optical microscope was utilized for identifying the characteristic parallel extinction of the orthorhombic enstatite and nonparallel extinction for the clinoenstatite. In any specimen it is difficult to identify rhombic enstatite in the presence of large amounts of clinoenstatite, and vise versa. Consequently, the type of pyroxene listed in Tables III to V applies to the major part of the meteorite specimen. X-ray diffraction data were also used to classify the enstatites in terms of the two polymorphs, clinoenstatite and rhombic enstatite.

By careful microprobe analysis, most inclusions in the enstatite grains can be avoided. The concentrations of Fe, Ca, Mn and Cr, the only elements likely to influence the luminescence spectrum and which occur in detectable concentrations, were determined. The abundance of silicon was simultaneously measured in order to eliminate the effects of possible variations in counting rates that would result from differences in grain thickness or by encountering a different phase in the sample. This was accomplished by calculating X:Si ratios, where X represents Fe, Ca, Mn or Cr. For these high purity specimens, standard corrections for absorption, fluorescence and atomic number effects are not required for the microprobe determination of the trace elements.

Individual grains, 10 to 200 μ in diameter were selected for analysis, and these samples were embedded in ¼ inch diameter plastic rods. Polishing was done by sequential use of 6-, 3-, and 1 μ diamond paste, and ¼ μ "Gamol" polishing suspension.

Table III. Luminescence and Microprobe Data for Enstatite Meteorite Specimens

Sample and Position [a]	Element concentration (counts/10 sec.) [d]					λ [c]	I [b]
	Mn	Fe	Ca	Si	Cr		
A-1-1	531	20724	1371	16484		426	54
A-1-2	140	11928	6461	11344		426	43
A-1-3	420	6006	1219	10033		435	49
A-1-4	34	12694	1575	34899		435	112
A-1-5	213	57014	12102	14104		435	104
A-1-6	45	975	157	36506		435	140
A-1-7	126	19797	624	23901		435	51
A-1-8	104	17680	1138	24703		435	50
A-1-9	157	5773	3000	18304		435	61
A-1-10	139	6752	2866	29315		435	73
A-1-11	156	9001	3233	45681		435	66
A-1-12	5608	58455	2200	23446		435	36
A-1-13	45	1502	617	28657		435	110
A-1-14	.00001*	1835	187	32251		491	82
A-1-15	45	4089	728	36871		491	112
A-1-16	137	2993	413	12995		491	50
A-1-17	203	15754	794	10811		491	69
B-1-1	19	6560	78	45740	129	435	35
B-1-2	.00001	1259	66	46482	12	435	34
B-1-3	28	9127	159	37674	129	435	37
B-1-4	4	1486	82	44301	28	435	36
B-1-5	75	10242	533	40266	359	435	46
B-1-6	.00001	1181	214	45710	12	435	19
B-1-7	22	1381	120	36445	93	435	55
B-1-8	42	17233	236	36764	258	435	68
B-1-9	36	6397	199	35934	190	435	61
B-1-10	.00001	706	88	37364	.00001	435	72
B-1-11	.00001	2394	2017	34055	60	621	123

Table III. Continued

Sample and Position [a]	Element concentration (counts/10 sec.) [d]					λ [c]	I [b]
	Mn	Fe	Ca	Si	Cr		
B-1-12	.00001	1134	141	33832	24	621	118
B-1-13	25	1978	88	33254	20	621	116
B-1-14	28	568	81	34196	12	621	139
B-1-15	46	1850	230	36372	77	621	123
B-1-16	6	1402	147	36380	8	621	126
B-1-17	.00001	618	75	38256	20	621	102
B-1-18	.00001	668	68	37955	.00001	621	109
B-1-19	84	1709	93	38402	.00001	621	106
B-1-20	30	2159	144	37758	36	621	93
C-2-1	20	920	599	32522	14	435	284
C-2-2	30	1716	504	28446	6	435	277
C-2-3	45	3894	508	30307	186	435	244
C-2-4	15	1100	416	33749	11	435	284
C-2-5	30	964	499	31078	14	435	254
C-2-6	45	950	440	33758	.00001	686	792
C-2-7	36	3390	396	25841	6	686	710
C-2-8	10	1086	480	25660	.00001	686	762
C-2-9	5	1053	470	27714	3	686	1000
C-2-10	10	1118	466	27243	.00001	686	1170
E-1-1	.00001	.00001	3644	33759	.00001	435	11
E-1-2	.00001	1160	2895	17940	.00001	491	23
E-1-3	.00001	.00001	3178	36952		534	39
E-1-4	.00001	.00001	3311	38093	46	578	29
E-1-5	10	111	872	16480	5	621	267
E-1-6	.00001	127	3945	31041	.00001	621	47
E-1-7	.00001	.00001	4019	38744	.00001	578	19
E-1-8	6	.00001	3886	40779	.00001	534	27
E-1-9	.00001	11	3686	44848	.00001	491	15

Table III. Continued

Sample and Position [a]	Element concentration (counts/10 sec.) [d]					λ [c]	I [b]
	Mn	Fe	Ca	Si	Cr		
E-1-10	10	13	3812	34833	.00001	435	7
E-1-11	22	47	943	36971	.00001	409	167
L-7-1	26	314	737	35600	4	435	55
L-7-2	9	82	705	33532	.00001	435	70
L-7-3	18	48	786	38076	26	435	61
L-7-4	10	59	778	34608	.00001	435	67
L-7-5	12	173	699	28441	35	435	62
L-7-6	10	52	762	34107	.00001	621	162
L-7-7	20	3124	846	37731	26	621	105
L-7-8	86	5171	798	33287	235	621	143
L-7-9	14	72	835	32110	4	621	151
L-7-10	24	115	819	32663	13	621	142
L-7-11	9	28	70	56578	4	621	100
L-7-12	26	64	814	40587	4	621	171
L-7-13	4	108	793	39007	.00001	621	162
L-7-14	22	911	843	39157	.00001	621	144
L-7-15	36	2806	798	39791	26	621	157
L-7-16	.00001	217	748	36913	.00001	435	60
L-7-17	.00001	56	835	40408	.00001	435	72
L-7-18	45	1896	836	38925	4	435	64
L-7-19	28	286	873	31945	70	435	49
L-7-20	.00001	72	3415	36077	.00001	409	50
D-1-1	27	.00001	594	31708	.00001	435	162
D-1-2	66	9	770	35555	.00001	491	191
D-1-3	.00001	38	553	30350	.00001	534	117
D-1-4	35	.00001	521	20912	12	578	191
D-1-6	23	27	712	28651	.00001	435	146
D-1-7	14	5	809	29957	15	491	145

Table III. Continued

Sample and Position [a]	Element concentration (counts/10 sec.) [d] Mn	Fe	Ca	Si	Cr	λ [c]	I [b]
D-1-8	39	26	766	32315	.00001	534	227
D-1-9	20	19	724	30987	.00001	578	228
D-1-10	.00001	.00001	439	22924	.00001	621	260
D-1-11	28	58	673	28677	12	621	541
D-1-12	13	12	842	34188	12	643	446
D-1-13	12	21	731	29973	.00001	664	630
D-1-15	29	21	712	36499	5	686	558
D-1-16	27	30	676	37976	5	409	173
D-1-17	24	20	673	33190	10	700	399
D-1-18	36	6	459	27193	.00001	409	99
F-1-1	193	143	466	25216	21	435	594
F-1-2	46	80	553	29044	7	435	607
F-1-3	53	79	688	24833	16	435	634
F-1-4	71	84	518	22057	10	435	680
F-1-5	42	89	233	27272	5	435	568
F-1-6	69	137	607	25876	15	686	1760
F-1-7	66	108	579	29507	17	686	1070
F-1-8	91	69	589	26926	22	686	1230
F-1-9	96	48	615	28934	6	686	1380
F-1-10	61	60	434	28069	11	686	1520
J-1-1	.00001	15	620	20885	.00001	686	1180
J-1-2	.00001	6	581	18167	.00001	686	980
J-1-3	.00001	7	634	20499	7	686	1230
J-1-4	16	.00001	629	19804	.00001	686	1200
J-1-5	7	14	611	19839	4	686	1330
J-1-6	7	59	128	7833	.00001	435	205
J-1-7	30	122	393	15143	.00001	435	76
J-1-8	.00001	22	603	23029	.00001	435	167

Table III. Continued

Sample and Position [a]	Element concentration (counts/10 sec.) [d]					λ [c]	I [b]
	Mn	Fe	Ca	Si	Cr		
J-1-9	22	.00001	569	23443	.00001	435	320
J-1-10	22	21	511	22256	4	435	294
M-1-1	43	3	456	27989	20	435	337
M-1-2	55	13	457	27632	9	435	238
M-1-3	59	12	456	24670	10	435	277
M-1-4	55	37	414	23588	13	435	271
M-1-5	43	30	402	33276	16	435	264
M-1-6	36	37	480	35082	13	686	578
M-1-7	69	60	498	33705	20	686	521
M-1-8	54	38	414	34567	.00001	686	634
M-1-9	35	40	412	32968	24	686	649
M-1-10	40	25	466	34144	6	686	634
0-1-1	17	.00001	80	32382	58	435	538
0-1-2	.00001	1	75	34045	.00001	435	389
0-1-3	.00001	14	51	29513	.00001	435	462
0-1-4	.00001	.00001	73	22862	.00001	435	380
0-1-5			58	27800		435	660
0-1-6			68	30254		435	356
0-1-7			58	30360		435	389
0-1-8			66	31954		435	370
0-1-9			58	28428		435	376
0-1-10			60	32405		435	393
0-1-11			74	30037		435	399
0-1-12			86	29227		435	360
0-1-13			78	32713		435	380
0-1-14			74	29574		435	465

Table III. Continued

Sample and Position [a]	Element concentration (counts/10 sec.) [d]					λ [c]	I [b]
	Mn	Fe	Ca	Si	Cr		
0-1-15			72	32889		435	449
0-1-16	1	.00001	148	32257		435	1120
0-1-17	.00001	.00001	126	40258		435	1000
0-1-18	.00001	.00001	160	38072		435	960
0-1-19	.00001	.00001	163	36658		435	760
0-1-20	.00001	.00001	99	42362		435	1340
0-1-21	.00001	.00001	462	38538		686	2838
0-1-22	.00001	.00001	113	37807		686	1920
0-1-23	4	.00001	220	42847		686	2020
0-1-24	.00001	44	94	12133		686	1790
0-1-25	.00001	.00001	132	40147		686	2080
G-1-1	3	242	835	42617		435	192
G-1-2	1	265	875	43729		435	184
G-1-3	4	272	887	43749		435	119
G-1-4	.00001	300	859	43354		435	233
G-1-5	.00001	1687	3003	46549		435	166
G-1-6	.00001	2359	1895	45347		686	591
G-1-7	5	667	2518	43158		686	251
G-1-8	.00001	430	3635	45955		686	198
G-1-9	.00001	711	933	39150		686	832
G-1-10	.00001	806	910	36824		686	805
I-1-1	9	591	730	28202		435	330
I-1-2	19	985	641	26025		435	231
I-1-3	10	430	659	30505		435	521
I-1-4	10	270	590	26180		435	277
I-1-5	19	285	626	21975		435	342
I-1-6	19	104	735	29464		686	2170

Table III. Continued

Sample and Position [a]	Element concentration (counts/10 sec.) [d] Mn	Fe	Ca	Si	Cr	λ [c]	I [b]
I-1-8	.00001	94	716	27352		686	2140
I-1-10	31	141	777	32588		686	800
I-1-11	3	95	682	29578		686	760
I-1-12	.00001	219	428	26801		686	1200
N-1-1	72	21	699	25778		435	900
N-1-2	63	37	702	28757		435	750
N-1-3	58	14	640	26754		435	780
N-1-4	69	16	658	29361		435	840
N-1-5	58	47	716	29335		435	880
N-1-6	70	41	739	26039		686	1800
N-1-7	64	6	691	32828		686	1840
N-1-8	61	34	702	33686		686	2050
N-1-9	48	15	711	37554		686	2360
N-1-10	65	21	760	37145		686	1650

a. Sample designation:
- A-1 Abee Meteorite; clinoenstatite chondrite
- B-1 Adhi Kot Meteorite; clinoenstatite chondrite
- C-2 Atlanta Meteorite; rhombic enstatite chondrite
- E-1 Blithfield Meteorite; rhombic enstatite chondrite
- L-7 Khairpur Meteorite; rhombic enstatite chondrite
- I-1 Jajh deh Kot Lalu Meteorite; rhombic enstatite chondrite
- G-1 Hvittis Meteorite; rhombic enstatite chondrite
- D-1 Bishopville Meteorite; rhombic enstatite achondrite
- F-1 Cumberland Falls Meteorite; rhombic enstatite achondrite
- J-1 Khor Temiki Meteorite; rhombic enstatite achondrite
- O-1 Shallowater Meteorite; rhombic enstatite achondrite
- N-1 Pesyanoe Meteorite; rhombic enstatite achondrite

Table III. Continued

M-1 Norton County Meteorite; rhombic enstatite achondrite

b. I is the photomultiplier tube output, representing intensity of luminescence emission for a particular monochromator wavelength setting; in arbitrary units.

c. λ is in nm; represents the particular monochromator wavelength setting.

d. The intensity of the characteristic X-ray lines for the various elements is represented in counts/10 sec.

* Computer computations using the above data to generate Tables IV - VII require that any zero values for counts/10 sec. be expressed as an "insignificantly small number". Thus, the number chosen to represent zero in the original data is .00001.

Table IV. Dispersion of Element Concentration: Geometric Means

Groups	Element concentration (counts/10 sec.) [a]				
	Mn	Fe	Ca	Si	Cr
Abee (chondrite)	159(3)16	8318(3)17	1230(3)17	21880(2)17	
Adhi Kot (chondrite)	28(2)13	2143(3)20	148(2)20	38020(1)20	48(3)17
Atlanta (chondrite)	21(2)10	1380(2)10	479(1)10	29510(1)10	14(4)7
Blithfield (chondrite)	12(2)4	71(5)6	2818(2)11	32360(1)11	
Khairpur (chondrite)	20(2)17	209(5)20	759(2)20	36310(1)20	17(4)12
Jajh deh Kot Lalu (chondrite)	14(2)8	240(2)10	646(1)10	27540(1)10	
Hvittis (chondrite)	4(2)4	562(2)10	1380(2)10	42660(1)10	
Bishopville (achondrite)	26(2)14	20(2)13	661(1)16	30200(1)16	10(1)7
Cumberland Falls (achondrite)	72(2)10	87(1)10	513(1)10	26920(1)10	13(2)10
Khor Temiki (achondrite)	16(2)6	22(3)8	490(2)10	18200(1)10	6(1)3
Pesyance (achondrite)	63(1)10	23(2)10	708(1)10	30200(1)10	
Shallowater (achondrite)	6(3)3	11(5)3	96(2)25	31620(1)25	
Norton County (achondrite)	49(1)10	25(2)10	447(1)10	30200(1)10	14(2)9
All chondrites	29(4)72	871(6)93	676(3)98	32360(1)98	26(4)38
All achondrites	36(2)53	27(3)54	324(2)81	28840(1)81	12(2)30

Table IV, Continued

Groups	Element concentration (counts/10 sec.) [a]				
	Mn	Fe	Ca	Si	Cr
All clinoenstatite	72(4)29	3890(4)37	389(4)37	29510(2)37	48(3)17
All rhombic enstatite	25(2)96	96(6)110	513(3)142	30900(1)142	13(2)51

a. Format for data: geometric mean(standard deviation)N, where N is the number of positions for which data were obtained for the particular element indicated.

Table V. Distribution of Element Concentration: Geometric Means of Element:Si Ratio Values

Groups	Element:Si Values [a]			
	Mn/Si	Fe/Si	Ca/Si	Cr/Si
Abee (chondrite)	76(4)16	3802(4)17	575(4)17	
Adhi Kot (chondrite)	8(2)13	537(3)20	39(2)20	14(3)17
Atlanta (chondrite)	8(2)10	468(2)10	162(1)10	6(3)7
Blithfield (chondrite)	5(2)4	28(7)6	871(2)11	
Khairpur (chondrite)	6(2)17	59(5)20	209(2)20	5(3)12
Jajh deh Kot Lalu (chondrite)	6(2)8	87(2)10	234(1)10	
Hvittis (chondrite)	2(1)4	132(2)10	324(2)10	
Bishopville (achondrite)	9(2)14	7(2)13	219(1)16	4(2)7
Cumberland Falls (achondrite)	28(2)10	33(1)10	191(1)10	5(2)10
Khor Temiki (achondrite)	10(2)6	13(3)8	269(1)10	3(1)3
Pesyanoe (achondrite)	25(2)10	9(2)10	263(2)10	
Shallowater (achondrite)	3(2)3	6(5)3	31(2)25	
Norton County (achondrite)	17(1)10	9(2)10	148(1)10	5(1)9
All chondrites	11(4)72	275(7)93	214(4)98	8(3)38
All achondrites	14(2)53	11(3)54	118(3)81	5(2)30

Table V. Continued

Groups	Element:Si Values[a]			
	Mn/Si	Fe/Si	Ca/Si	Cr/Si
All clinoenstatite	28(5)29	1318(5)37	135(6)37	14(3)17
All rhombic enstatite	9(2)96	34(5)110	170(3)142	5(2)51

a. Format for data: geometric mean(standard deviation)N, where N is the number of positions for which data were obtained for the particular element:Si value indicated.

The samples were carbon-coated to a thickness of about 200 - 400 Å to provide a conducting path for absorbed electrons, and were placed in a brass holder in the microprobe chamber for analysis.

Intensity of luminescence was recorded on a Varian dual pen strip recorder. The wavelength range from 400 to 700 nm was investigated in two ways: at monochromator settings to monitor and compare the blue and red portion of the spectrum (for enstatite, the host crystal luminescence is in the blue, and the activator induced luminescence emission is in the red portion of the spectrum), and at a variety of settings to obtain oscillographic displays of the luminescence for comparison with conventional electron backscatter and X-ray images.

All the X-ray measurements were made on an Applied Research Laboratories Model EMX microprobe equipped with three dispersive channels. X-ray intensities were read from three Hamner six-decade scalers on the basis of preset time or printed by a teletype machine. The probe was operated with a 1 μ spot size. The majority of the intensities were measured on a 4 inch LiF spectrometer using a sealed 0.001 inch beryllium window argon detector (argon Exatron); silicon intensities were measured using a 4 inch ADP (ammonium di-hydrogen phosphate) spectrometer with a 0.004 mm thick, carbon coated, nonsupported, mylar window, and a flow proportional counter with P-10 gas at atmospheric pressure. The LiF spectrometer was used to scan for the K_{α} X-ray

emission lines of the elements Ca, Fe, Mn and Cr; the ADP spectrometer was used to identify the K_{α} X-ray emission lines for Si.

The procedure for making X-ray intensity measurements was to select each grain by use of the reflected light microscope, and then simultaneously record the luminescence signal from the instant the electron beam impinged on the specimen, and the X-ray signals. For the individual grains derived from the larger samples, Fe, Mn, Cr, Ca and Si were determined. The intensity of the Si K_{α} X-ray emission line signal was utilized to monitor the phase (in this case, enstatite, $MgSiO_3$). The Fe, Ca and Cr were monitored so as to determine their influence on the optical fluorescence response of the enstatite host. Although Group IVB oxides can increase the host luminescence (in the blue), they were not monitored since their presence in these meteorites is well below the one weight % necessary to enhance the enstatite blue emission band.

Operational technique was as follows: 1. to obtain the luminescence intensity measurements, 2. to record five replications at each element odometer setting and at the background odometer setting for that element for a series of points within a grain or grains, and 3. to photograph luminescence oscillographic displays, and the conventional cathode ray tube electron backscatter image and X-ray images. Several review articles detail the standard analytical procedures in microprobe analysis (Campbell, et al., 1966;

Heinrich, 1962b; Keil, 1967a; Long, 1963).

For purposes of correlation studies, the quantitative data are obtained by examining a number of 1 μ diameter positions on the specimen surface. The excitation of local X-ray and optical fluorescence emission is produced by means of a focused electron beam. Since a 30 keV beam can penetrate several microns of material, the excitation volume can be a few cubic microns. The characteristic X-ray lines for various elements are analyzed by means of three curved crystal spectrometers, and the composition of the sample is determined from the wavelength and intensity of these characteristic lines. The information is assembled by simultaneously recording the intensities for the chosen elements and the luminescence intensity (the photomultiplier tube output) for each monochromator setting.

Multivariate statistical analytical techniques (Dixon and Massey, 1957; Snedecor and Cochran, 1962) were utilized to process the data. From this information it was possible to determine to what extent optical fluorescence spectra of the meteorites vary from sample to sample and to correlate the intensity and wavelength of optical fluorescence with chemical composition. Since some zero concentration values for the elements were measured (corresponding to the probe analysis detection limit for the element), the data transformation log (X + 1) was appropriate for the statistical analysis, where X was the element count rate.

By scanning of the electron beam, the distribution of

a given element over the surface of the sample can be obtained by monitoring the intensity of a particular characteristic X-ray line. The standard method used for producing X-ray and electron (backscattered electron and beam current) images is horizontal linear scanning (raster spot scanning). The various detector outputs are amplified to control the intensity of the synchronized electron beam in a cathode ray tube. The image elements correctly reproduce the entire image on an oscilloscope with a long persistence phosphor (P-7 phosphor with a decay time of about 20 sec.).

The AC pulse amplifier accepts negative pulses from the standard A. R. L. X-ray detector preamplifiers; these do not include the backscattered electron detector or sample current or optical fluorescence. The AC pulse amplifier produces approximately a 30 volt pulse of 1 μ sec. duration.

The DC amplifier is used with the sample current, backscattered electron, and optical fluorescence detectors. The rise time of the DC amplifier is 10 μ sec.

The advantage of forming an image from the high energy backscattered electrons is high contrast and resolution. This image has approximately 4X better resolution than the X-ray image. As the backscattering increases, the image on the cathode ray tube increases in intensity. This increased intensity indicates an increase in sample mass density. The use of the backscattered electron image gives increased resolution over the optical microscope. The image formed is similar to the optical image obtained in oblique illumination.

Information can be photographically recorded as in the case of an optical fluorescence display on an oscilloscope. The oscilloscope displays correspond to brightness patterns, over a narrow wavelength range of interest, generated by the electron beam raster over the sample face, detected and discriminated by the monochromator-photomultiplier unit, and projected on the oscilloscope screen. By rastering the electron beam over a specimen surface and recording either the X-ray fluorescence or the optical fluorescence signal, an image can be constructed on a synchronized cathode ray tube, and photographed in less than one second. The area scanned ranges from about 45 x 45 μ to 200 x 200 μ. The patterns, photographically recorded, selectively delineate the emitting area of the specimen and permit comparisons of a particular color, intensity of that color, and any obvious associations with specific element distributions.

Oscillographic recording was done on Polaroid Type 47 film (ASA 3000). The image from the Type 561 Tektronix oscilloscope was recorded with an Oscillograph record camera at an f/5.6 aperture setting with one Type 67 Time-Base set at 0.5 sec./div and the other Type 67 Time-Base set at 2 msec./div. The number of lines that reproduce the image on the oscilloscope is obtained by dividing the frame rate (0.5) by the line rate (0.002), and in this example equals 250 lines. The electron beam scanned a 200 x 200 μ area in ½ to 5 seconds. The problem of possible deterioration of

the material under the action of the electron beam was recognized, and consequently any area was exposed to the beam for as short a time as possible to successfully obtain a complete set of the luminescence display photographs and not appreciably alter the luminescence output for that area. Typically, the electron beam would scan a particular 1 μ diameter spot in 10^{-5} seconds.

The luminescence photographs were obtained using the assembly described previously, with an RCA 1P28 photomultiplier tube of the type commonly used in a Beckman DK-2A spectrophotometer for the visible region of the spectrum. The signals from the weakly luminescent silicates are adequate and do not require photomultiplier-differential current amplifier circuits for their detection and quantitative measurement.

The recording of optical fluorescence spectra is accomplished by positioning the 1 μ diameter electron beam (30 keV, 0.03 μ amperes) at a position of interest on an individual grain or bulk specimen. The optical fluorescence is then detected at the monochromator-photomultiplier unit. By varying the monochromator settings, a complete emission spectrum of the fluorescence can be displayed on a strip chart recorder. In addition, the option exists to simultaneously record the luminescence intensity (at a particular wavelength) and the presence of a particular element of interest on a dual pen strip chart recorder. In

this case, the specimen is translated under the fixed electron beam so that both the optical fluorescence and X-ray fluorescence signal can be compared directly.

III. PRESENTATION AND DISCUSSION OF RESULTS

A. Correlation and Interpretation of Measurements and Observations

When the samples were observed microscopically during electron bombardment, large differences in both the intensity and wavelength of the resulting luminescence were evident. Different portions of a single mineral sample emitted at wavelengths ranging to both limits of the visible spectrum. Fluorescence was most intense in the red portion of the spectrum. Almost all of the strong luminescent samples contained very little iron or calcium, and the achondrite enstatite meteorites luminesced stronger than the chondrites throughout the visible spectrum.

Fluorescence spectral data and the Mn, Fe, Ca, Si and Cr content of the meteorite samples are given in Table III. Selected grains examined by the electron microprobe revealed that the dispersion of the concentrations of these elements in the samples is large. This variability indicates why a variety of intensity and wavelength responses may be possible within a specimen.

As is common with trace element data, the concentrations are not normally distributed, that is, they cannot be adequately represented by a normal or gaussian frequency distribution curve. Points on the cumulative frequency curve can be reasonably fitted with a straight line when plotted on log probability paper, indicating that the distribution of the

data is better described by a log-normal frequency distribution curve than by one which is normal. Accordingly, for statistical analysis of the data they have been transformed by converting concentrations to log concentrations in order to normalize the distribution. The statistics representing the "average" concentration and the spread of values around the "average" are then the geometric mean and the geometric standard deviation respectively.

Higher Mn concentration is indicated for the achondrite specimens when compared with the chondrite specimens. Iron is higher, and Ca, Si and Cr are slightly higher in the chondrites than in the achondrites. Comparison of the types of enstatite shows that Mn, Fe and Cr are more concentrated in the clinoenstatite than in the orthorhombic form. The Ca concentration for these specimens appears slightly higher in the rhombic enstatite than for the clinoenstatite. These measurements clearly demonstrate the high variability in the Fe concentration and the more uniform Ca concentrations when the specimens are compared on both the basis of chondrites and achondrites and of clinoenstatite and rhombic enstatite. Plots of the geometric means taken from Table IV show this clearly in Figure 4. Similar relations would be indicated if the geometric means from Table V were plotted instead.

The values also demonstrate the trend of concentration of Fe and of Cr in the pyroxene that would be expected for more reducing conditions (higher purity pyroxene). Thus,

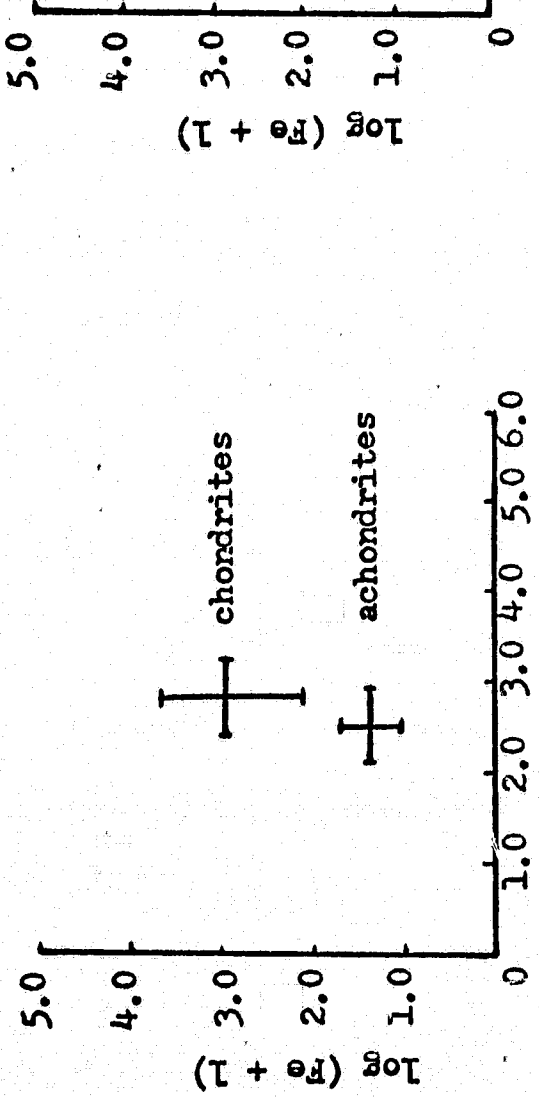

(a)

(b)

Figure 4. Meteorite Class and Phase Distinction as Determined by Microprobe Analysis:
a. Geometric means for iron and calcium for chondrite and achondrite specimens,
b. Geometric means for iron and calcium for clinoenstatite and rhombic enstatite specimens.

the amount of Fe is highest in the clinoenstatite chondrites, less in the rhombic enstatite chondrites, and least in the rhombic enstatite achondrites. The same trend is shown by Cr.

When the intensity of optical fluorescence at a particular wavelength, represented by the photomultiplier tube output, is compared with either the type or class of meteorite, important relationships can be seen. Table VI contains both the arithmetic and geometric means of intensity values for the red and blue portions of the visible spectrum. The short wavelength intensity value is higher for the achondrites than for the chondrites, and for rhombic enstatite than for clinoenstatite. The same trend is indicated in the red region for both grouping comparisons. Also, the long wavelength values are considerably greater than the short wavelength values for the chondrites and the achondrites, and for clinoenstatite and rhombic enstatite.

Figure 5 represents the variation of the geometric means of the short wavelength optical fluorescence output for individual meteorite specimens with respect to the Fe and Ca concentration differences for these specimens. Similar relationships are evident when the long wavelength outputs are plotted. A considerable number of significant relationships are featured on this diagram. The trend of the positions of the specimens on the diagram, considered from the upper left corner to the lower right corner is in agreement with the following relationships: change of meteorite class;

Table VI. Optical Fluorescence Intensity for Meteorite Type and Class

Type and Class	Statistic	Intensity, arbitrary units[a] (at 435 nm)	(at 621 nm)	(at 686 nm)
Chondrites	Arithmetic mean and standard deviation	124 ± 111	132 ± 41	945 ± 561
Achondrites	Arithmetic mean and standard deviation	513 ± 287		1415 ± 619
Clinoenstatite	Arithmetic mean and standard deviation	63 ± 31	116 ± 13	
Rhombic enstatite	Arithmetic mean and standard deviation	383 ± 290	182 ± 118	1243 ± 634
Chondrites	Geometric mean and standard deviation	85 ± 2		794 ± 2
Achondrites	Geometric mean and standard deviation	437 ± 2		1288 ± 2
Clinoenstatite	Geometric mean and standard deviation	54 ± 2	115 ± 1	
Rhombic enstatite	Geometric mean and standard deviation	269 ± 2	159 ± 2	1072 ± 2

a. Intensity of optical fluorescence, represented by the phototube output.

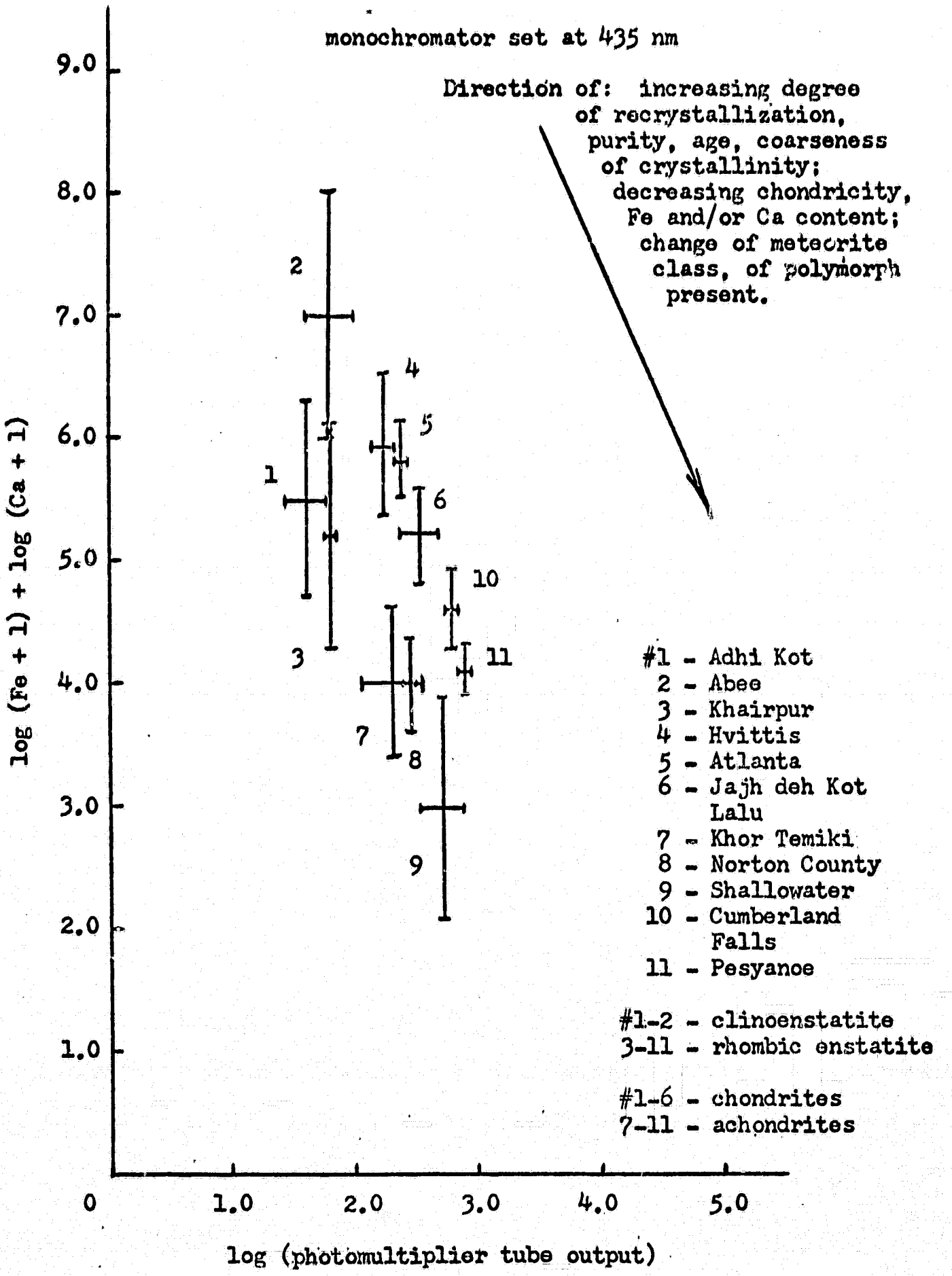

Figure 5. Meteorite Optical Fluorescence Intensities Comparison With Chemical Composition

purity; decreasing total Fe, and decreasing Fe in the pyroxene structure; change in chondricity; age; phase present; degree of recrystallization; increasing coarseness of crystallinity; and increase in luminescence output. The clinoenstatite chondrites, rhombic enstatite chondrites, and rhombic enstatite achondrites are positioned in this fashion. The clinoenstatite chondrite specimens are chondritic, have the highest Fe concentrations in the series, and represent rapid crystallization, smallest grain size, and shortest cosmic ray exposure ages (approximately 10^6 years) in the series. The rhombic enstatite chondrite specimens can be described as poorly chondritic, having a lower Fe concentration, slower crystallization, larger grain size, and longer cosmic ray exposure ages (approximately 2×10^7 years; Mason, 1966) in the series. The rhombic enstatite achondrites are nonchondritic, have the lowest Fe concentrations, slowest crystallization history, usually larger grain size, and the longest cosmic ray exposure ages (approximately 4×10^7 years, a representative value for all of the enstatite achondrites; Urey, 1967) in the series.

As discussed previously, an increase in luminescence output for a particular wavelength region might be expected if one enstatite specimen compared with another specimen had higher purity and lower concentrations of elements such as Fe which would tend to suppress optical fluorescence; higher symmetry and less lattice distortion (i.e., rhombic enstatite compared with clinoenstatite); and a history of slower

crystallization which would result in higher purity material and larger grain size. That the relations are consistent is clearly demonstrated.

Consequently, although previously unexplained, it is not surprising that the luminescence of terrestrial enstatites is lower than that for the higher purity extraterrestrial enstatites represented by these enstatite chondrite and achondrite specimens. Only the orthorhombic polymorph is known to occur in terrestrial rocks.

Multivariate statistical analytical techniques were utilized to process the transformed data so as to evaluate the significance of the relationships that are indicated by the measurements. The test of a hypothesis that the variables X and Y are independent is made using the sample correlation coefficient, r. If this hypothesis is rejected, then there is sufficient reason to believe, at the specified level of significance, that X and Y are correlated.

Tables VII and VIII contain correlation statistics for the individual meteorite specimens; rhombic enstatite and clinoenstatite groupings; and chondrite and achondrite groupings. The corresponding values in the two tables are similar, and the statistics in Table VIII demonstrate the value of using the element to Si ratios to take into account irregularities of the sample surface and variations in thickness. The significance of the correlations improves slightly compared to the corresponding values in Table VII that were not divided by Si.

Table VII. Correlation Statistics Based on Log Transformation of Data

Groups	Variables [a] 1	2	r_{12} [b]	Significance level [c] 0.1%	1%	2%	5%	10%
Abee (chondrite)	Mn	Fe	0.625		*			
	Fe	Ca	0.690		*			
	Mn	$I_{435\ nm}$	-0.752		*			
	Fe	$I_{435\ nm}$	-0.536					*
Adhi Kot (chondrite)	Mn	Cr	0.639				*	
	Fe	Ca	0.433					*
	Fe	Cr	0.860	*				
	Ca	Cr	0.420					*
	λ	I	0.867	*				
	Si	$I_{435\ nm}$	-0.808		*			
	Cr	$I_{435\ nm}$	0.751			*		
	Si	$I_{621\ nm}$	-0.662				*	
Atlanta (chondrite)	λ	I	0.971	*				
	Ca	$I_{435\ nm}$	-0.885				*	
Blithfield (chondrite)	Fe	Si	-0.788					*
Khairpur (chondrite)	Mn	Fe	0.723		*			
	Fe	Cr	0.499					*
	Ca	Si	-0.601		*			
	λ	I	0.947	*				
	Ca	$I_{621\ nm}$	0.655				*	
Jajh deh Kot Lalu (chondrite)	λ	I	0.876	*				

Table VII. Continued

Groups	Variables [a] 1	2	r_{12} [b]	Significance level [c] 0.1%	1%	2%	5%	10%
Hvittis (chondrite)	Ca	Si	0.593					*
	λ	I	0.727			*		
	Ca	$I_{686\ nm}$	-0.948			*		
Bishopville (achondrite)	Ca	Si	0.664		*			
	λ	I	0.854	*				
Cumberland Falls (achondrite)	λ	I	0.952	*				
Khor Temiki (achondrite)	Fe	Ca	-0.634					*
	Ca	Si	0.952	*				
	λ	I	0.927	*				
Pesyanoe (achondrite)	λ	I	0.973	*				
	Mn	$I_{686\ nm}$	-0.886			*		
Shallowater (achondrite)	Ca	Si	0.400					*
	λ	I	0.824	*				
	Ca	$I_{435\ nm}$	0.740	*				
	Si	I_{435}	0.672		*			
	Ca	$I_{686\ nm}$	0.934			*		
Norton County (achondrite)	λ	I	0.969	*				
	Ca	$I_{686\ nm}$	-0.829					*

Table VII. Continued

Groups	Variables [a] 1	2	[b] r_{12}	Significance level [c] 0.1%	1%	2%	5%	10%
All chondrites	Mn	Fe	0.701	*				
	Mn	Ca	0.258				*	
	Mn	Si	-0.532	*				
	Mn	Cr	0.516		*			
	Fe	Si	-0.353		*			
	Fe	Cr	0.633	*				
	Ca	Si	-0.254				*	
	λ	I	0.548	*				
	Si	$I_{621\ nm}$	-0.393					*
	Ca	$I_{686\ nm}$	-0.711		*			
	Si	$I_{686\ nm}$	-0.699		*			
All achondrites	Mn	Fe	0.305				*	
	Mn	Ca	0.424		*			
	Ca	Cr	-0.440			*		
	λ	I	0.579	*				
	Si	$I_{435\ nm}$	0.499		*			
All clinoenstatite	Mn	Fe	0.661	*				
	Mn	Ca	0.681	*				
	Mn	Si	-0.614	*				
	Mn	Cr	0.639				*	
	Fe	Ca	0.734	*				
	Fe	Si	-0.499		*			
	Fe	Cr	0.860	*				
	Ca	Si	-0.616	*				
	Ca	Cr	0.420					*
	λ	I	0.476		*			

Table VII. Continued

Groups	Variables [a] 1	2	[b] r_{12}	Significance level [c] 0.1%	1%	2%	5%	10%
	Cr	$I_{435\ nm}$	0.751			*		
	Si	$I_{621\ nm}$	-0.662				*	
All rhombic enstatite	Mn	Fe	-0.201					*
	Mn	Cr	0.293					*
	Fe	Ca	0.222				*	
	Fe	Cr	0.335				*	
	Ca	Si	0.194				*	
	λ	I	0.446	*				
	Mn	$I_{435\ nm}$	0.311					*
	Ca	$I_{435\ nm}$	-0.564	*				
	Si	$I_{621\ nm}$	-0.457					*
	Fe	$I_{686\ nm}$	-0.394				*	
	Ca	$I_{686\ nm}$	-0.526	*				
	Si	$I_{686\ nm}$	-0.276					*

a. I is the intensity over the visible wavelength range, or at the wavelength specified; λ is the wavelength

b. r is the sample correlation coefficient

c. level at which correlation coefficient is statistically significant

Table VIII. Correlation Statistics Based on Log Transformation of Element:Si Ratio Data

Groups	Variables[a] 1	2	r_{12}[b]	Significance level[c] 0.1%	1%	2%	5%	10%
Abee (chondrite)	Mn	Fe	0.741		*			
	Mn	Ca	0.534				*	
	Fe	Ca	0.783	*				
	Mn	$I_{435\ nm}$	-0.739		*			
	Fe	$I_{435\ nm}$	-0.569					*
Adhi Kot (chondrite)	Mn	Ca	0.517					
	Mn	Cr	0.640				*	
	Fe	Ca	0.445				*	
	Fe	Cr	0.870	*				
	Ca	Cr	0.440					
	λ	I	0.867	*				
	Cr	$I_{435\ nm}$	0.758			*		
Atlanta (chondrite)	λ	I	0.973	*				
	Mn	$I_{435\ nm}$	-0.823					*
Blithfield (chondrite)	none							
Khairpur (chondrite)	Mn	Fe	0.740	*				
	λ	I	0.947	*				
	Ca	I_{621}	0.647				*	
Jajh deh Kot Lalu (chondrite)	λ	I	0.875	*				

Table VIII. Continued

Groups	Variables [a] 1	2	[b] r_{12}	Significance level [c] 0.1%	1%	2%	5%	10%
Hvittis (chondrite)	λ	I	0.727			*		
	Ca	$I_{686\ nm}$	-0.968		*			
Bishopville (achondrite)	Ca	Cr	0.911		*			
	λ	I	0.854	*				
Cumberland Falls (achondrite)	Mn	Cr	0.588					*
	Ca	Cr	0.553					*
	λ	I	0.952	*				
Khor Temiki (achondrite)	Fe	Ca	-0.749			*		
	λ	I	0.927	*				
Pesyanoe (achondrite)	Mn	Fe	0.574					*
	Mn	Ca	0.962	*				
	Fe	Ca	0.613					*
	λ	I	0.973	*				
	Mn	$I_{686\ nm}$	-0.872					*
Shallowater (achondrite)	λ	I	0.824	*				
	Ca	$I_{435\ nm}$	0.577					
Norton County (achondrite)	Mn	Ca	0.772		*			
	λ	I	0.969	*				
	Cr	$I_{435\ nm}$	0.890				*	
	Ca	$I_{686\ nm}$	-0.836					*

Table VIII. Continued

Groups	Variables [a] 1	2	[b] r_{12}	Significance level [c] 0.1%	1%	2%	5%	10%
All chondrites	Mn	Fe	0.431	*				
	Mn	Ca	0.478	*				
	Mn	Cr	0.472		*			
	Fe	Cr	0.583	*				
	λ	I	0.561	*				
	Ca	$I_{686\ nm}$	-0.672		*			
All achondrites	Mn	Fe	0.431		*			
	Mn	Ca	0.472	*				
	Ca	Cr	-0.372				*	
	λ	I	0.579	*				
All clinoenstatite	Mn	Fe	0.782	*				
	Mn	Ca	0.788	*				
	Mn	Cr	0.640				*	
	Fe	Ca	0.820	*				
	Fe	Cr	0.870	*				
	Ca	Cr	0.440					*
	λ	I	0.648	*				
	Cr	$I_{435\ nm}$	0.758		*			
All rhombic enstatite	Mn	Cr	0.312				*	
	λ	I	0.445	*				
	Mn	$I_{435\ nm}$	0.376		*			
	Ca	$I_{435\ nm}$	-0.538	*				
	Fe	$I_{686\ nm}$	-0.315					*
	Ca	$I_{686\ nm}$	-0.377		*			

Table VIII. Continued

a. I is the intensity over the visible wavelength range, or at the wavelength specified; λ is the wavelength

b. r is the sample correlation coefficient

c. level at which correlation coefficient is significant

Highly significant positive correlations are evident for Mn and Fe, Fe and Ca, Fe and Cr, Ca and Cr, Mn and Ca, and Mn and Cr. This is consistent with the crystal chemical relations discussed previously for the pyroxene structure. Where Mn, Fe and Ca are present in relatively large amounts, such as in the clinoenstatite specimens or in the chondrite specimen class, compared with the high purity achondrite members, there are highly significant negative correlations with Si, as large concentrations of impurities tend to depress the Si count rate from the pyroxene phase.

Within an individual meteorite specimen, the variation in intensity and/or wavelength of optical fluorescence can be explained by the corresponding variation in chemical composition. Higher concentrations of Fe and Ca tend to suppress fluorescence. Because of structural and other differences, such as the history of the specimen, a given trace element pattern will not quantitatively produce the same effect in different meteorite specimens. The concentration of Mn may be too low, for example, to exert an obvious enhancement of long wavelength visible luminescence. Manganese-Fe and Mn-Ca are positively correlated with a high degree of statistical significance, and since both Fe and Ca effectively reduce the optical fluorescence emission in both the blue and red region of the visible spectrum, it is to be expected that the influence of Mn would be minor. However, in the Abee specimen, Mn is present in a relatively high concentration for the meteorite specimens and the influence of Mn in depressing the short wavelength host emission band is

shown to be highly significant.

Definite relations are present for a particular specimen, wavelength-intensity response, and meteorite class. The high purity of the achondrites favors a higher intensity of response in the visible range than is the case with the chondrites. Homogeneous distribution of trace elements and low concentration of impurities is reflected in the highly significant positive correlations for intensity and wavelength for all of the achondrite specimens. For all individual specimens (except the Abee meteorite, where the blue luminescence overrides any red contribution), for clinoenstatite, for rhombic enstatite, for chondrites, and for achondrites there are significant positive correlations for intensity and wavelength (i.e., the emission in the red region of the visible spectrum is greater than that for the blue region).

To convert the microprobe data in Table III to concentrations, a reliable chemical analysis for the enstatite from the Khairpur meteorite is included at this point (Mason, 1966): SiO_2, 58.92 weight %; Al_2O_3, 1.18%; MgO, 39.62%; CaO, 0.32%; TiO_2, 0.00%; MnO, 0.02%; FeO, 0.04%; from neutron activation analysis, Mn: 66 ppm, Cr: 5 ppm. Other analyses for the meteorites used in this investigation are reported by Wiik (1956), Morimoto, et al., (1960), and Keil (1967b). The counts per second above background on standards used for compiling Table III (for a 1 μ diameter beam spot, 30 keV, and adjusted count rate to 0.03 μ amperes) are as follows: $CaWO_4$, 2,238; Fe, 39,126; Si, 32,277; Mn, 39,288; and Cr, 31,653. The X-ray intensity from a given element compared

to the standard is a straight line function for these specimen values where all impurities (Mn, Fe, Ca and Cr) are present in the pyroxene in an amount less than 15 weight %. For example, the Mn metal standard signal was 39,288 counts/sec. which represents 100% Mn or 10^6 ppm of Mn. Thus, 4 counts/sec. above background would represent 0.01% Mn or 100 ppm, or one count/sec. above background for each 25 ppm of Mn. This compares favorably with the reliable chemical analysis value for the Khairpur meteorite enstatite of 66 ppm Mn and the microprobe geometric mean value listed in Table IV of 2 counts/sec. which would be equivalent to 50 ppm on the basis of the adjusted metal standard value. The arithmetic mean and standard deviation can be improved by applying a counting correction, $s_{mean} = \frac{s}{\sqrt{N}}$, where s is the standard deviation of the arithmetic mean (equals 2 counts/sec., in this case) and N is the number of readings for that position and element (equals 5, in this case) (White, 1967). Therefore the adjusted value is 2 ± 1 counts/sec. or 50 ± 25 ppm for Mn. Good agreement is also obtained for the Ca, Fe and Cr concentrations for this method compared with the chemical analysis values for the Khairpur.

For homogeneous samples and standards, count rates of the order of 1000 per second have a standard deviation of $\pm$ 2% and represent measurements of high precision. For typical low count rates for Mn and Cr the standard deviation is less than $\pm$ 7% for five replications for an element at a position on the pyroxene specimen. This variance is strongly influenced by the geochemical variance, and by sampling errors, sample

reduction errors, and analytical errors.

The accuracy of the method can be evaluated by comparing the true mean and the mean of the measured values. The true value will depend on the degree to which the data for the grains represent the subsample and the degree to which these data represent the pyroxene in the entire meteorite. To a high degree, this is confirmed by comparing the trends indicated by the various oscillographic displays, representing much larger sampling areas. The microprobe trace values agree within 25% of the trace values quoted for the chemical trace element analysis; the mean microprobe trace element detection level is of the order of 50 ppm for a particular trace element. Thus, the measurements are sufficiently precise and accurate for the purpose of comparing optical fluorescence spectral data and chemical composition for specimens of microscopic size.

B. Discussion of Oscillographs

Photographs of the 200 x 200 μ area displays (corresponding to approximately 285X magnification) for each specimen are presented in Figures 6 - 18 for cathodoluminescence and conventional X-ray oscillographic displays.

Depending on the meteorite specimen, some of the luminescence photographs are more revealing than others concerning obvious correlations with the element distribution indicated by the X-ray detector displays. This variation is mirrored and confirmed in the correlation statistics for the individual specimen. In some of the photographs, the

luminescence display enhances the outlines of cracks, flaws and grain boundaries, or may primarily show as a color and intensity gradation from the outer to the inner portion of the grain. This difference may be caused by reactions between the surface layers and the atmosphere or environment during heating and cooling, coupled with slow rates of diffusion of reaction products into interiors of the crystals.

Examples of several of the effects are displayed for the chondrites in Figures 6 - 12 and for the achondrites in Figures 13 - 18, such as the quenching effect of Fe and Ca on luminescent emission, Mn as an activator, and exsolution lamellae. Previous attempts to record visible cathodoluminescence (Korda, et al., 1967; Saller, 1967) did not utilize wavelength discrimination, such as provided by the microprobe attachments described in this work, and consequently the capability for detailed analysis and correlation studies had been absent.

If necessary, the wavelength of the visual fluorescence colors can be determined by using the Munsell (1929) color system. For example, a purple luminescence color for a meteorite observed under electron excitation might be designated 5.0 RP 5/6; the notation 5.0 RP 5/6 indicates a Munsell hue of 5.0 red-purple, a Munsell value of 5/ (which is equally separated from black and white), and a Munsell chroma of /6 (which means six steps away from gray (N5/) of the same Munsell value. The Munsell terms can be identified as follows: value indicates how colors vary in lightness, and chroma indicates how colors vary in saturation.

However, although color perception can be associated with scales of constant hue, saturation and lightness, the chemical variability and the associated color variability for the specimens limit the application and usefulness of this system. The color patterns for the various specimens clearly demonstrate why there was confusion in the literature when interpretations of fluorescence colors from bulk materials were attempted. With an analytical procedure and capability of obtaining point analyses, such as presented in the preceding section, and with the oscillographic displays, presented in this section, meaningful explanations have been made.

Oscillographic displays for the Adhi Kot meteorite are shown in Figure 6. From these photographs, minor inclusions can be identified and delineated. The quenching effect of both Fe and Ca is demonstrated by comparing the cation displays with the series of optical fluorescence photographs. For example, in the lower right corner of Figure 6b a large Fe concentration is indicated; the outline of this feature appears on all of the optical fluorescence photographs as a black area since the color emission is suppressed. Similarly, in Figure 6c a large Ca concentration is indicated in the far right-center of the photograph. In each fluorescence display, this area remains dark. The Mn display is useful to demonstrate that Mn quenches the blue response (Figure 6h). For example, there is a Mn concentration in the upper left portion of the

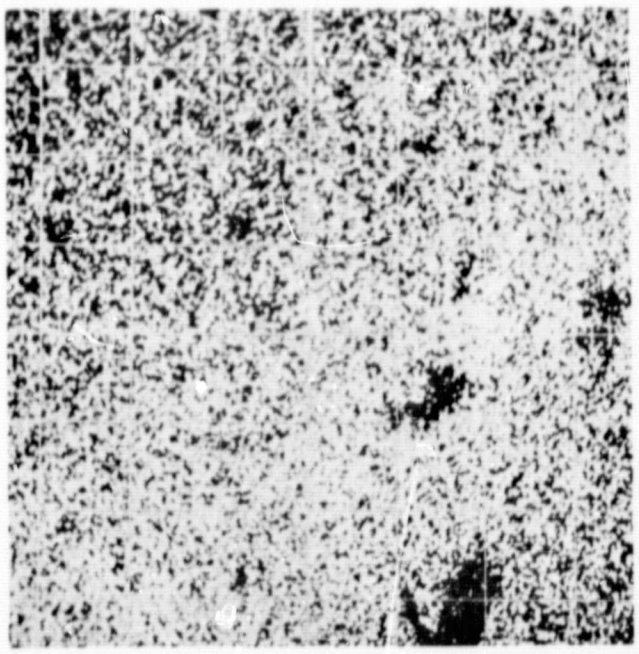

a. Si K_{α}

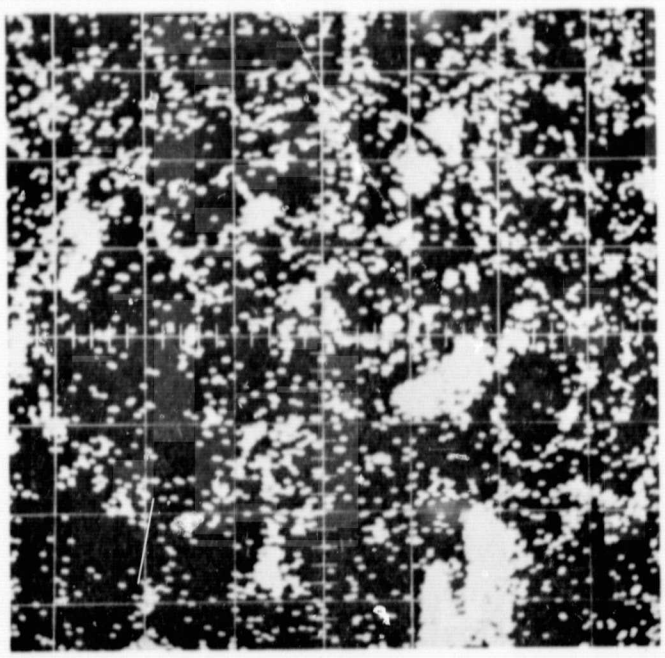

b. Fe K_{α}

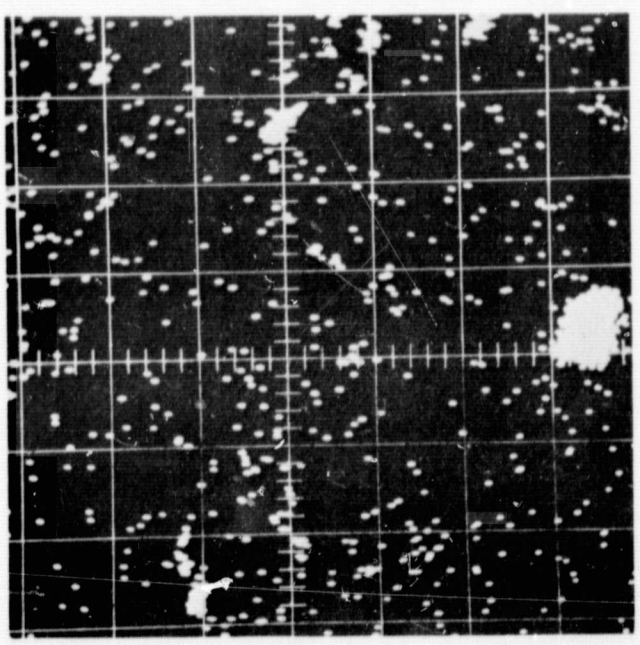

c. Ca K_{α}

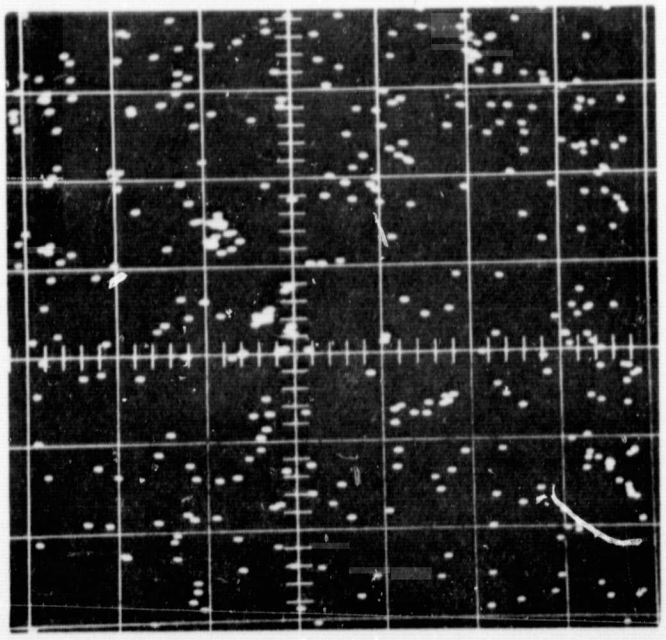

d. Mn K_{α}

Figure 6. Adhi Kot Chondrite Oscillographic Displays

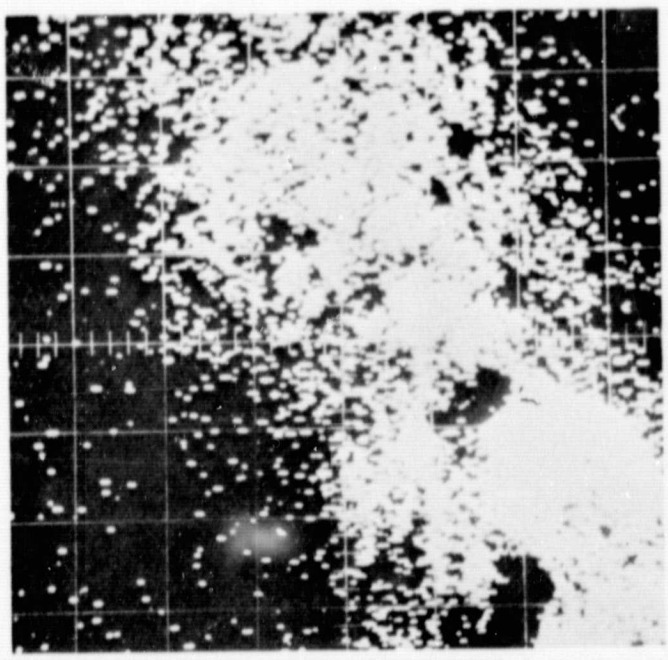

e. 435 nm

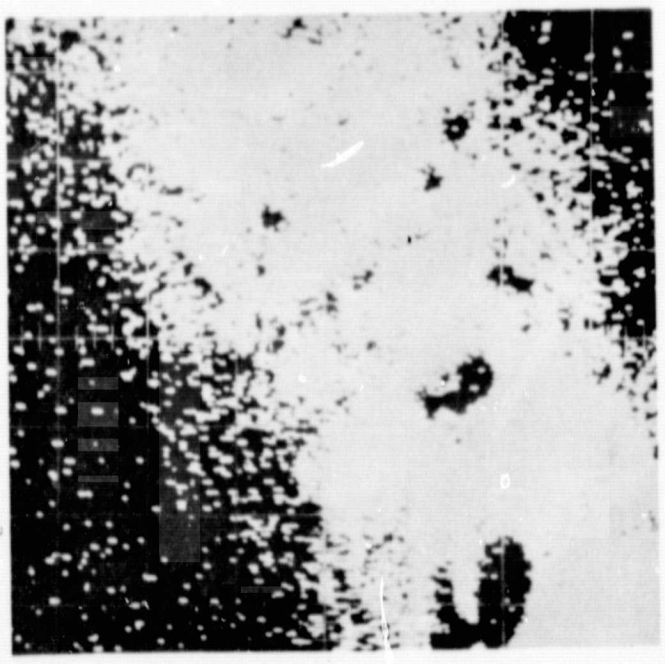

f. 534 nm

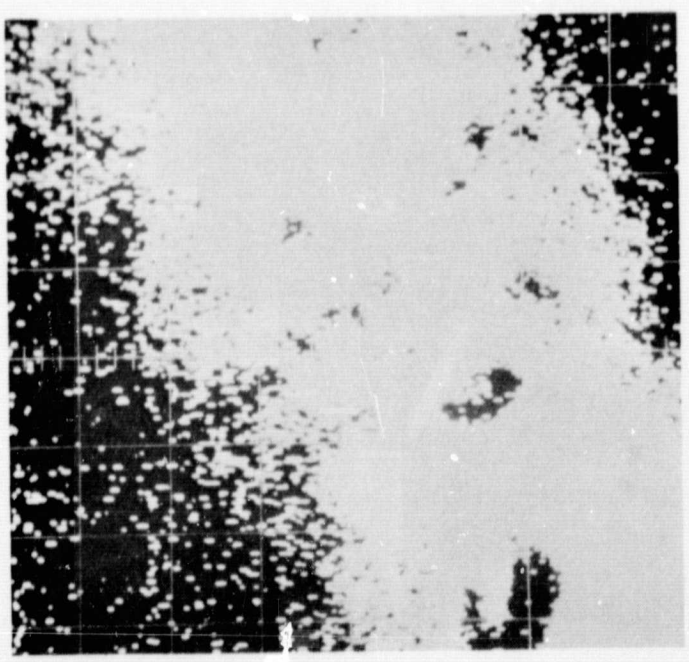

g. 621 nm

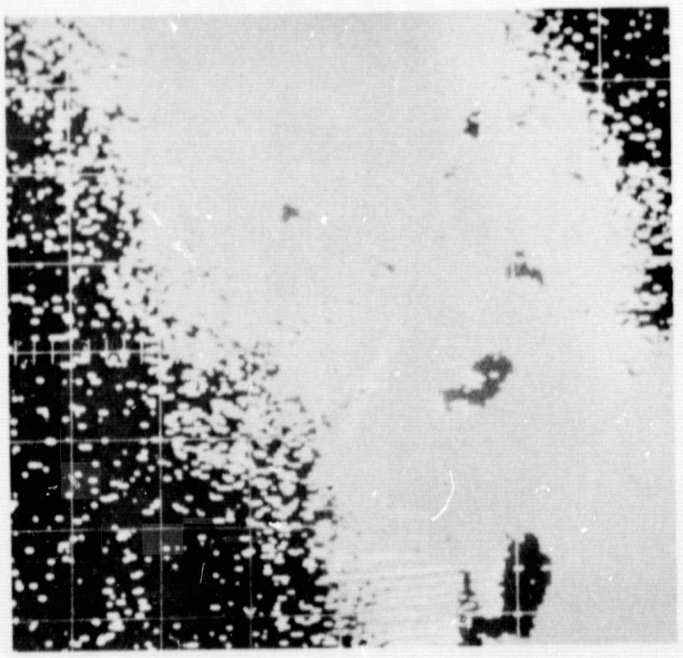

h. 664 nm

Figure 6. Adhi Kot Chondrite Oscillographic Displays

photograph that exhibits the corresponding influence on the color displays. The blue luminescence overrides the red contribution and the specimen appears to luminesce blue.

Figure 7 pictures a specimen obtained from the Abee chondrite. Again the quenching influence of Fe, Ca and/or Mn in attenuating the short wavelength visible emission is clearly demonstrated for a large number of positions on the optical fluorescence photographs. The dark areas on Figures 7e and 7f can each be explained in terms of the presence of high Fe, Ca or Mn concentrations. This fine-grained specimen luminesces blue in areas of lower impurity concentrations.

In Figure 8, special attention is devoted to the Ca distribution and its effect on the various luminescence photographs for the Blithfield chondrite specimen. The 621 nm display represents areas where the higher-Ca pyroxene and the lower-Ca pyroxene areas are contrasted by the lack of luminescent response for the higher-Ca areas. The areas of lowest Ca rim the grain and clearly luminesce red. These luminescent rims can also be visually observed, and they surround areas that luminesce blue. Subsolidus exsolution of a more calcic pyroxene is probably responsible for the heterogeneities in the Ca patterns. In the slowly cooled pyroxenes, a high degree of ordering is possible, and in such crystals unmixing of the Ca-rich phase generally occurs. A more rapid cooling situation may prevent exsolution of the Ca-rich phase.

Careful examination of Figure 9 reveals a considerable

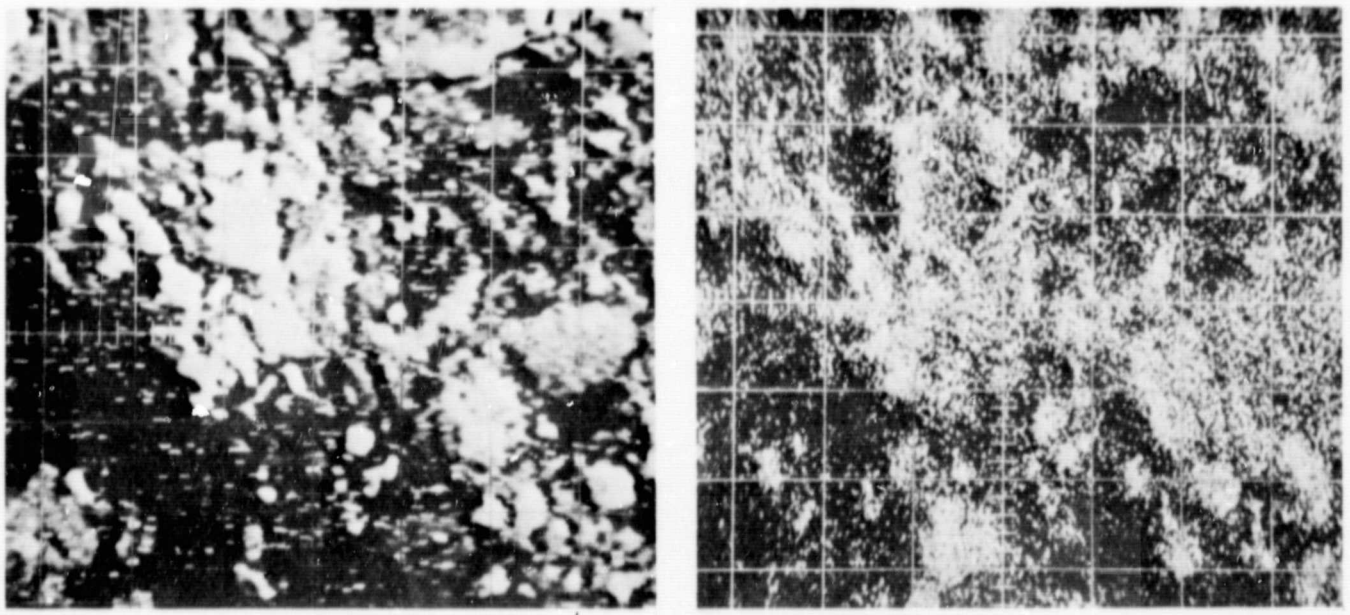

a. E. B. S.
(Electron Backscatter)

b. Fe K_{α}

c. Si K_{α}

d. Mn K_{α}

Figure 7. Abee Chondrite Oscillographic Displays

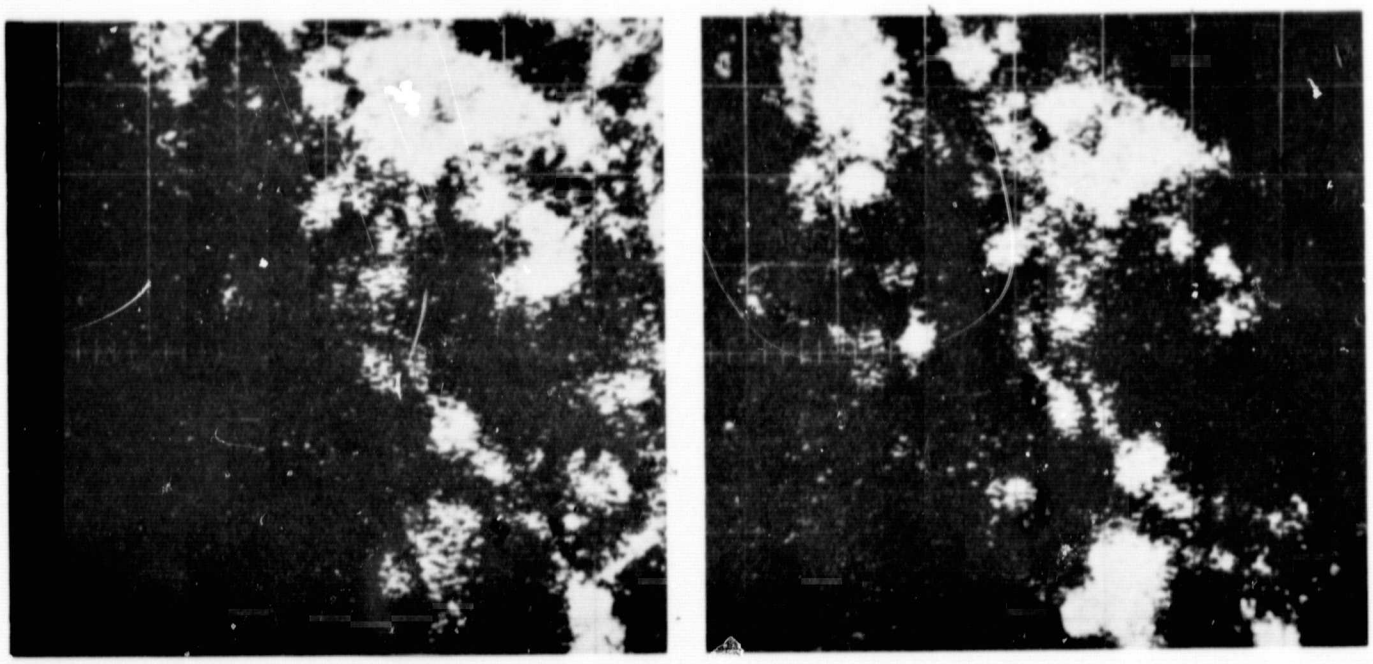

e. 435 nm f. 492 nm

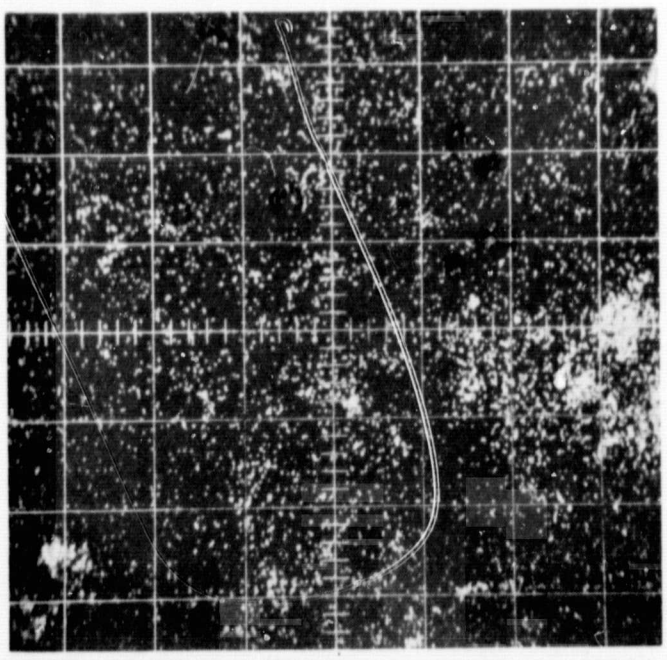

g. Ca K_{α}

Figure 7. Abee Chondrite Oscillographic Displays

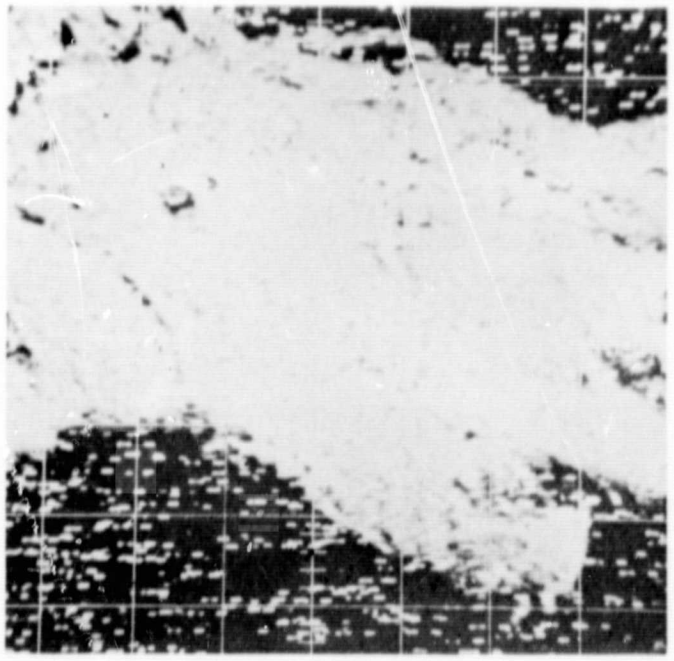

a. E. B. S.

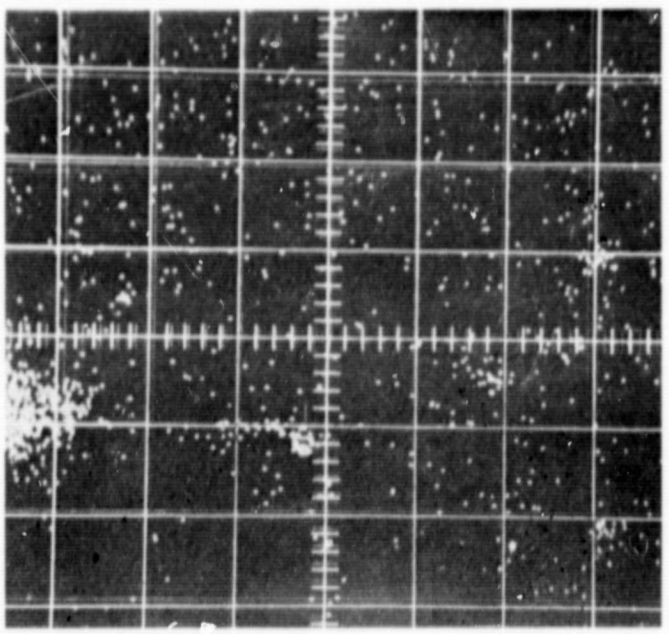

b. Fe K_{α}

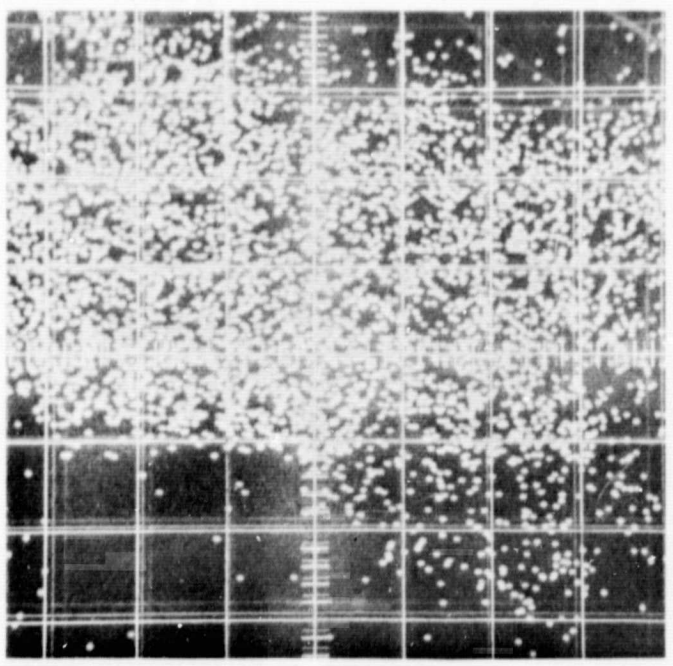

c. Ca K_{α}

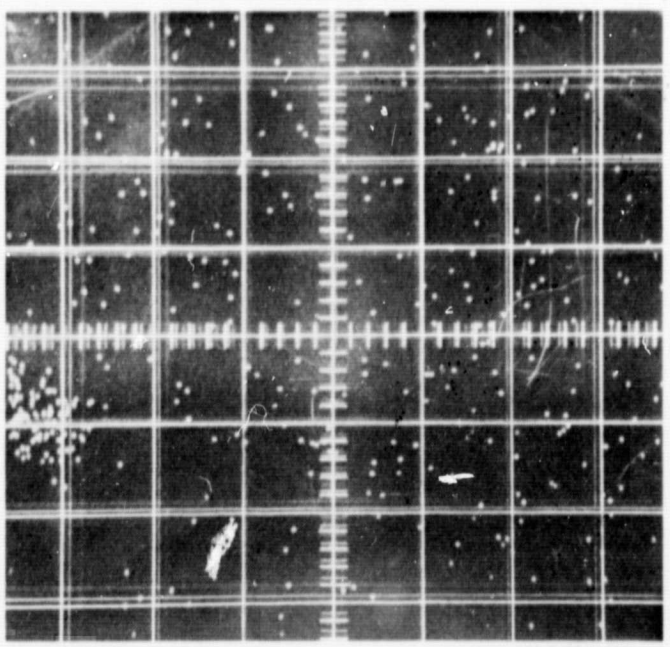

d. Mn K_{α}

Figure 8. Blithfield Chondrite Oscillographic Displays

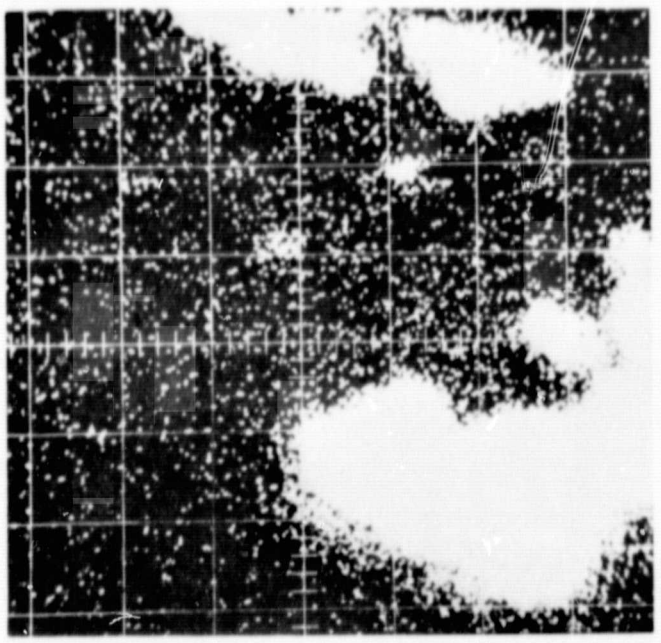

e. 435 nm

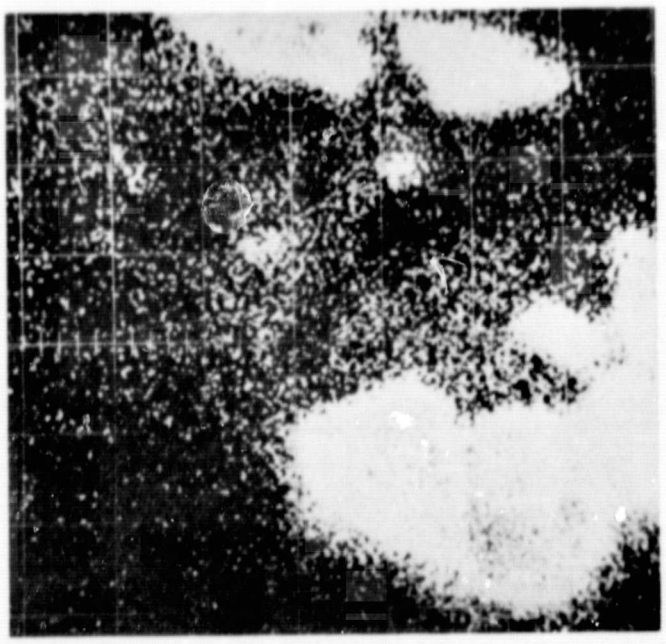

f. 491 nm

g. 534 nm

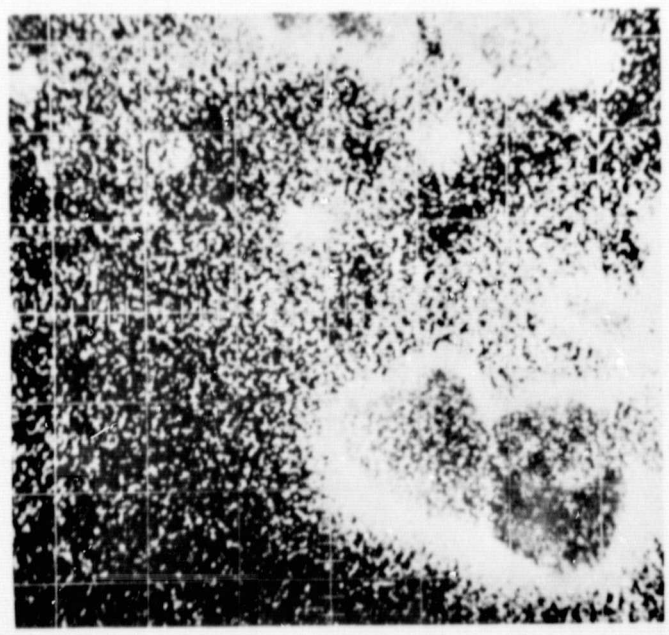

h. 621 nm

Figure 8. Blithfield Chondrite Oscillographic Displays

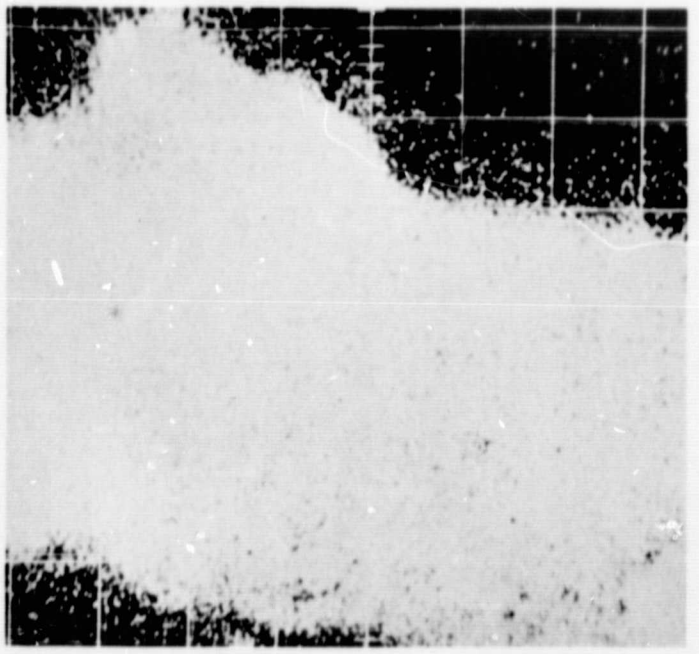

1. Si K_{α}

Figure 8. Blithfield Chondrite Oscillographic Displays

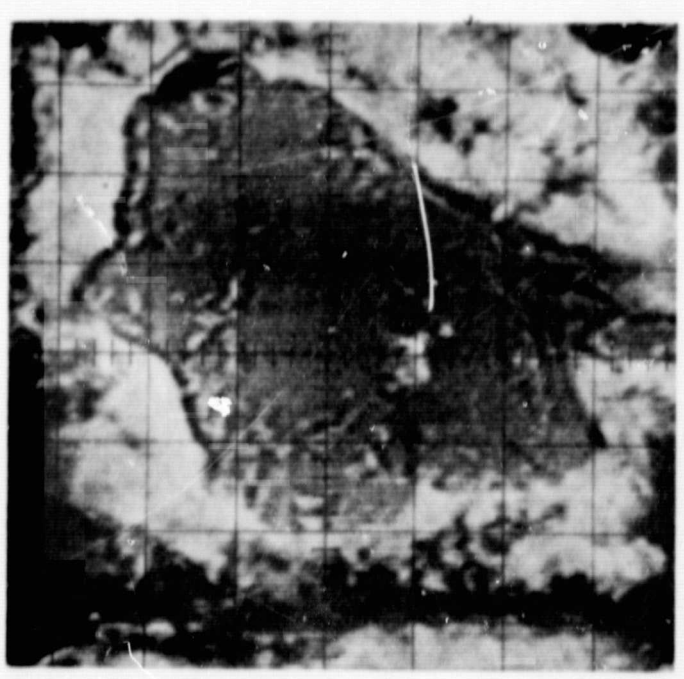

a. Specimen Current Image

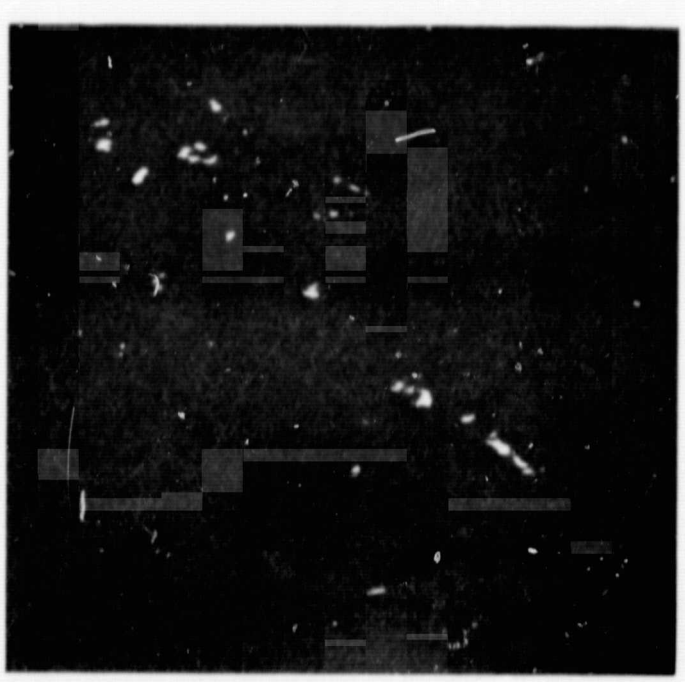

b. Fe K_{α}

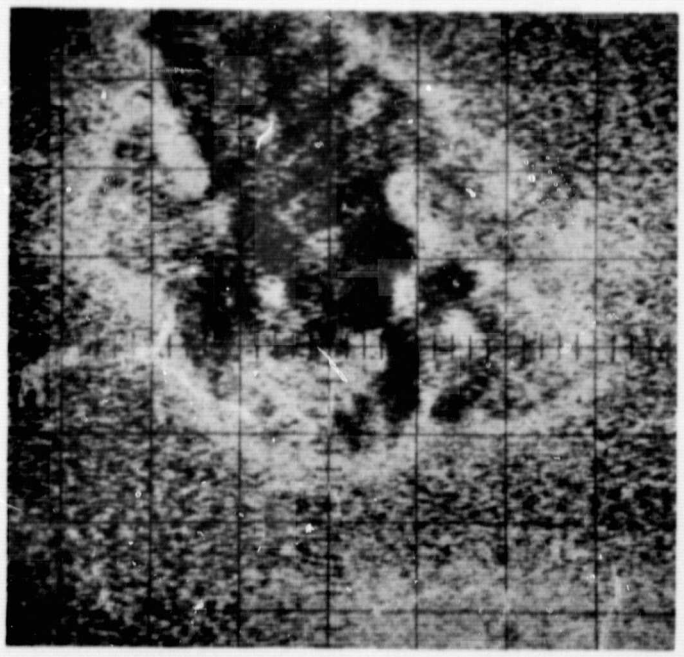

c. 700 nm

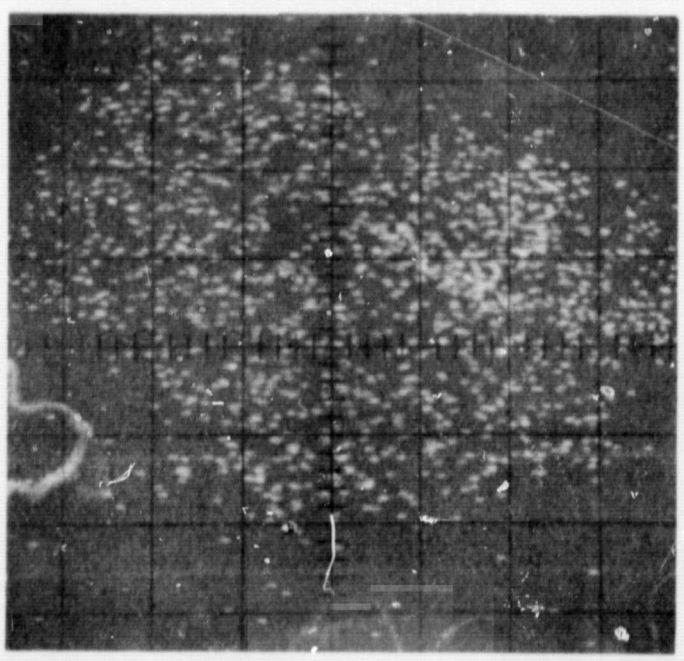

d. Ca K_{α}

Figure 9. Khairpur Chondrite Oscillographic Displays

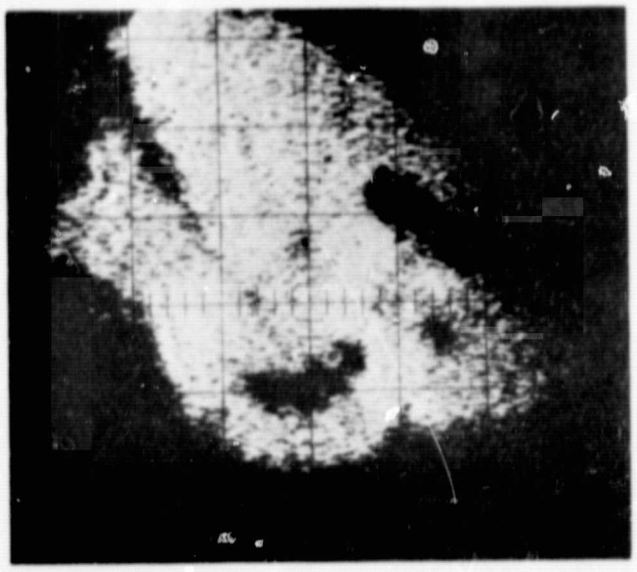

e. 409 nm

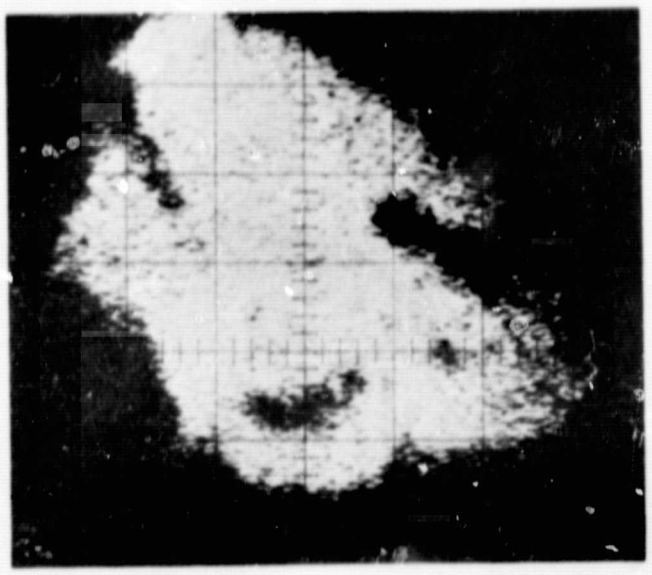

f. 491 nm

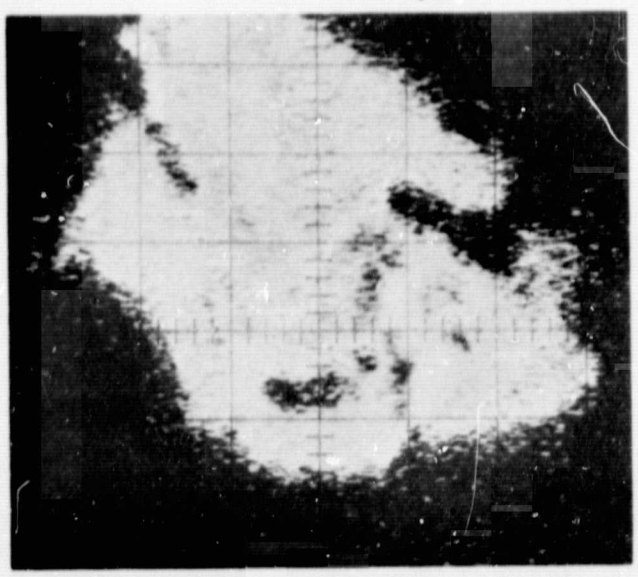

g. 578 nm

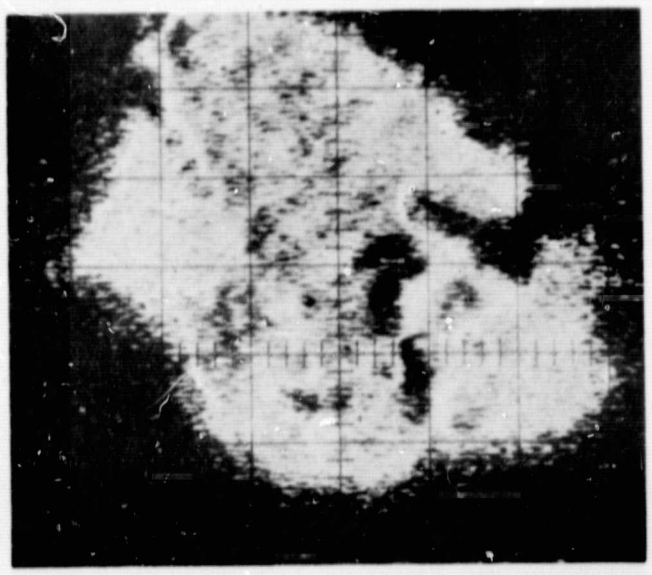

h. 686 nm

Figure 9. Khairpur Chondrite Oscillographic Displays

amount of information, and permits an explanation of the apparent blue and red visual luminescence. In Figure 9a, the specimen current image outlines the specimen grain obtained from the Khairpur enstatite chondrite meteorite. Figure 9f indicates the blue, 491 nm, color distribution for the same grain. Figure 9h represents the 686 nm display, and emphasizes exsolution lamellae which would be difficult to detect for this specimen using other methods. In this sample, the higher-Ca pyroxene luminesces in the blue region of the spectrum, but not in the red. The low-Ca pyroxene is activated by Mn. The rhombic enstatite (low-Ca) and Ca-rich pyroxene solid solution are sharply contrasted, and establish a frozen in record of the temperature (Atlas, 1952; Boyd, et al., 1964a, 1964b) of equilibrium crystallization (in this case, below 700 °C).

The ratio between the length and thickness of the exsolution lamellae may be useful as an index of elongation to provide a rough index to the intensity of recrystallization. For the Khairpur chondrite in Figure 9, this ratio is approximately 10:1 and, for a pyroxene, would be indicative of a dynamothermal origin or strong dynamic metamorphism (Tyrrell, 1958). The least pressure direction would run parallel to the banding. The cleavage planes are parallel to the banding ((110) cleavage for pyroxene), i.e., perpendicular to the direction of greatest pressure. It is of interest to comment that the Fe concentration trend also parallels the cleavage.

A similar effect of Ca depressing the optical fluorescence output is shown in Figure 10 for the Hvittis chondrite. An area of high Mn concentration is indicated in the left-central region of the Mn K_{α} photograph. Again, the high Mn region suppresses the blue luminescence as indicated by the corresponding dark area for the 415 nm display and enhances the red luminescence as indicated by the corresponding white area of the 700 nm display. Within the specimen a rim caused by a higher intensity fluorescence signal for the optical fluorescence displays is apparent, and this is associated with the corresponding lower impurity concentrations for these regions. The blue luminescence overrides the red contribution, and the specimen appears to luminesce blue to a viewer.

Figure 11 presents displays for a number of various size grains from the Atlanta chondrite. A series of optical fluorescence displays for different wavelength settings of the monochromator-photomultiplier detection unit demonstrates the discrimination capability of the system, as indicated by the various color patterns and absence of any color pattern for the 425 nm setting. The specimen luminescence appears as blue and red; various hues of purple are possible when the colors due to the host and activator bands mix. The chemical variability within grains is responsible for the variation and pattern of optical fluorescence emission. In general, the central portions of a grain luminesce blue, and the outer portions luminesce red; the luminescing regions tend

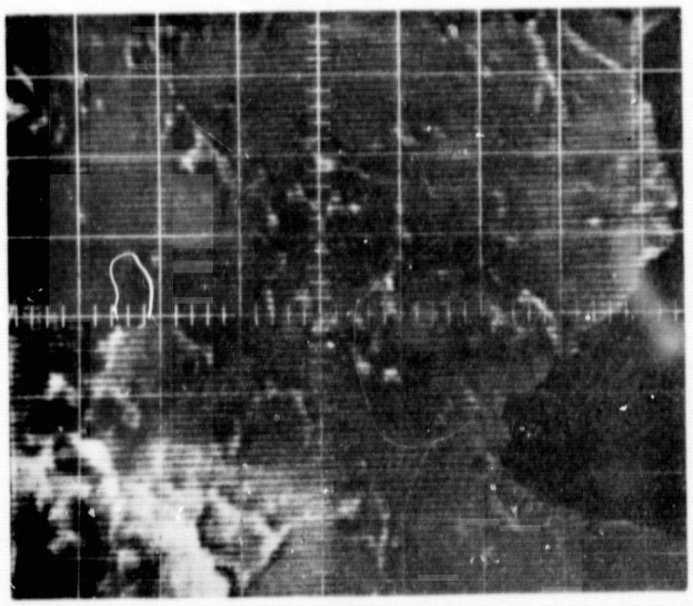

a. Specimen Current Image

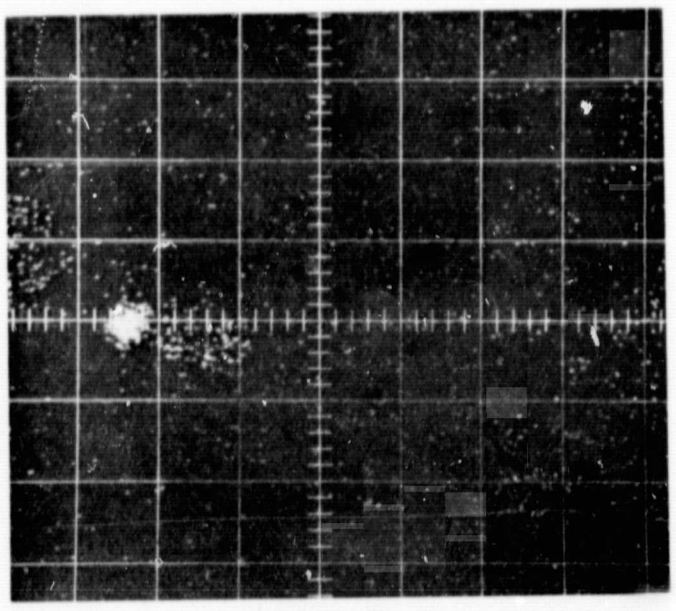

b. Mn K_{α}

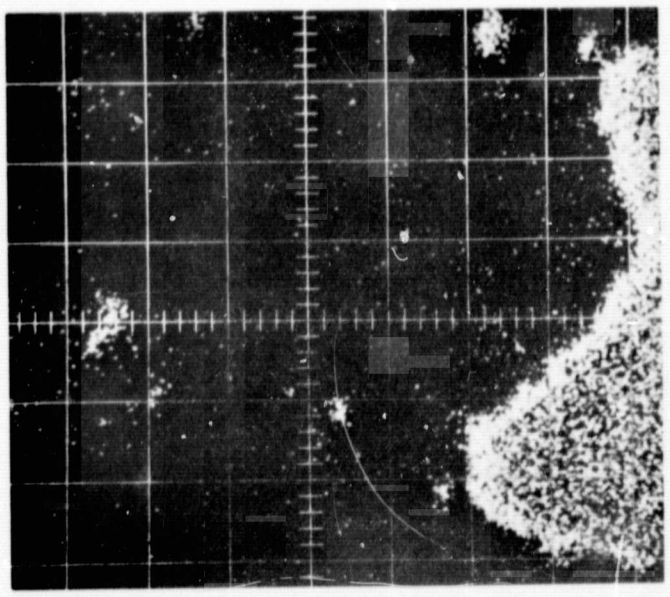

c. Fe K_{α}

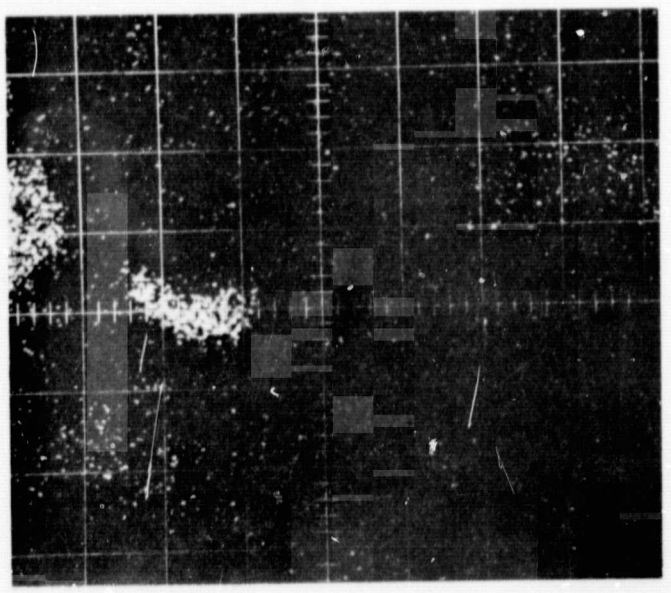

d. Ca K_{α}

Figure 10. Hvittis Chondrite Oscillographic Displays

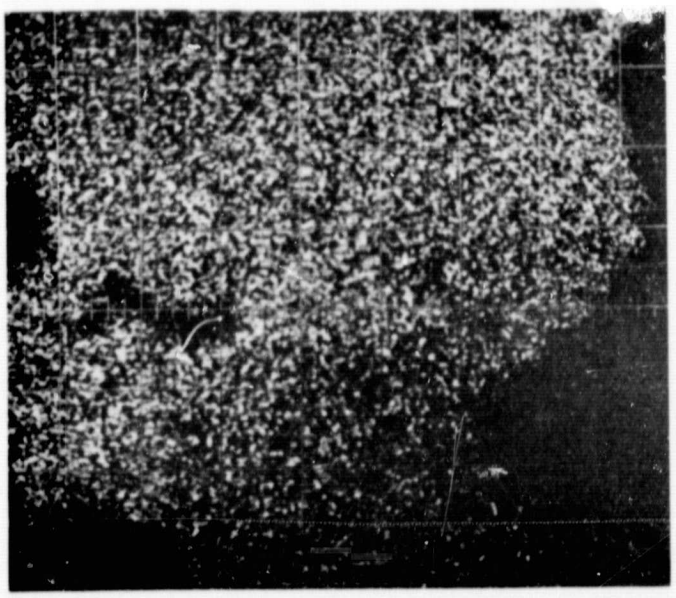

e. Si K_{α}

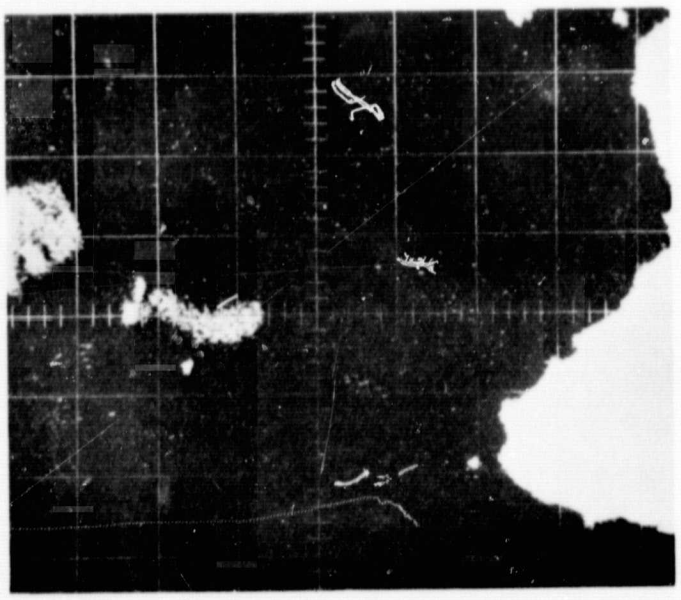

f. E. B. S.

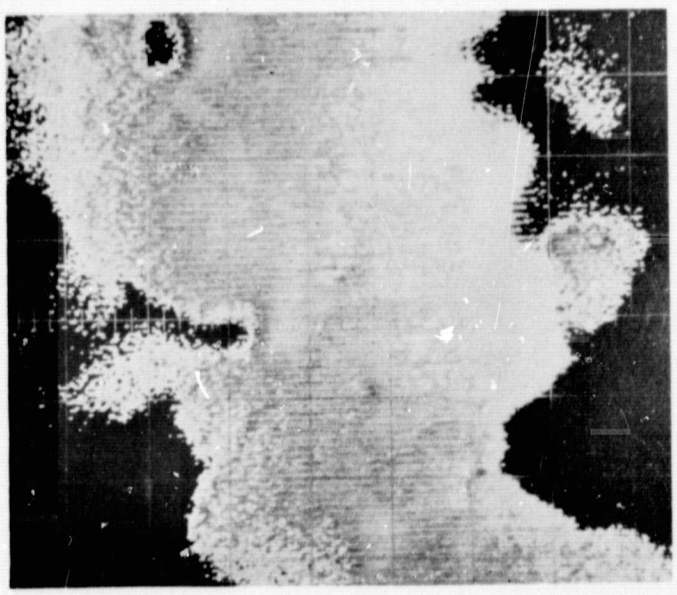

g. 415 nm

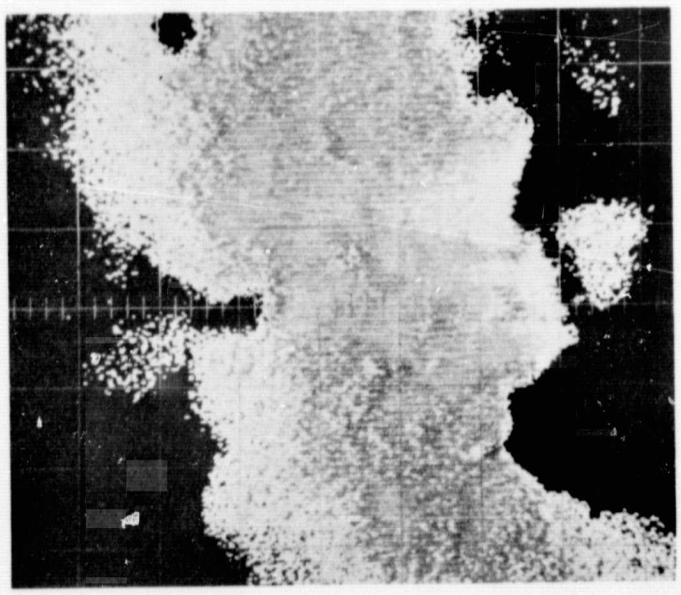

h. 435 nm

Figure 10. Hvittis Chondrite Oscillographic Displays

i. 475 nm

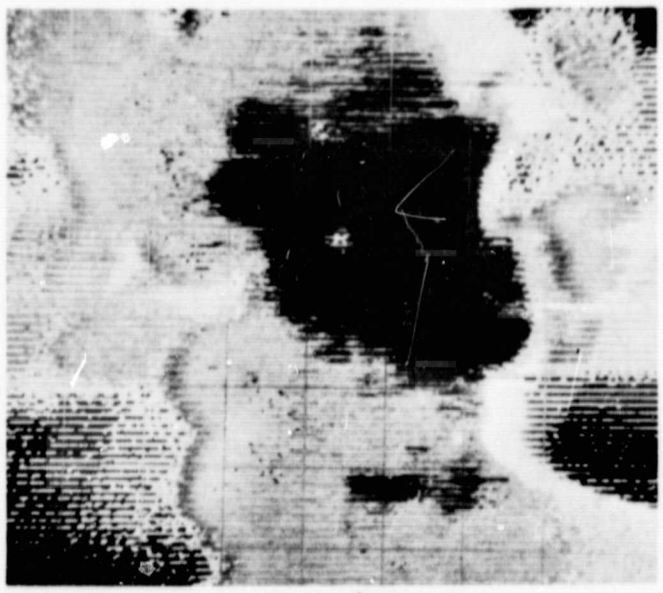

j. 600 nm

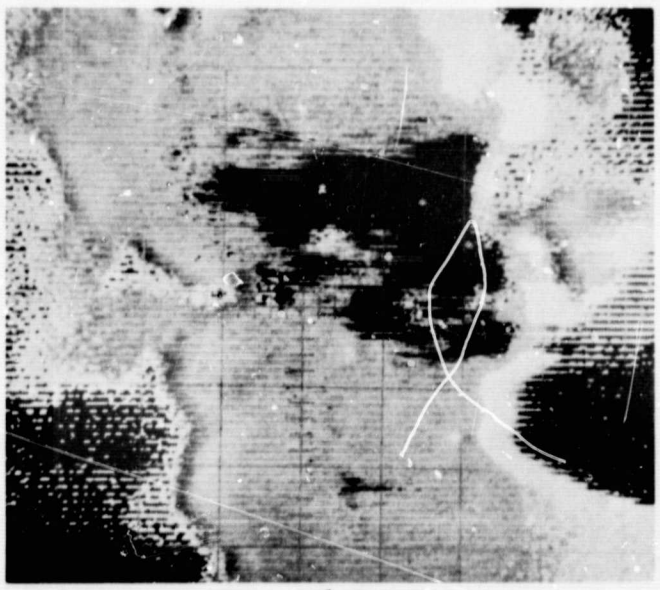

k. 650 nm

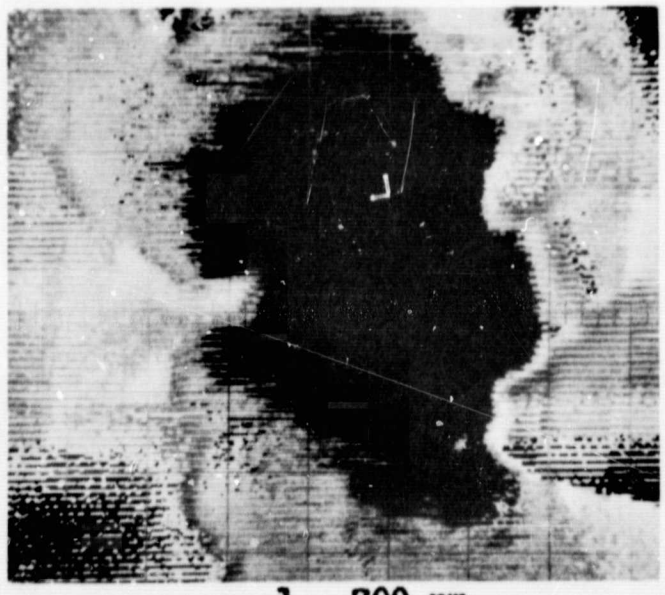

l. 700 nm

Figure 10. Hvittis Chondrite Oscillographic Displays

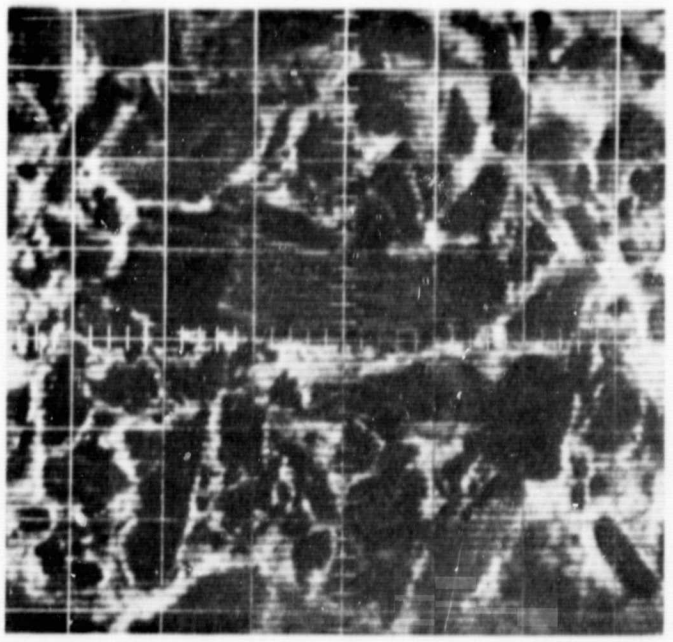

a. Specimen Current Image

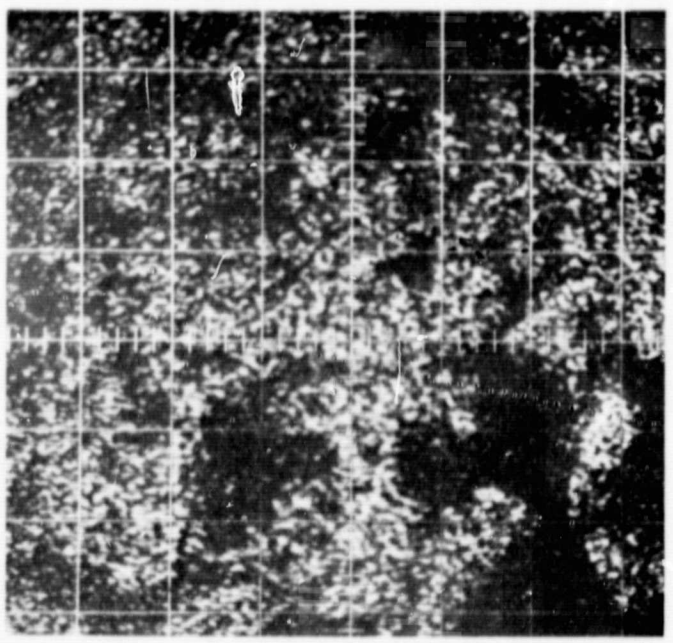

b. Si K_{α}

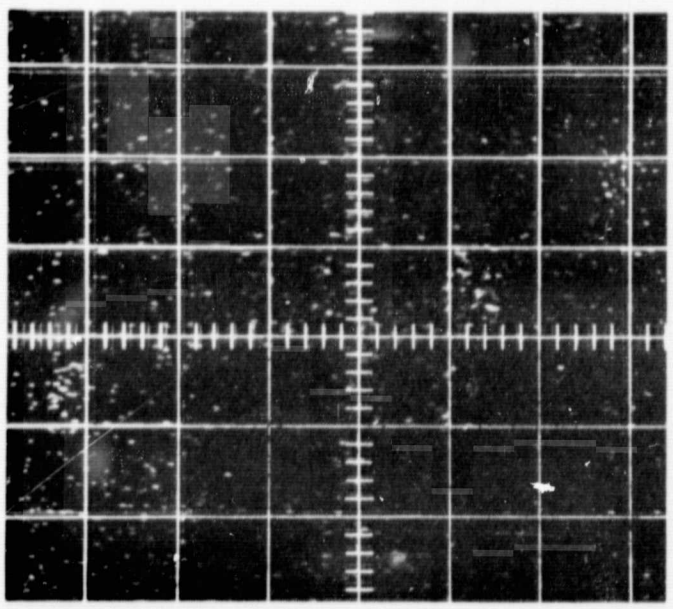

c. Ca K_{α}

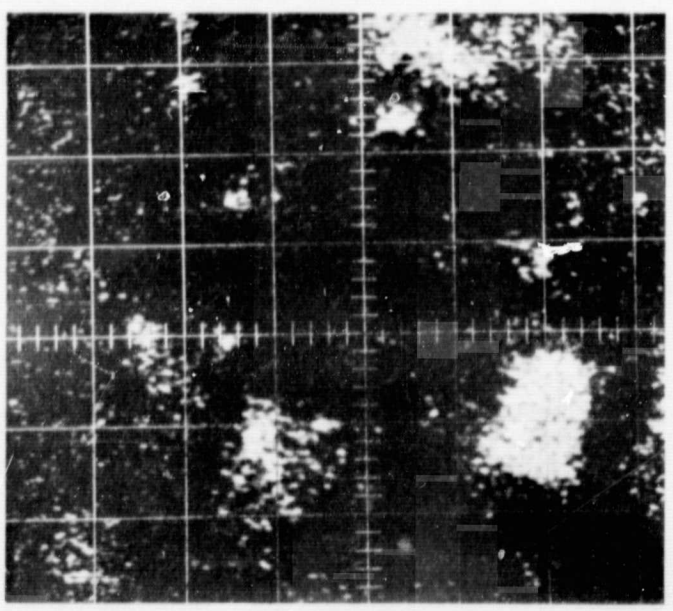

d. Fe K_{α}

Figure 11. Atlanta Chondrite Oscillographic Displays

e. 410 nm

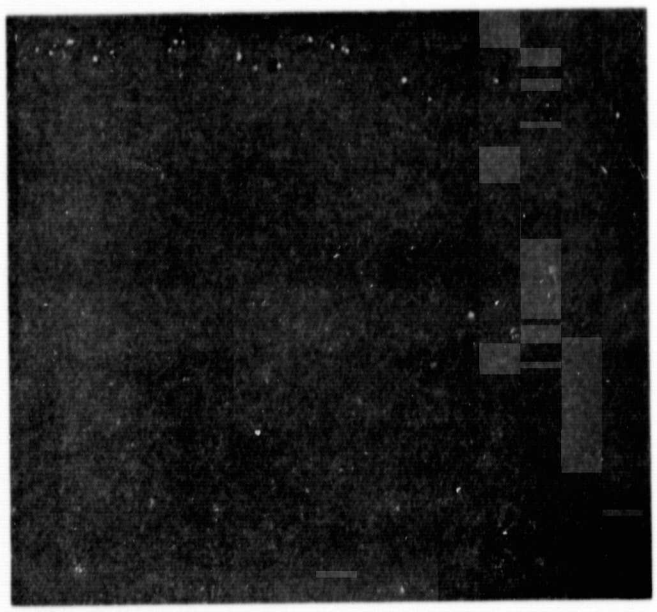

f. 425 nm

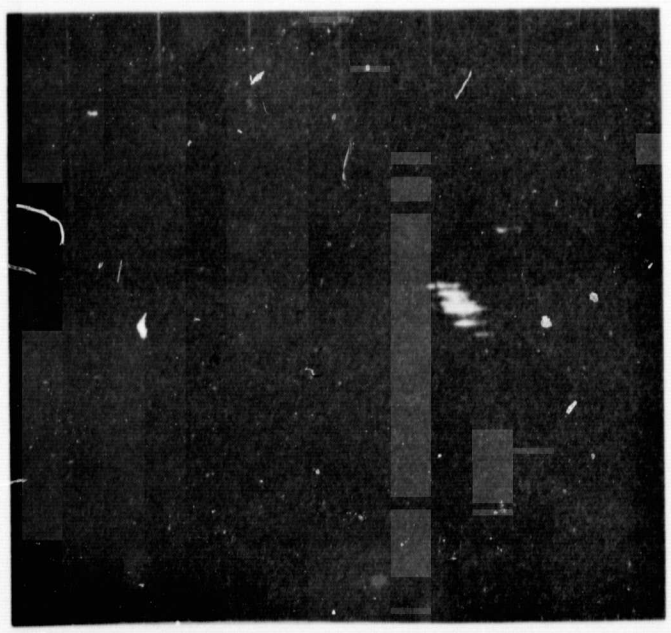

g. 475 nm

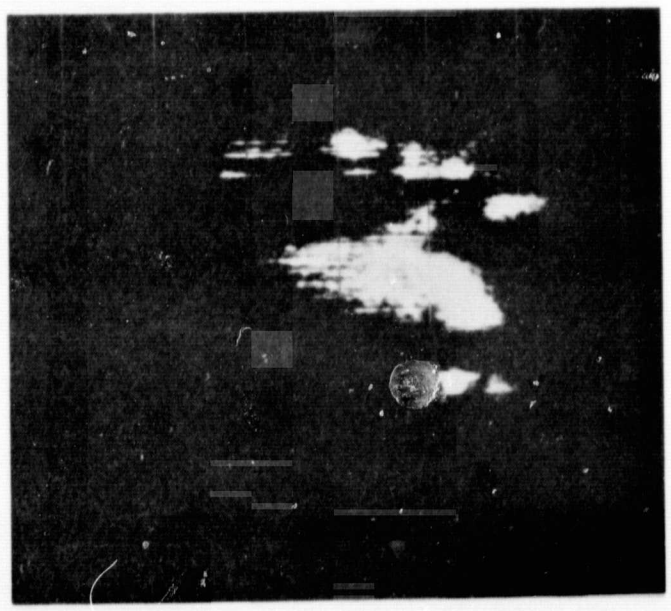

h. 500 nm

Figure 11. Atlanta Chondrite Oscillographic Displays

i. E. B. S.

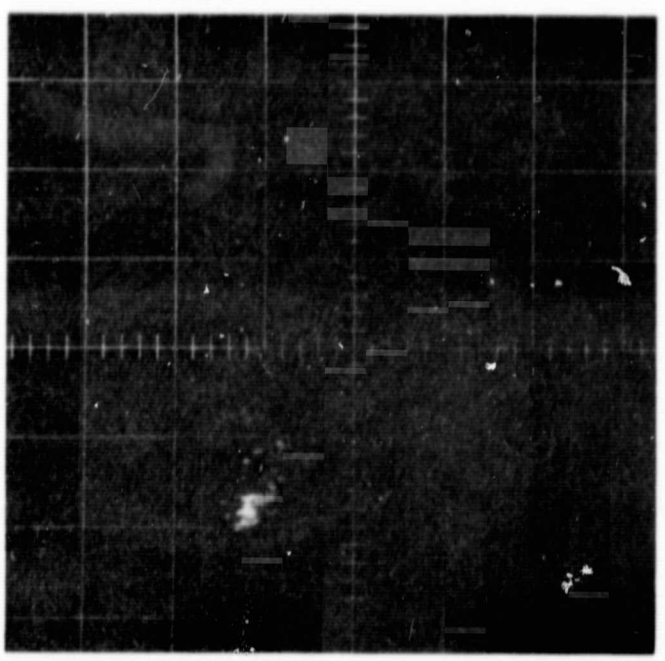

j. Mn K_{α}

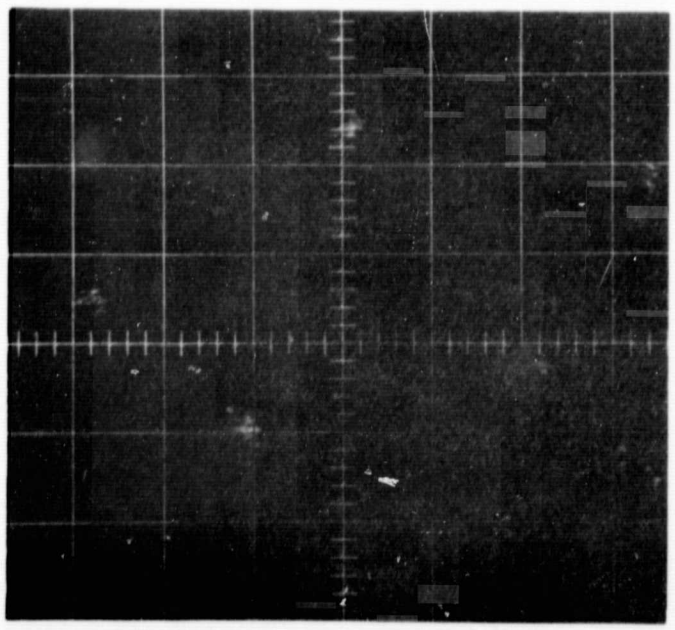

k. Cr K

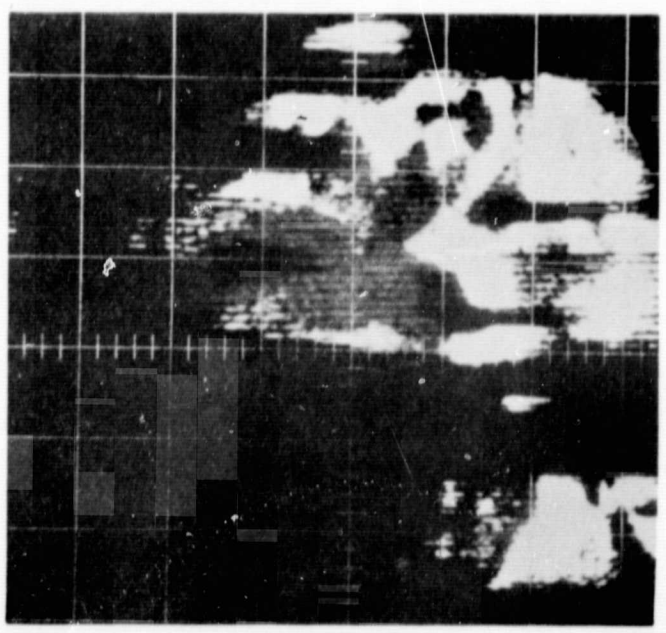

l. 700 mm

Figure 11. Atlanta Chondrite Oscillographic Displays

to appear elongated and parallel to the (110) cleavage.

The Jajh deh Kot Lalu chondrite luminesces a dark blue. From Figure 12, the uniform distribution of impurities (Fe and Ca) appears to be associated with the predominance of the blue fluorescence band when the Fe and Ca concentrations are not too high. No additional obvious associations are indicated.

The Bishopville achondrite in Figure 13 begins the photographic series for the achondrite specimens. The same general associations of the influence of the impurities present on the corresponding optical fluorescence pattern are present for the achondrites. The influence of Ca in depressing the fluorescent response is more apparent than are correlations for the other cation displays. Both the Ca pattern and the associated color patterns tend to parallel the (110) cleavage. An example of this is demonstrated by a Ca concentration that is identified from the top-center of the Ca K_α photograph and trending for a distance of approximately 35 μ toward the lower-right corner of the photograph. However, the pattern associations are not as well developed as for some of the specimens already discussed. The visual fluorescence is blue and red, as determined primarily by the presence and concentrations of Ca.

In Figure 14, the optical fluorescence patterns tend to parallel the (110) cleavage, as in other specimens. The visual color patterns seen under conditions of direct electron excitation are red luminescence with occasional blue areas;

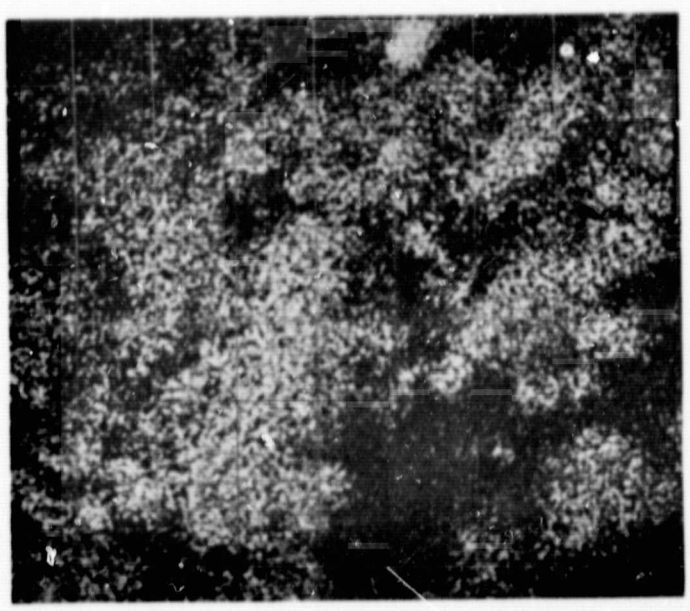

a. Si K_{α}

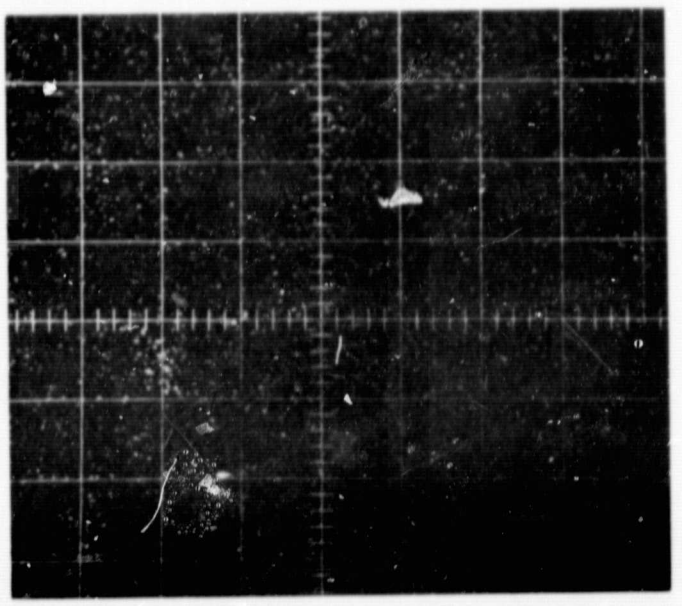

b. Ca K_{α}

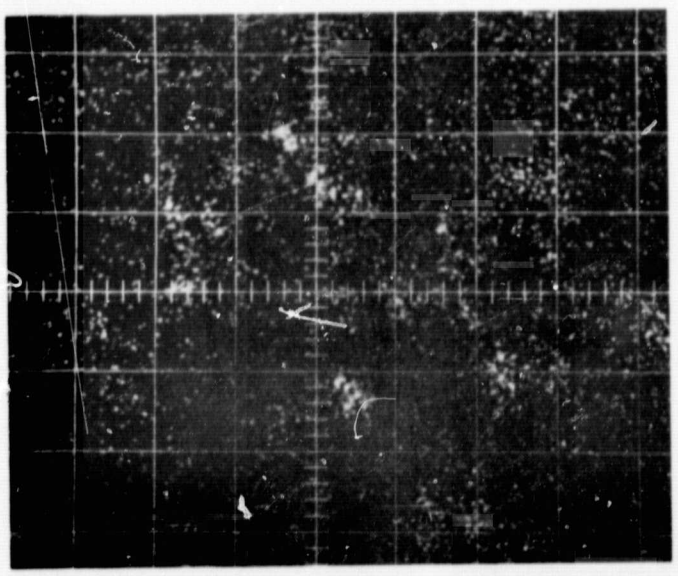

c. Fe K_{α}

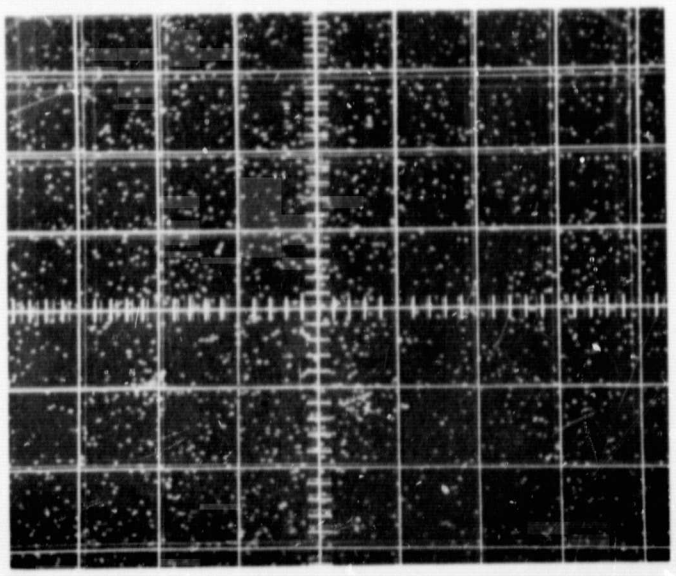

d. Mn K_{α}

Figure 12. Jajh deh Kot Lalu Chondrite Oscillographic Displays

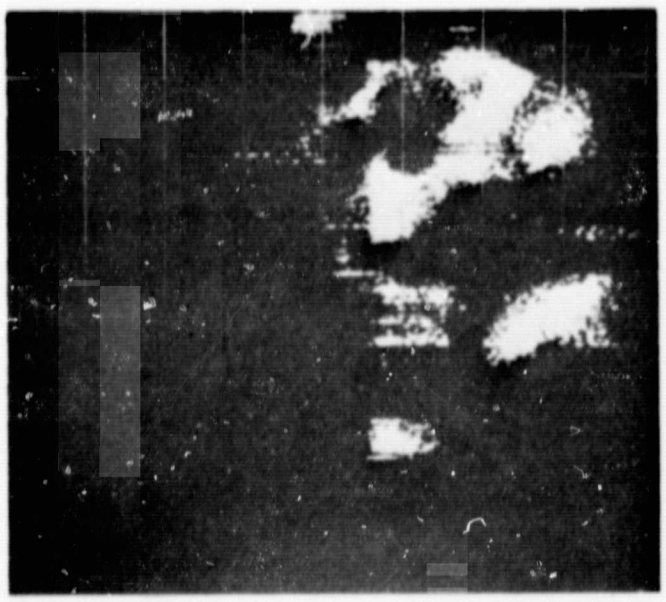

e. 415 nm

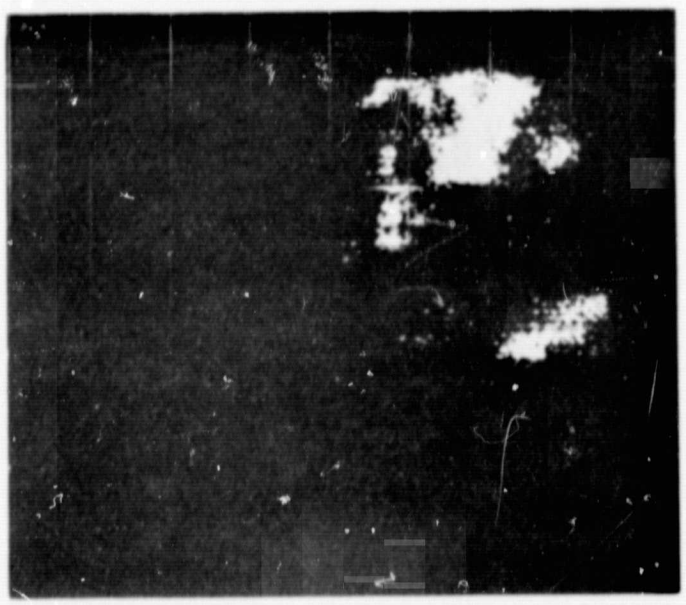

f. 435 nm

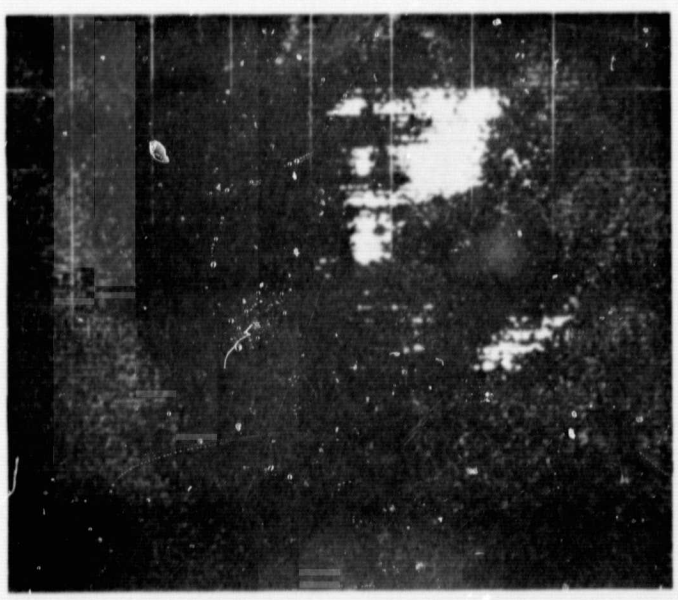

g. 465 nm

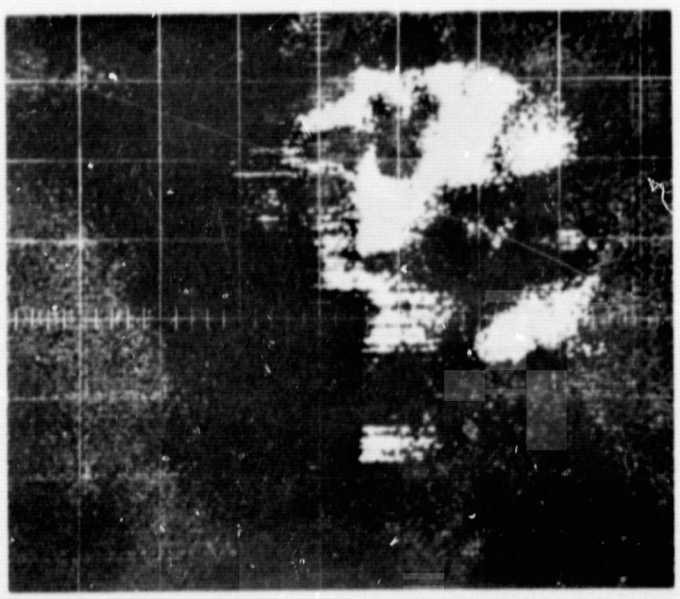

h. 500 nm

Figure 12. Jajh deh Kot Lalu Chondrite Oscillographic Displays

i. 550 nm

j. 600 nm

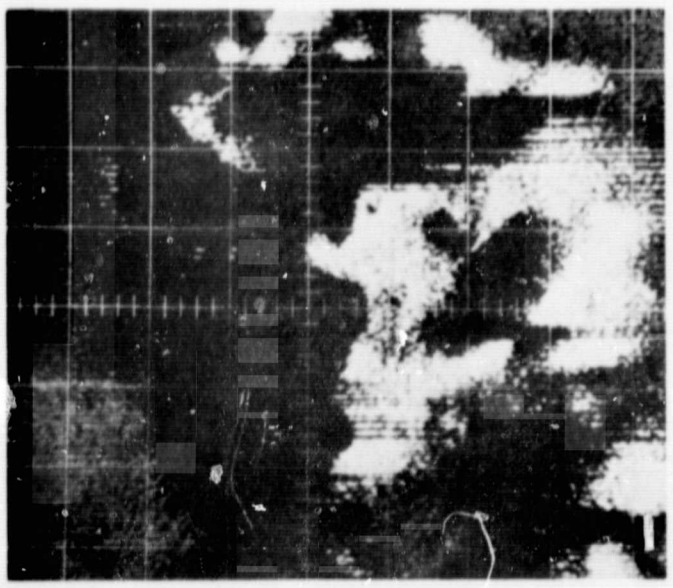

k. 650 nm

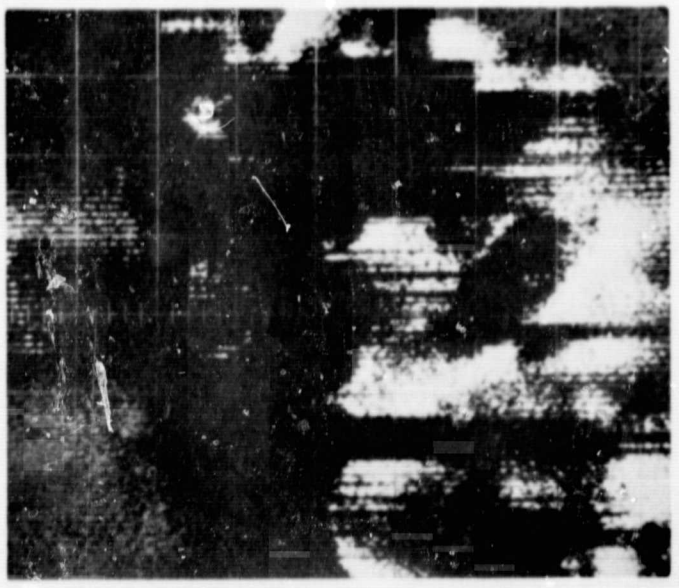

l. 668 nm

Figure 12. Jajh deh Kot Lalu Chondrite Oscillographic Displays

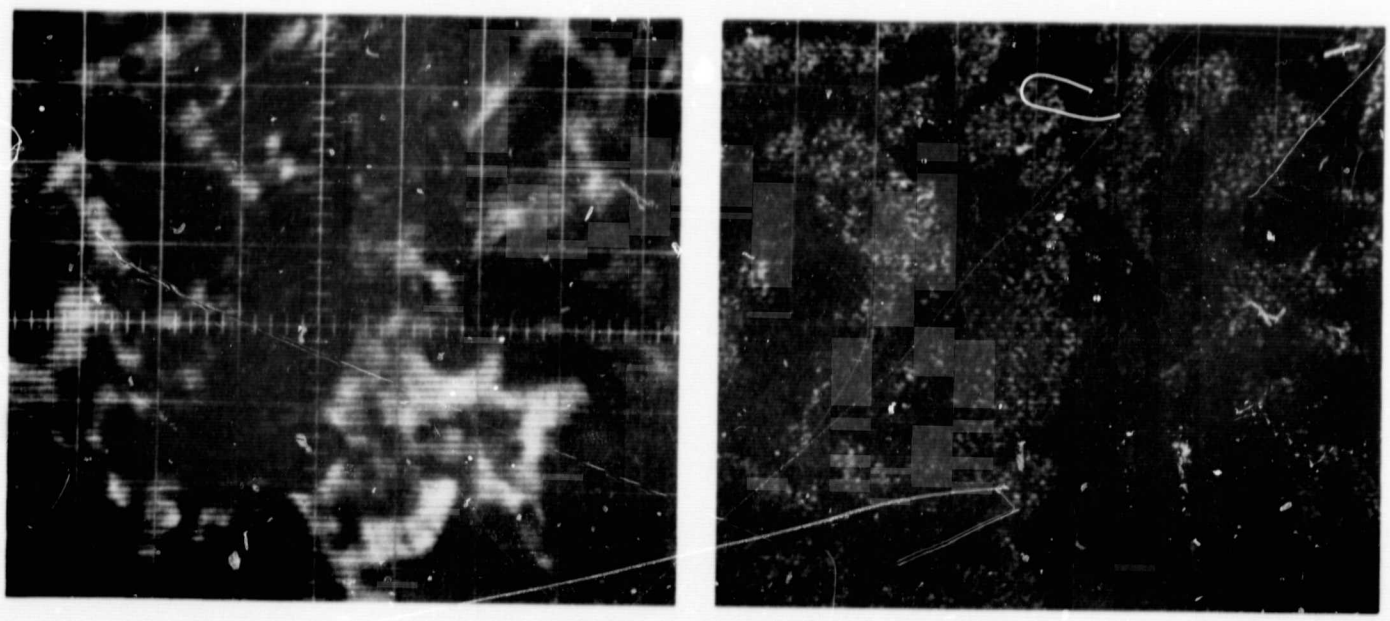

m. Specimen Current Image

n. E. B. S.

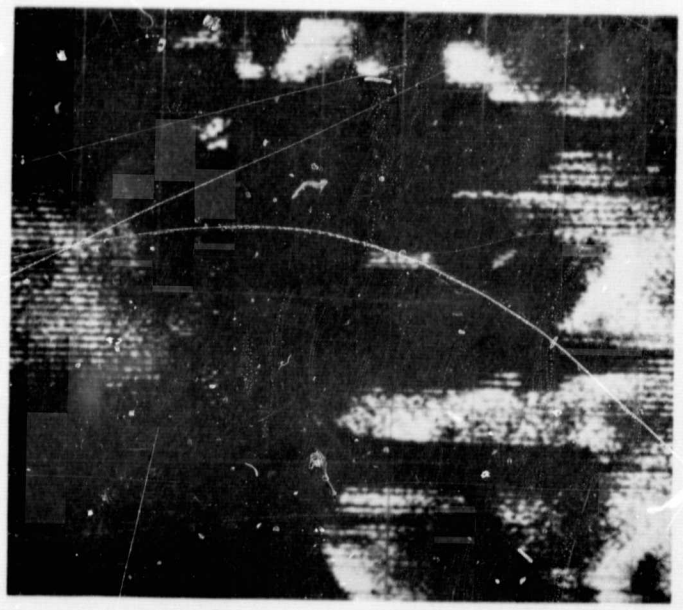

o. 700 nm

Figure 12. Jajh deh Kot Lalu Chondrite Oscillographic Displays

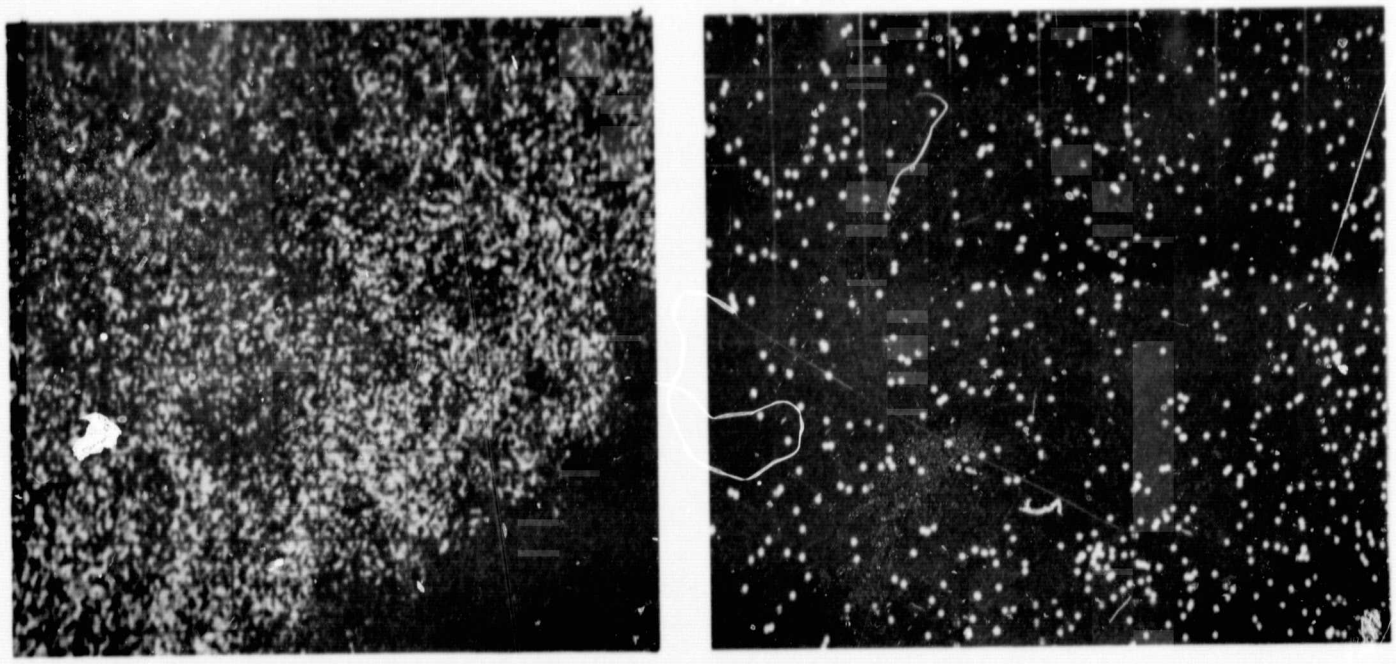

a. Si K_α

b. Fe K_α

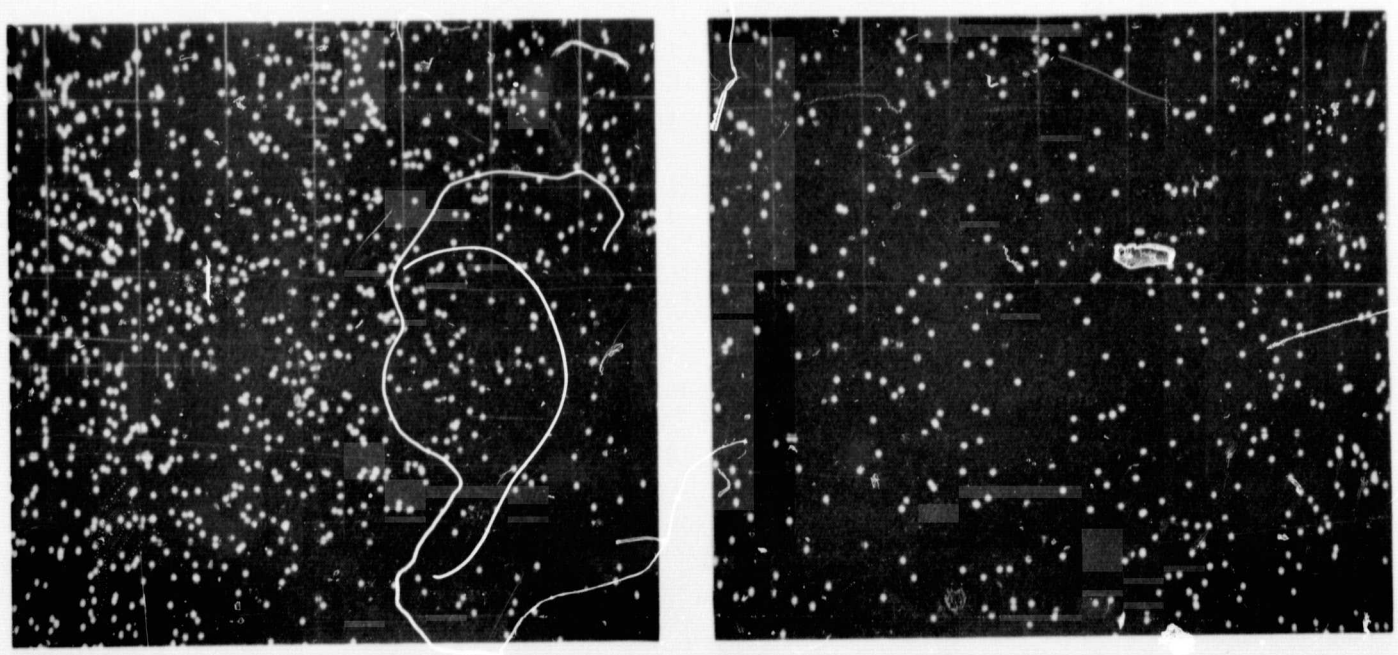

c. Ca K_α

d. Mn K_α

Figure 13. Bishopville Achondrite Oscillographic Displays

e. 409 nm

f. 491 nm

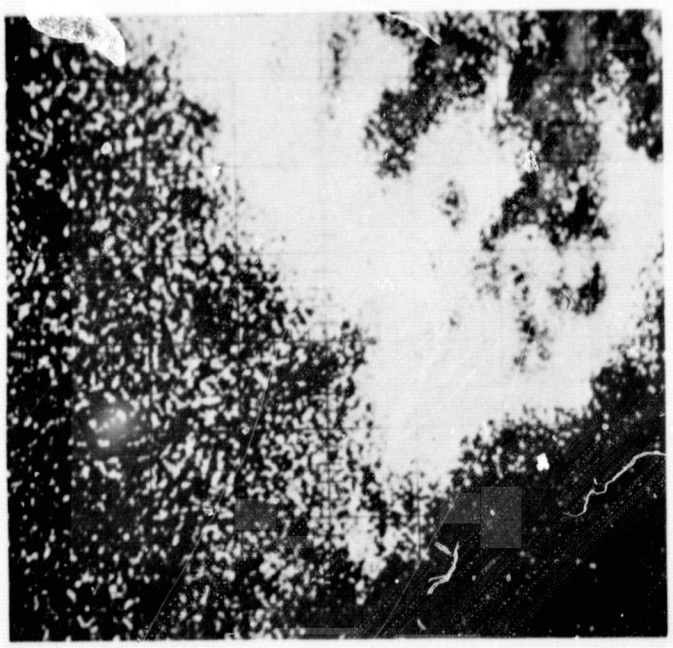

g. 578 nm

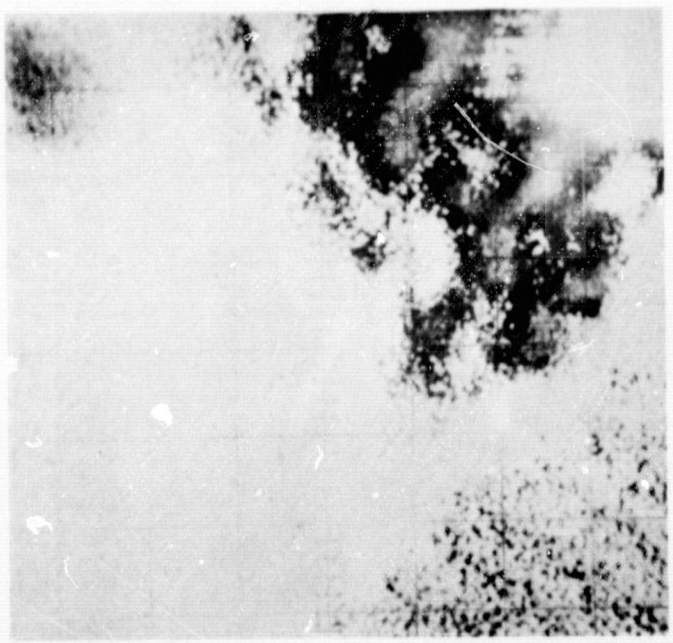

h. 700 nm

Figure 13. Bishopville Achondrite Oscillographic Displays

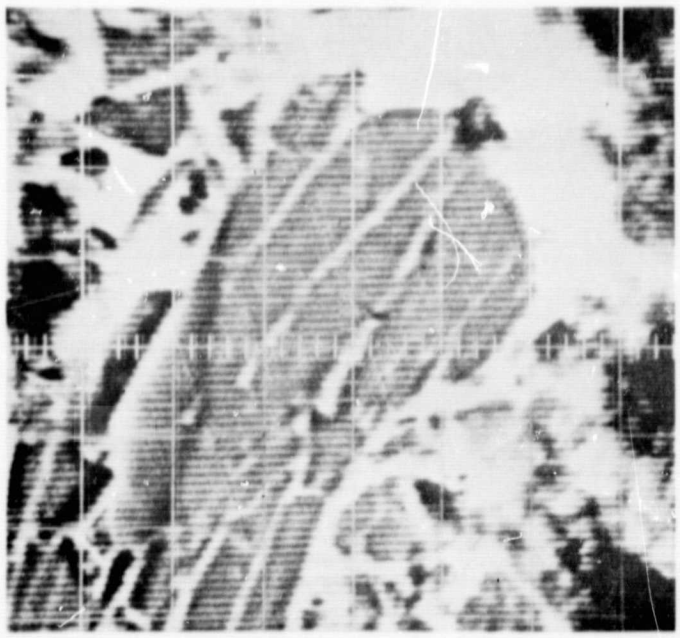

a. Specimen Current Image

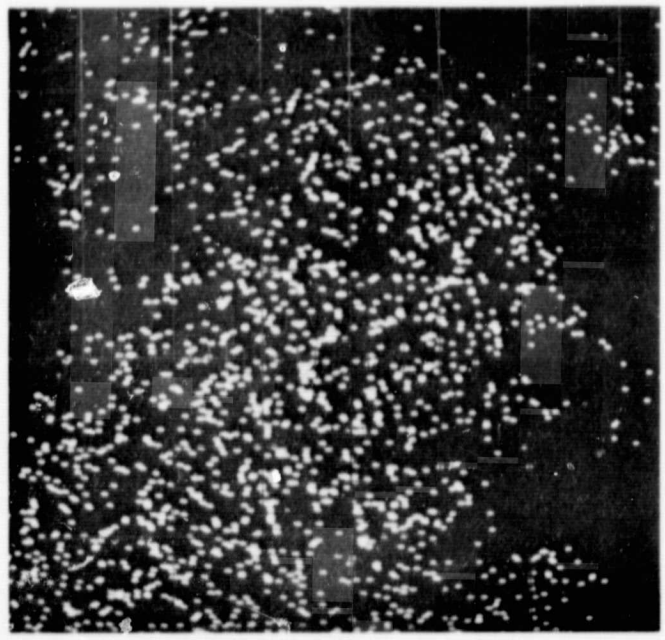

b. Si K_{α}

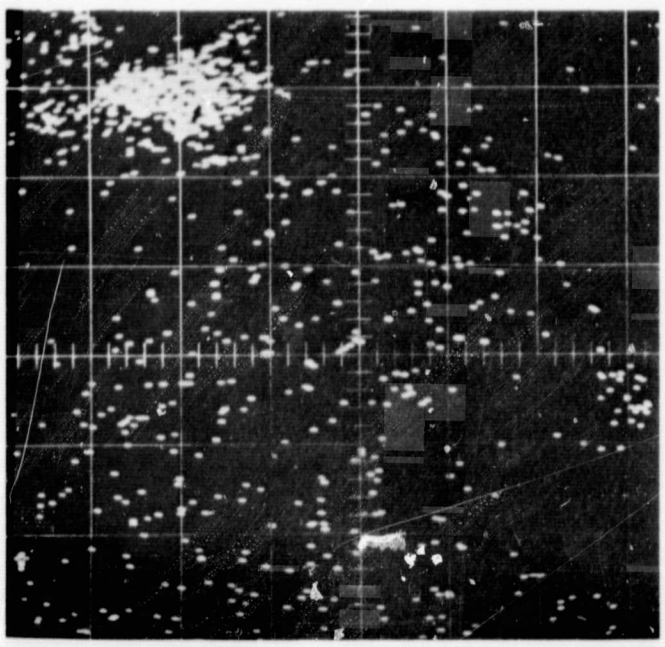

c. Ca K_{α}

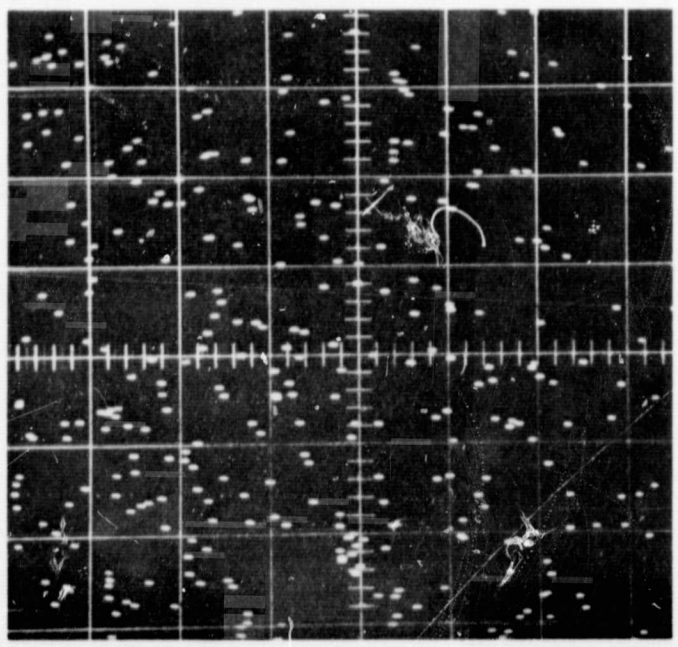

d. Fe K_{α}

Figure 14. Khor Temiki Achondrite Oscillographic Displays

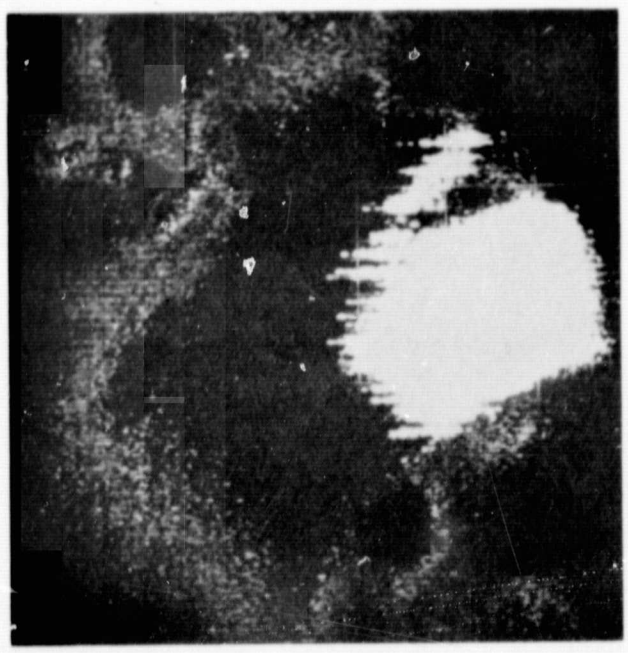

e. 405 nm

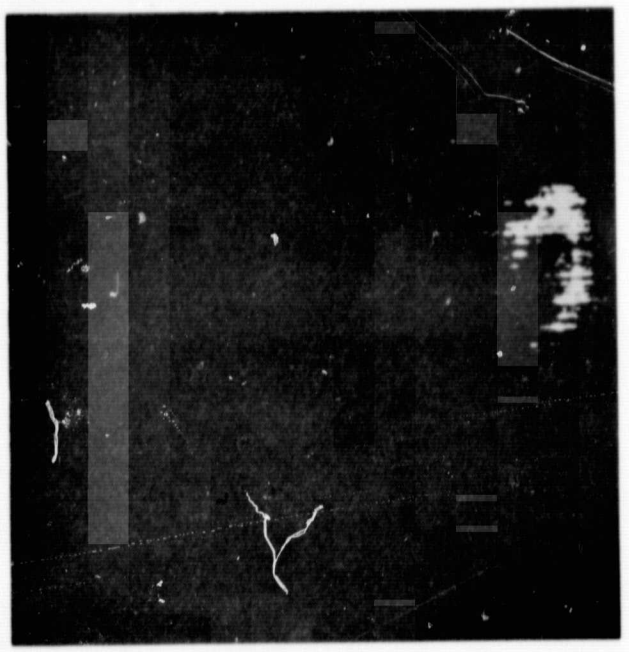

f. 450 nm

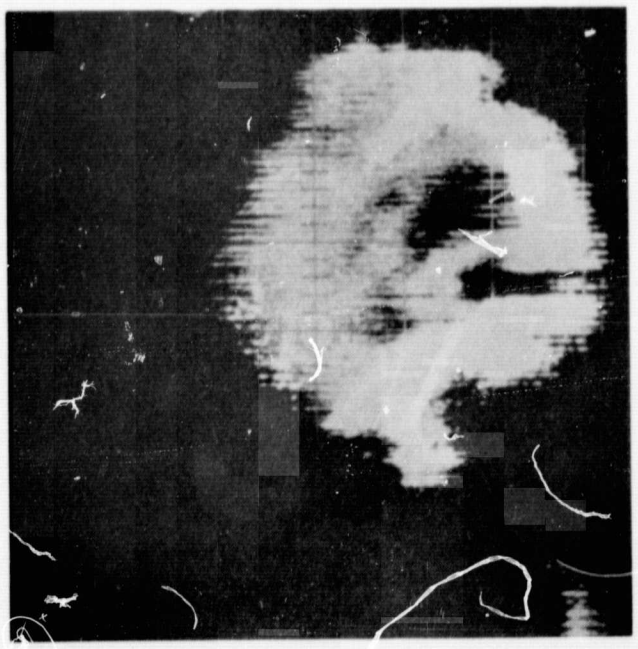

g. 650 nm

h. 700 nm

Figure 14. Khor Temiki Achondrite Oscillographic Displays

more precise color discrimination is shown by the optical fluorescence patterns in Figures 14e - 14h. These rows, flattened blebs, or lamellae are determined to a high degree by the presence and relative concentrations of Ca. For example, this is indicated on the 650 nm and 700 nm color displays in the upper-left area of the photographs.

As the specimen purity increases, color pattern associations with impurities become less distinct; however, general relations can still be described. In Figure 15, the Norton County achondrite oscillographic displays substantiate this. The grain represented by Figure 15 is centered in the photograph and extends slightly beyond the 200 x 200 μ boundaries of the various displays. The central portion of the grain luminesces blue, and the outer portion of the grain luminesces red as indicated by the 410 nm and 475 nm and the 600 nm and 700 nm displays, respectively. Visual observation of the grain during excitation detects the blue luminescence emission in the central portion of the grain, and a pink luminescence for the outer portion of the grain resulting from the mixture of the blue and red color emission bands that the eye detects.

Slow recrystallization for the Shallowater achondrite specimen resulted in high purity, and especially slightly higher purity for the outer portions of the grain shown in Figure 16. This manifests itself as a greater optical fluorescence output in the blue for the outer portions of

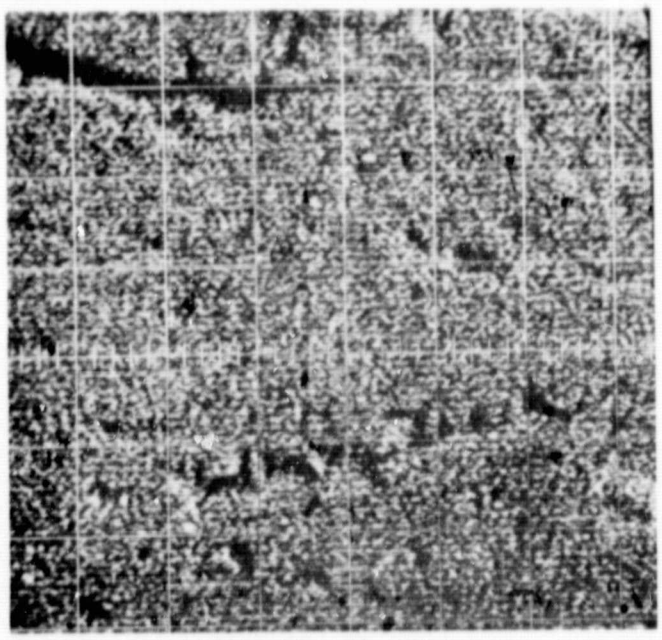

a. E. B. S.

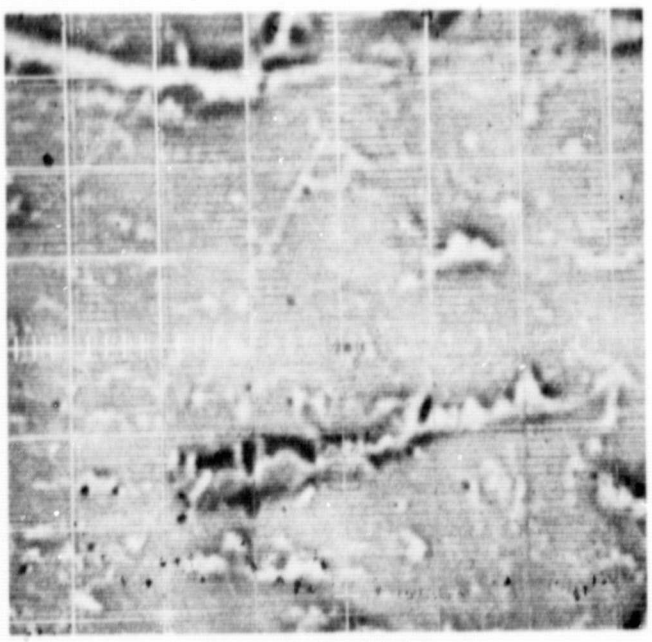

b. Specimen Current Image

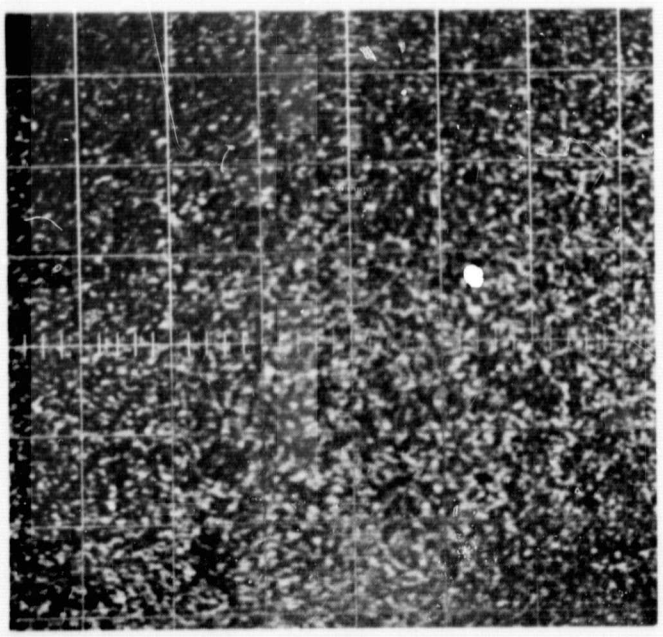

c. Si K_{α}

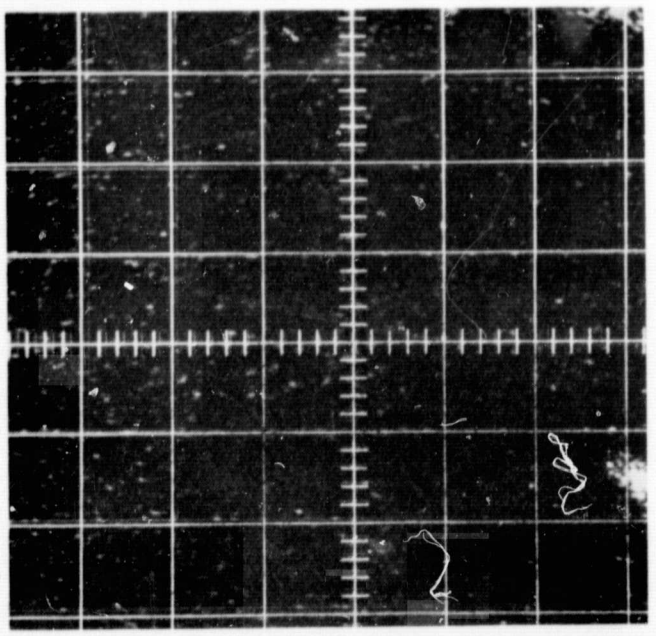

d. Ca K_{α}

Figure 15. Norton County Achondrite Oscillographic Displays

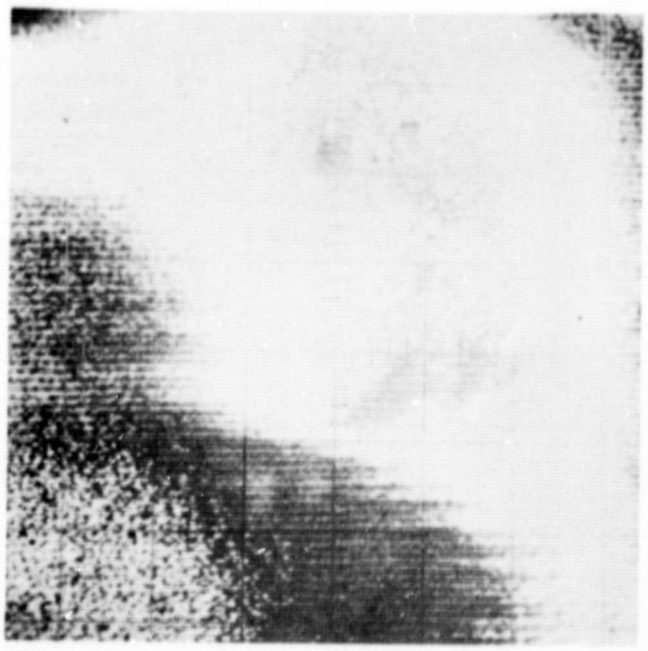

e. 410 nm

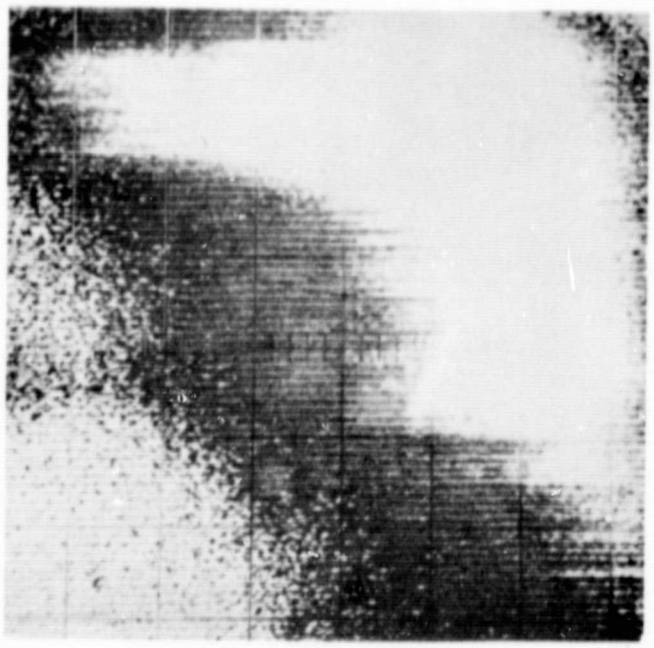

f. 475 nm

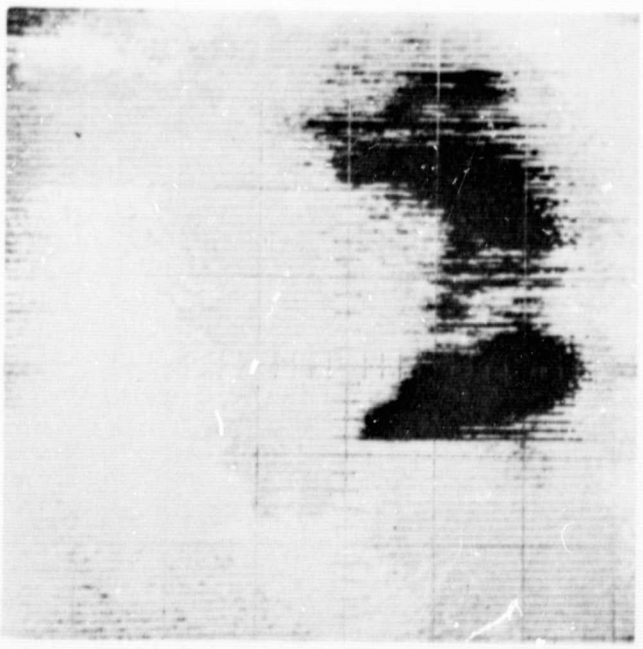

g. 600 nm

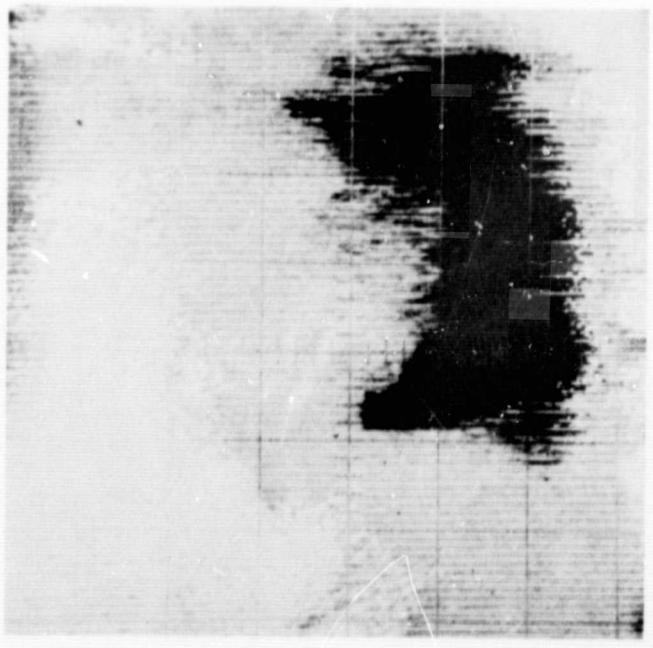

h. 700 nm

Figure 15. Norton County Achondrite Oscillographic Displays

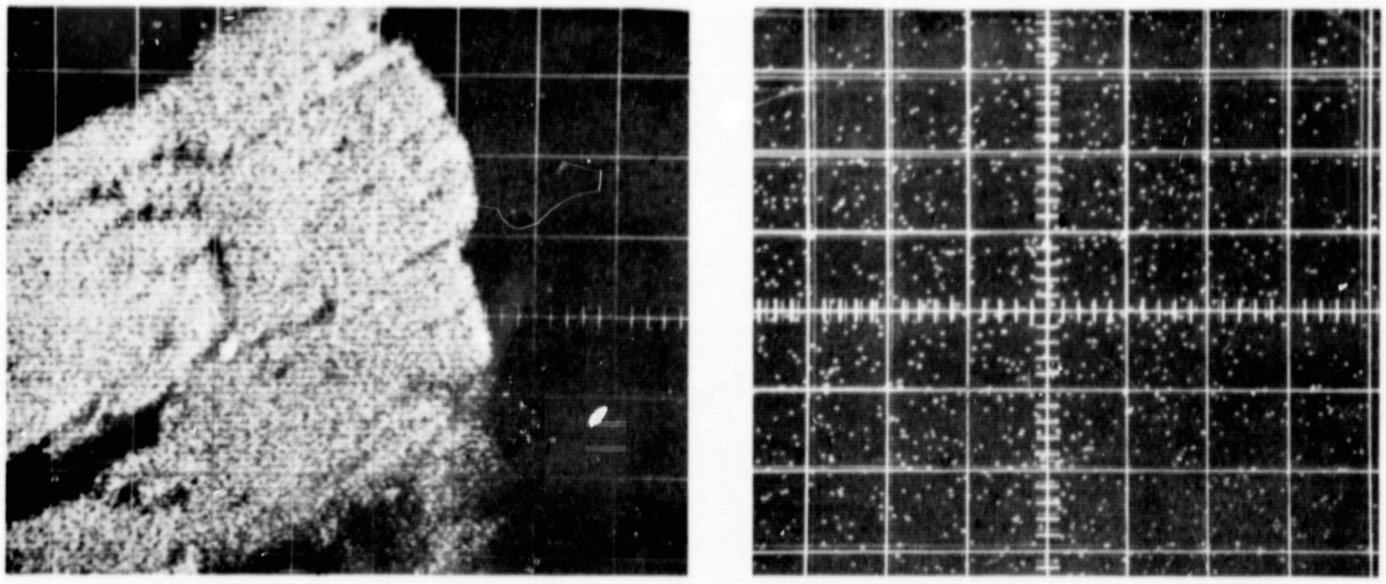

a. E. B. S.

b. Mn K_{α}

c. Si K_{α}

d. Fe K_{α}

Figure 16. Shallowater Achondrite Oscillographic Displays

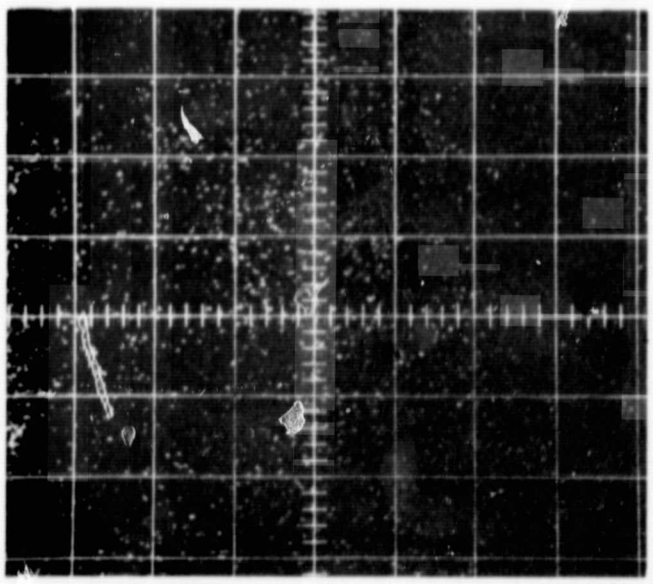

e. Ca K_{α}

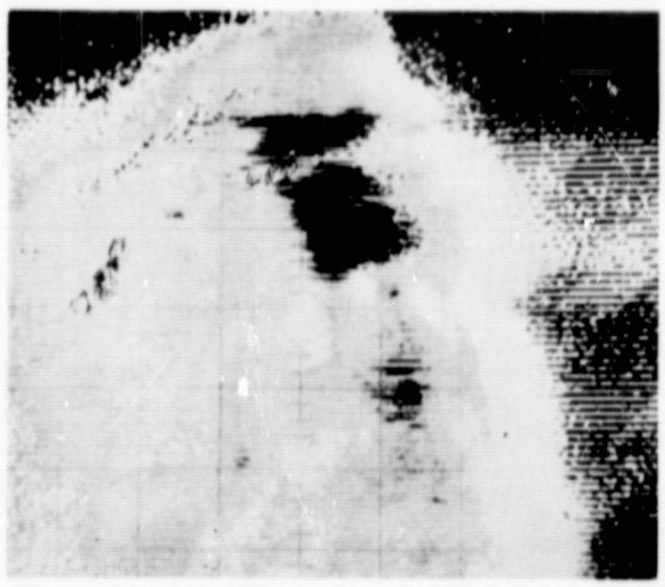

f. 415 nm

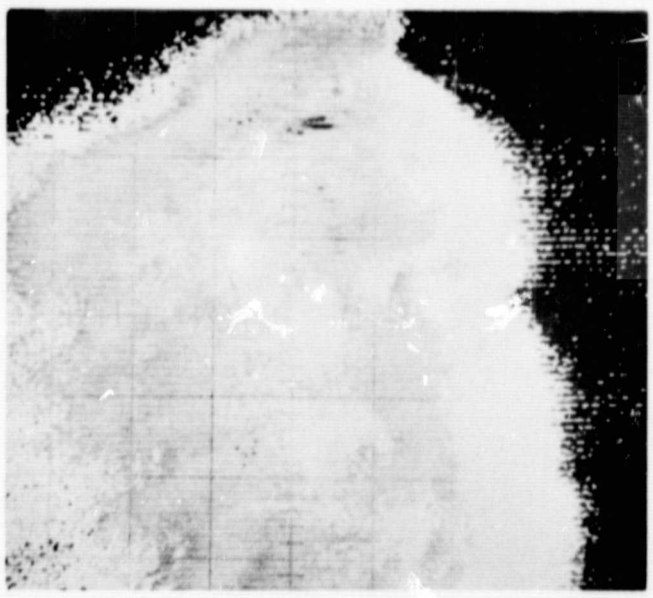

g. 435 nm

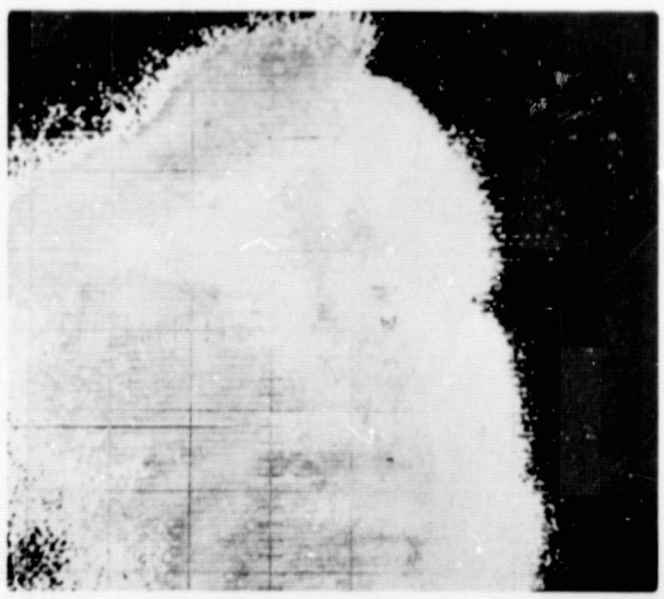

h. 450 nm

Figure 16. Shallowater Achondrite Oscillographic Displays

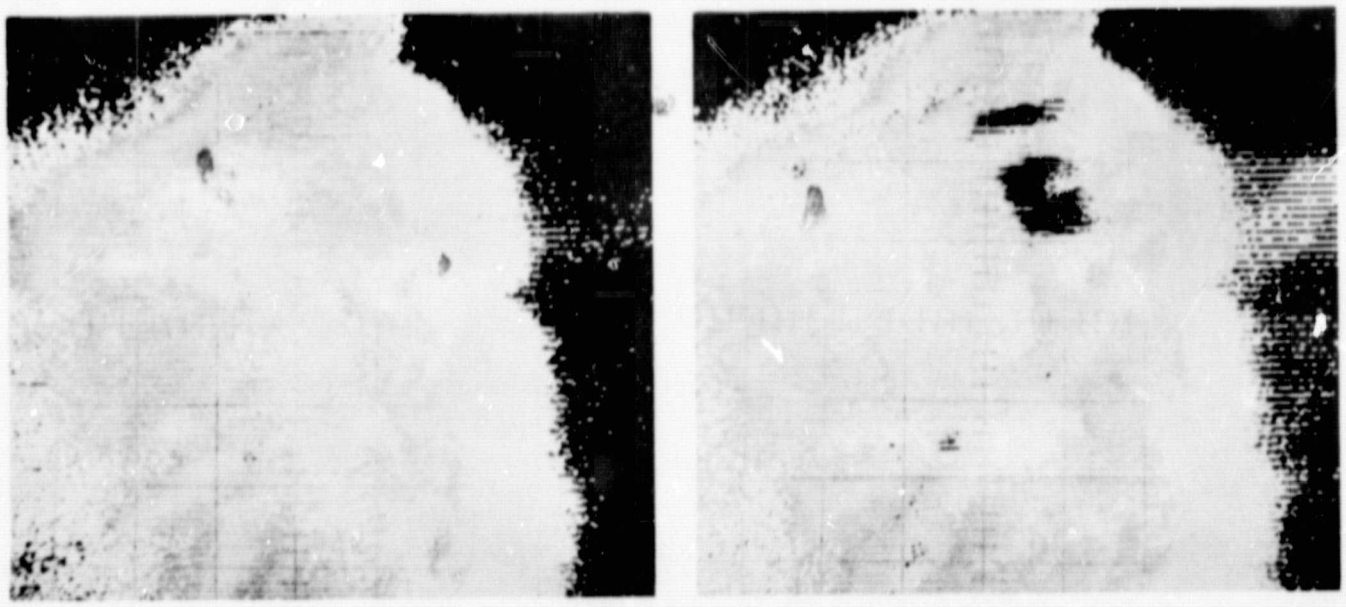

i. 475 nm

j. 500 nm

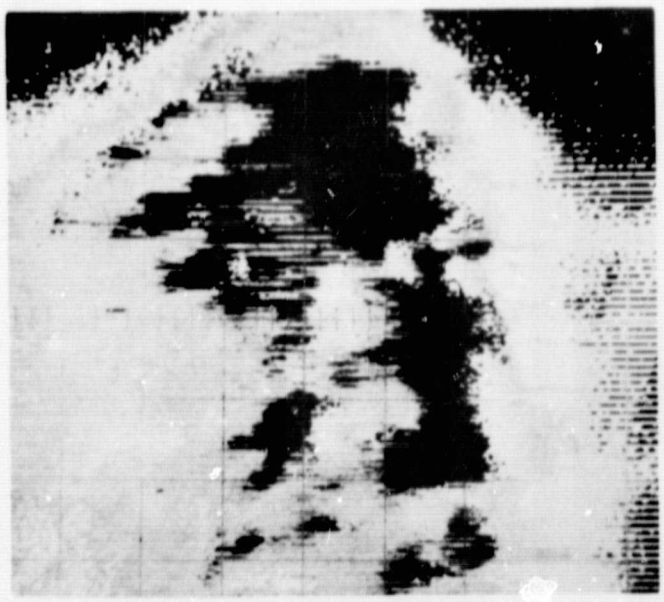

k. 525 nm

Figure 16. Shallowater Achondrite Oscillographic Displays

the grain. However, impurity inhomogeneities have also resulted in just distinguishable rows of Ca concentration blebs which parallel the (110) cleavage. This specimen fluoresces a blue color.

The Cumberland Falls achondrite exhibits a red rim around the periphery of the grain. As in the case for the Norton County achondrite specimen, the grain is large and slightly exceeds the field of view represented in the oscillographs for Figure 17. The central portion of the grain luminesces blue, and the outer portion luminesces red; this luminescence is associated with the high degree of recrystallization represented by the Cumberland Falls meteorite. There is a tendency for the color patterns to parallel the (110) cleavage. As is the case for all of the achondrite specimens, the impurities, when detectable, are uniformly distributed. In this example, Fe, Mn and Cr concentrations were not detectable in the respective oscilloscope displays.

The final specimen to be described is the Pesyanoe achondrite. The two primary features of Figure 18 are the higher intensity blue fluorescent rim that the grain exhibits and the higher intensity color response for areas of low Ca and Fe concentrations. The outer portion of the grain luminesces brighter than the inner portion as is characteristic for the recrystallization history of the achondrites where the outer portions of a pyroxene grain would have relatively lower impurity concentrations than the inner portions. In the

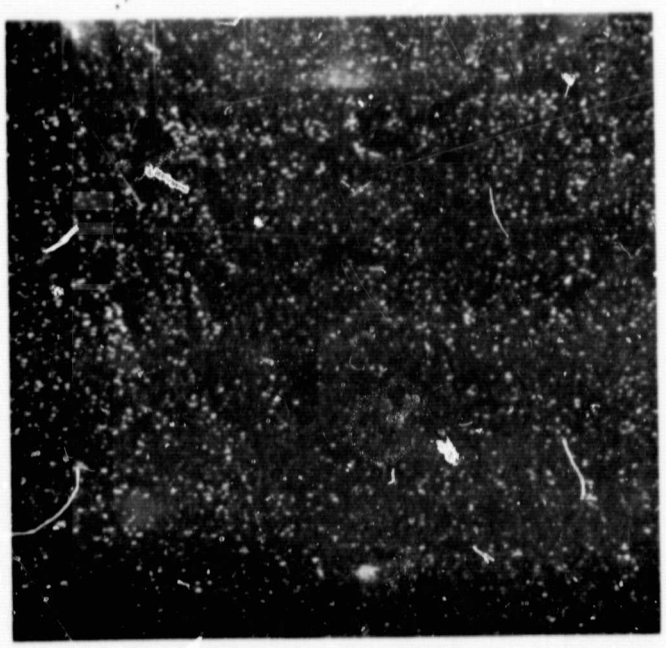

a. E. B. S.

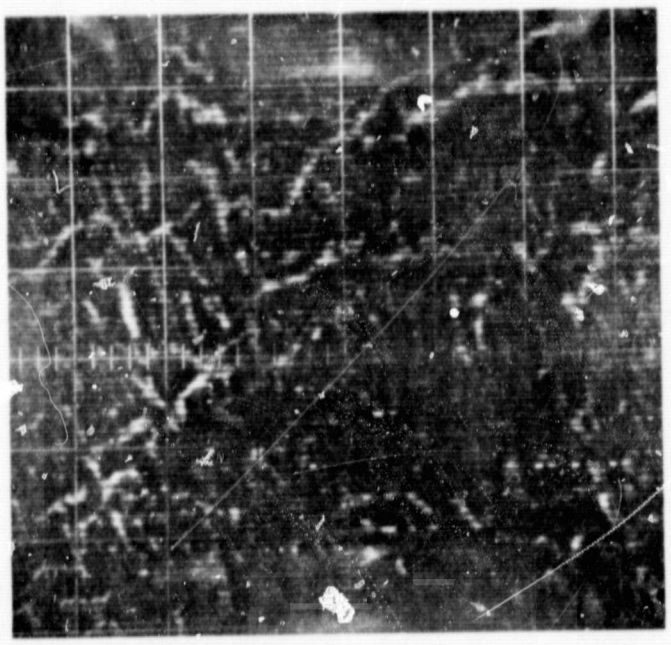

b. Specimen Current Image

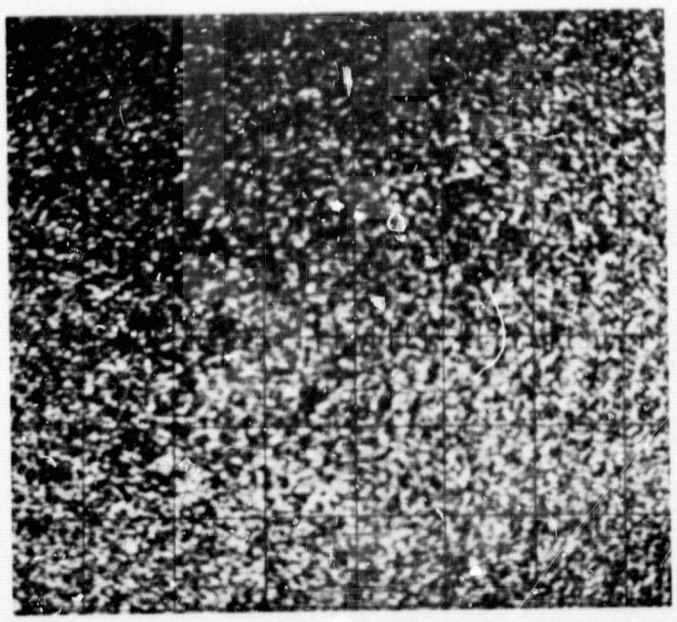

c. Si K

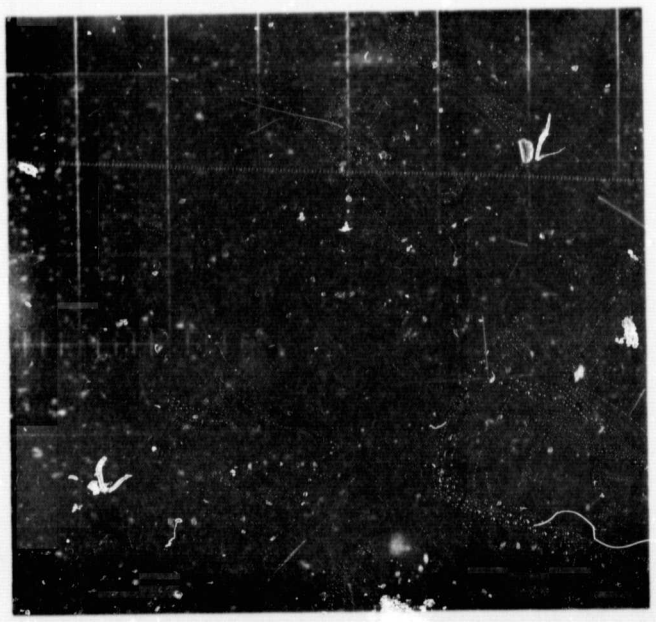

d. Ca K

Figure 17. Cumberland Falls Achondrite Oscillographic Displays

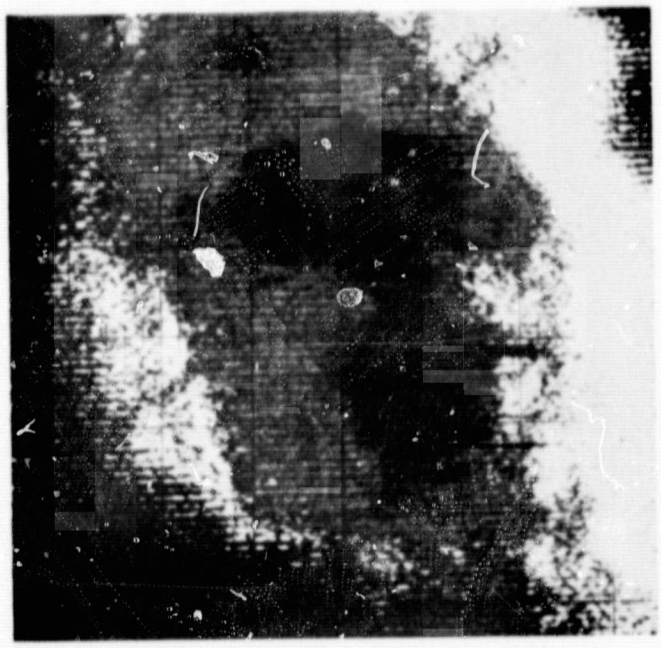

e. 410 nm

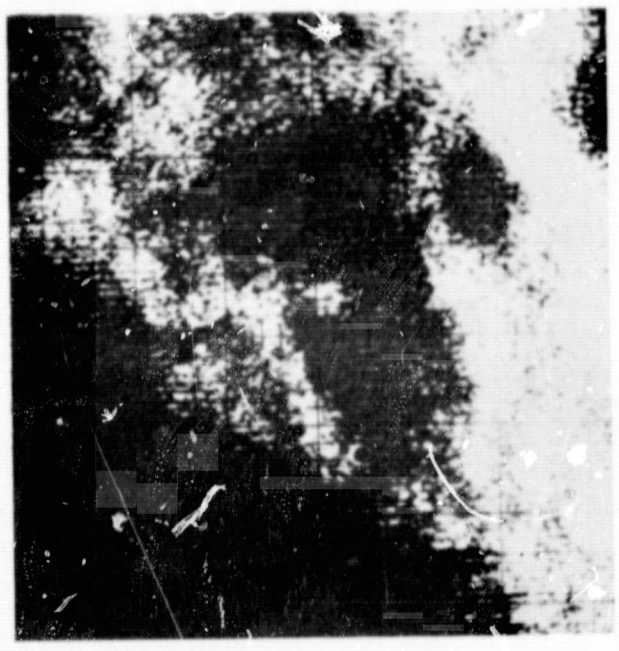

f. 450 nm

g. 500 nm

h. 575 nm

Figure 17. Cumberland Falls Achondrite Oscillographic Displays

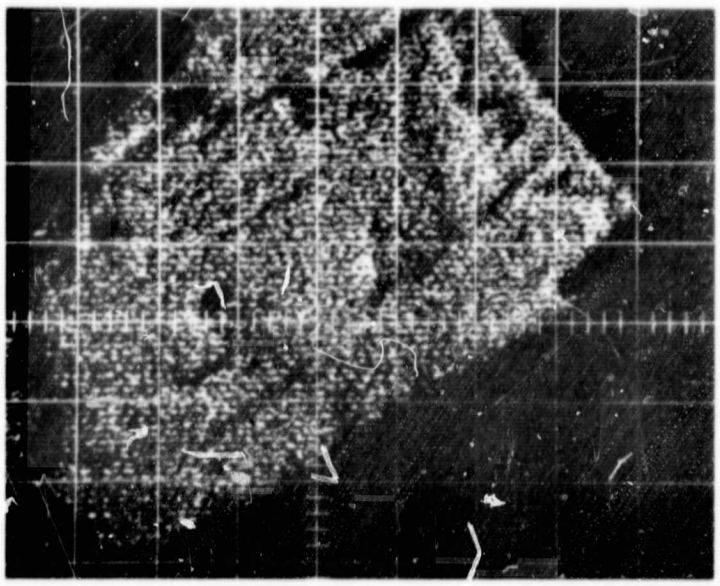

a. E. B. S.

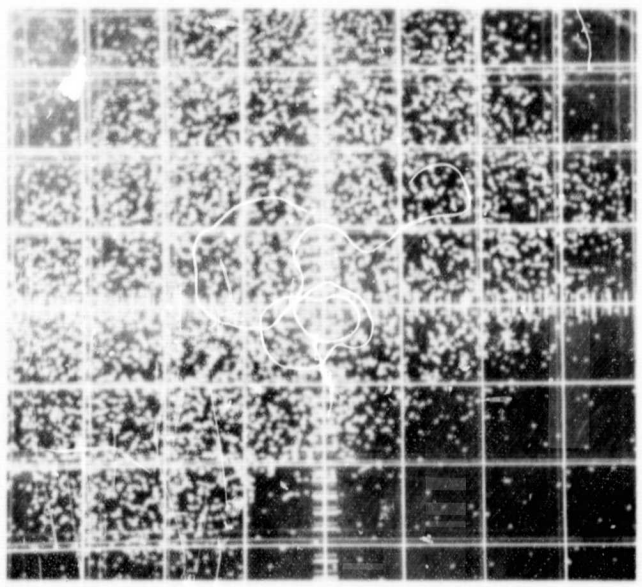

b. Ca K_{α}

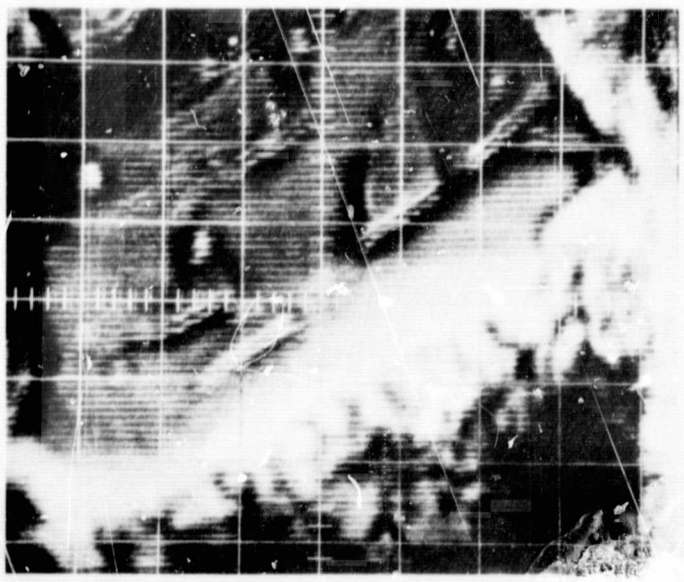

c. Specimen Current Image

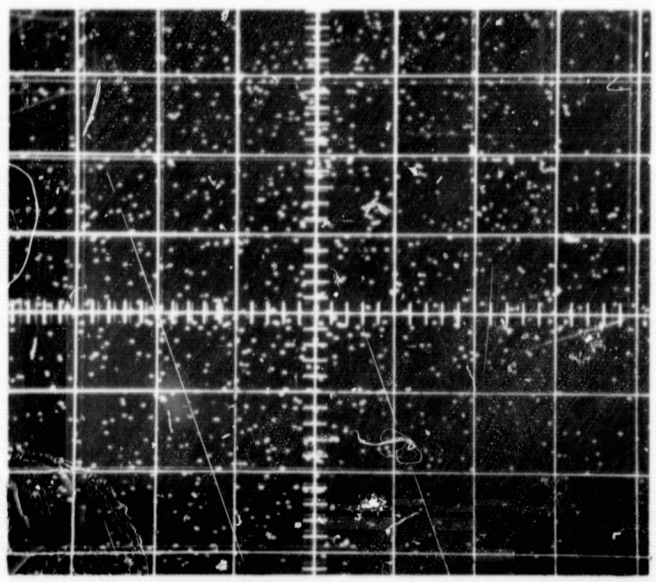

d. Mn K_{α}

Figure 18. Pesyanoe Achondrite Oscillographic Displays

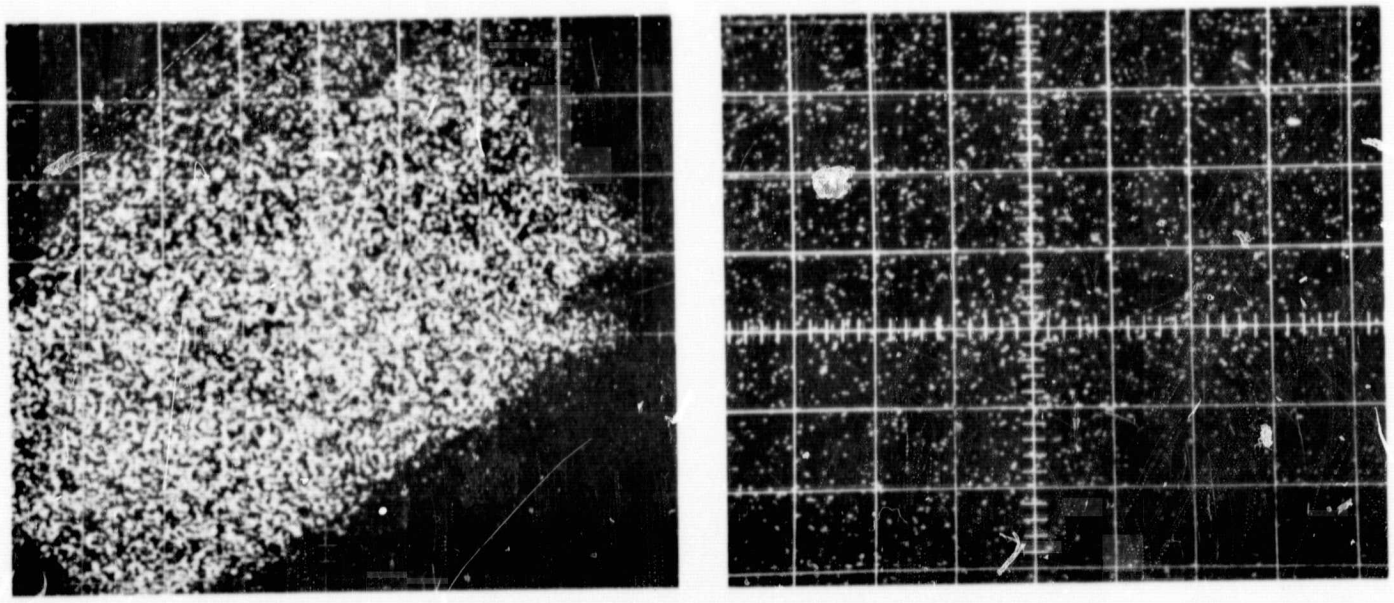

e. Si K_{α} f. Fe K_{α}

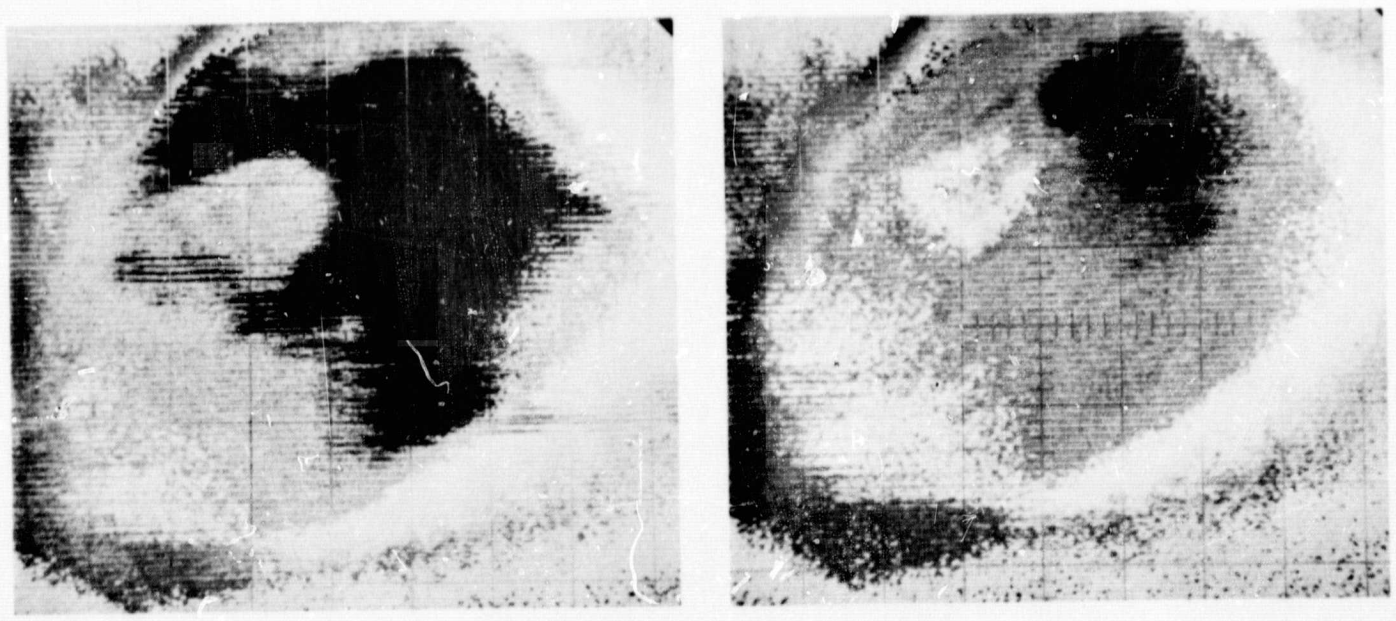

g. 415 nm h. 435 nm

Figure 18. Pesyanoe Achondrite Oscillographic Displays

i. 450 nm

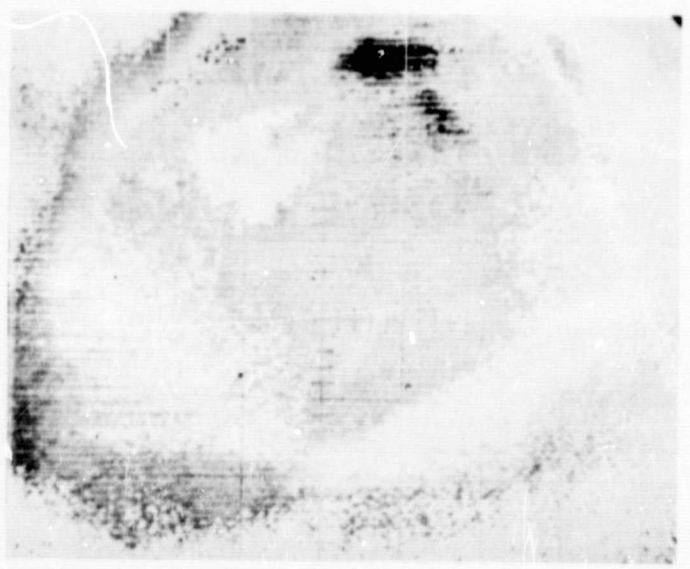

j. 465 nm

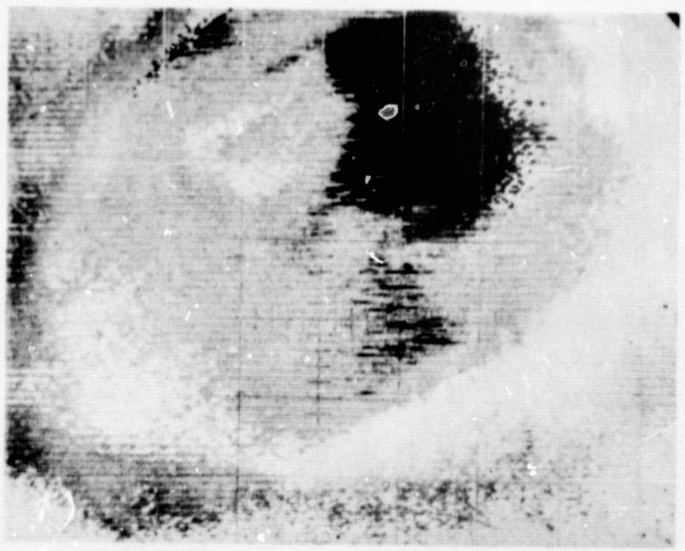

k. 500 nm

l. 550 nm

Figure 18. Pesyanoe Achondrite Oscillographic Displays

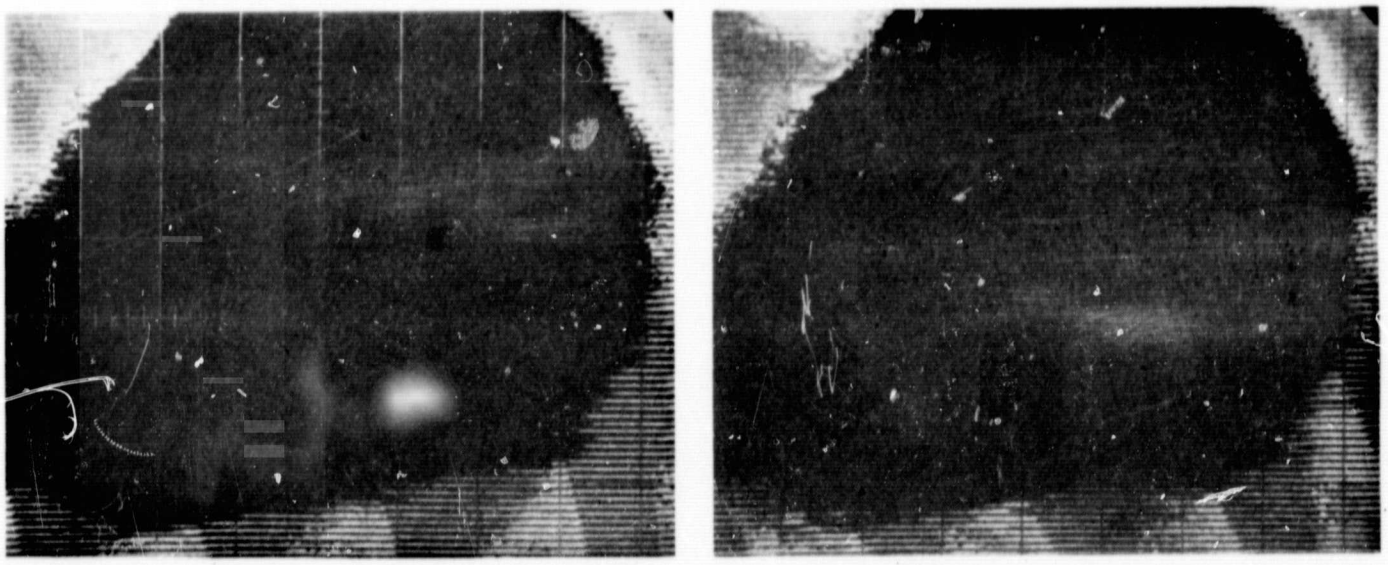

m. 600 nm

n. 650 nm

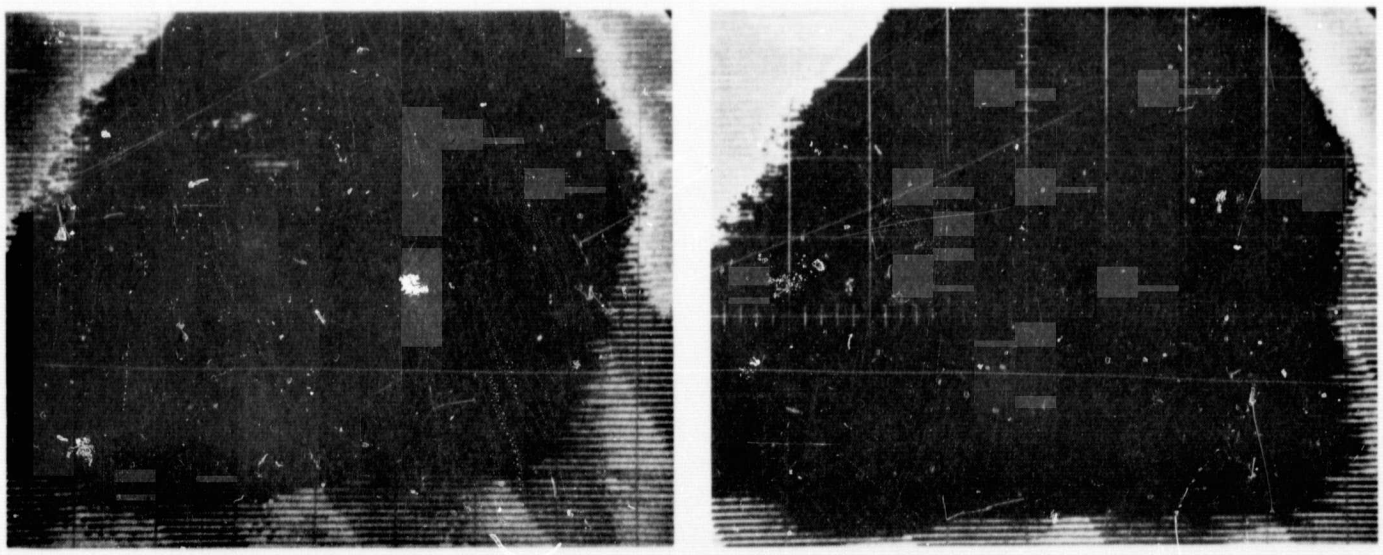

o. 686 nm

p. 700 nm

Figure 18. Pesyanoe Achondrite Oscillographic Displays

upper-left section of the blue and red optical fluorescence displays, there is an area that luminesces strongly. A comparison of these photographs with those for the Fe and Ca distribution displays indicates that the luminescing areas are areas of lower Fe and Ca than areas which do not exhibit luminescence. Again, there is a general trend for the color and Ca patterns to parallel the (110) cleavage.

C. Summary of Results

In the case of bulk specimens, the luminescence analytical technique is especially suitable for studying coexisting phase assemblages, their reaction interfaces, and the reaction mechanisms. It has been demonstrated that the phase boundaries coincide exactly with those displayed by cathodoluminescence stimulation (Brindley and Hayami, 1965; Greer, et al., 1967a; Long and Agrell, 1965).

Individual enstatite grains were separated from meteorites, and quantities of these grains from the individual specimens were grouped side by side and stimulated to demonstrate the variation in color response from specimen to specimen. The blue to red and the varying shades of purple are consistent with the relative position and intensity of the host crystal band (near 4200 Å) and the Mn-activated band (near 6700 Å) as discussed previously.

Studying individual grains appears to be the most promising in terms of quantity and quality of information that can be obtained by the luminescence analysis techniques.

Under the electron bombardment, separate grains display large variation in fluorescence characteristics which are interpreted by the numerous relations presented in the previous sections. These variations are primarily attributed to differences in crystal structure, host, activator concentration, and impurity level; in most cases, the influence of one of the variables overrides the others so that the differences are interpretable, and the contrasts useful in characterizing the particular specimen. For example, the trend of luminescence intensity for enstatite specimens separated from achondritic meteorites was usually greater throughout the visible portion of the spectrum as compared to that for enstatite specimens separated from chondritic meteorites. This general trend is associated with the greater purity of the achondrites, thus allowing a more efficient energy conversion to optical fluorescence. Also, the red luminescence observed is in agreement with both the concept of increasing the manganese concentration in the host crystal increases the intensity in the red emission region, while simultaneously decreasing the host crystal emission in the blue. The observed decrease in luminescent efficiency in going from an orthorhombic enstatite to a monoclinic enstatite specimen is consistent with the crystal field theory explanation concerning the environment of the atoms when the lattice spacing is altered, and also when there is a reduction in the site symmetry. In favorable cases, this type of information could be used to rapidly isolate high

pressure phases in a mixture, and consequently aid in establishing the pressure ranges experienced by the sample.

Thus, the luminescence response for several representative natural terrestrial, extraterrestrial (separated from meteorites) and synthetic silicates has been investigated by studying the interrelationships of crystal host, activator, and impurity as they influence the wavelength and intensity of the emission colors. The effect on luminescent response of impurities, polymorph present, and conditions of formation of the solid can be precisely evaluated both on a point by point basis (one micron diameter) and by two dimensional color raster patterns at different wavelengths for the specimen surface as was demonstrated by the measurements on the enstatite specimens. A modified Applied Research Laboratories EMX microprobe X-ray analyzer (Greer and White, 1967b) facilitated the investigation of a number of cathodoluminescence phenomena, and permitted the assembly of quantitative information for bulk specimens and powders, and detailed determinations of optical fluorescence emission and chemical composition for individual grains. The observed correlations and contrasts provide a reasonable basis to expect useful information from studying the luminescent response and patterns that can be obtained from lunar surface specimens.

D. Comparison With Other Investigations

Using proton irradiation in their investigations, Gaeke and Walker (1966, 1967) have reported luminescence spectra of

stony meteorites, and Nash (1966) has examined some of the common rock-forming silicate minerals. Many notes appear on the subject (Buddhue, 1940, 1941, 1942; Derham, et al., 1964a, 1964b; Garlick, 1964; Reid and Cohen, 1967); however, no systematic work has begun as yet. The majority of the meteorite spectra available in the literature (Derham, et al., 1964a, 1964b; Gaeke and Walker, 1966, 1967; Garlick, 1964) are misleading representations of the luminescent response. Useful data listings could have been accomplished by categorizing their observed wavelengths and intensities or using standard description techniques (Wyszecki and Stiles, 1967) as well as including chemical analyses.

This investigation, however, has quantitatively demonstrated relationships between wavelength, intensity, color distribution, element composition, sensitivity of luminescent phenomena to specimen purity, and meteorite class. In addition, for the first time, oscillographic displays for optical and X-ray fluorescence emissions, supported by essential statistical correlations for the specimens, have been tabulated and discussed.

Constant exposure of the specimen point to the electron beam causes a fatigue of the phosphor which is found to be described by a power-law decay relating intensity and time: $I = t^{-n}$, where I is the measured photomultiplier tube output at a given time, n is a constant evaluated for the particular curve, and t is the time in seconds. Under the conditions of operation of this investigation, the power to be

dissipated for a 1 μ spot exceeds 25,000 watts/cm^2, and it must be emphasized that most phosphors will exhibit detectable permanent changes in efficiency on prolonged steady excitation at this level. This type of decay is also consistent with, and to a lesser extent influenced by, the strain and fracturing that is associated with the history of the meteorites. Young (1953), Massey and Burhop (1952), Leverenz (1940, 1950), and others (Burton, 1947; Ehrenberg and King, 1963; NAS-NRC Pub. 1133, 1964) provide appropriate discussions of electronic and ionic impact, penetration, and reaction phenomena. Usually, any mention of these phenomena has been erroneously omitted and/or ignored in recent literature describing luminescence spectra for meteorites (see for example, Gaeke and Walker, 1966, 1967; Schutten and van Dijk, 1966).

IV. CONCLUSIONS

A. Significance and Scope of the Study

Although luminescent emission from most materials is complex, the application of optical fluorescence as a complementary tool for the characterization of lunar and planetary materials has been advanced by newly developed, quantitative, nondestructive analytical techniques. Several specimens of minerals likely to occur on the lunar surface have been selected to demonstrate the variety of information that can be obtained. Variations in the intensity and wavelength in the fluorescence spectra of natural materials can be correlated with chemical composition, and the distribution of individual mineral components in a multi-phase assemblage is readily made apparent. An advantage of exploiting optical fluorescence lies in its ability to provide quantitative data for specimens of microscopic size.

Classification of materials through remote sensing analysis or by laboratory application of luminescence analysis can be of considerable utility in the evaluation and eventual exploitation of indigenous resources. Such information may be applied in an effort to broadly classify the mineralogical composition of lunar surface material and possibly aid the understanding of the topographic conditions under which the lunar soil series (soils having horizons of similar origin, character, and arrangement in the soil profile which were derived from similar parent material)

and catenas (groups of soils within a particular region which developed from similar parent material but differ in the characteristics of their profiles because of the varying topographic and erosion conditions under which they formed; Thornbury, 1954) develop.

B. Findings

When the samples were observed microscopically during electron bombardment, large differences in both intensity and wavelength of the resulting luminescence were evident. Different portions of a single mineral sample emitted at wavelengths ranging to both limits of the visible spectrum. Within an individual specimen the variation in intensity and/or wavelength of fluorescence appears to be accounted for by corresponding variation in chemical composition. Higher concentrations of Fe, Ca and Cr tend to suppress fluorescence. In many cases, exsolution phenomena representing areas of high Ca and low Ca pyroxene are sharply contrasted by monitoring the optical fluorescent emission intensity with the monochromator set in the red portion of the visible spectrum. Both the high and low Ca pyroxene luminesce in the blue; however, the high Ca quenches strong luminescence in the red and consequently the oscillographic displays clearly show the location of each type.

Fluorescence is most intense in the red portion of the spectrum. Almost all of the strong luminescent samples contain very little Fe or Ca, and the achondrite enstatite

specimens luminesce stronger than the chondrites throughout the visible spectrum.

This behavior is also observed for the clinoenstatite specimens which luminesce with relatively low efficiency and primarily in the blue, and for the orthorhombic enstatite specimens which luminesce with relatively higher efficiency both in the blue and in the red part of the visible spectrum. Iron readily substitutes for Mg in enstatite and diopside, and is in larger concentrations in the clinoenstatite. The presence of Fe quenches luminescence and also can effectively reduce the Mn luminescent emission contribution to red emission. In numerous measurements the Mn and Fe indicated a significant positive correlation, and this association usually decreased the red contribution to the luminescent response for the specimens. In addition, the observed decrease in luminescent efficiency in going from an orthorhombic enstatite to a monoclinic enstatite specimen is consistent with the crystal field theory explanation concerning the environment of the atoms when the lattice spacing is altered, and also when there is a reduction in site symmetry.

Selected mineral grains examined by the electron microprobe revealed that the dispersion of concentrations of Fe, Mn, Cr and Ca in these samples is also large. This variability indicates why a variety of intensity and wavelength responses may be possible within a specimen. These chemical pecularities effectively define the two

groups (Keil, 1967b; Larimer, 1967; Larimer and Anders, 1967; Mason, 1962; Reid and Cohen, 1967; Van Schmus and Wood, 1967; Wiik, 1956) as well as tend to delineate the enstatite polymorph present. The enstatite chondrites are characterized by a high degree of reduction. The principal mineral is pure or nearly pure $MgSiO_3$ as rhombic enstatite, or clinoenstatite in part. Some chondrules show well-developed chondritic structure, others are primarily granular aggregates of enstatite. The luminescence efficiency tends to follow the textural relationships in terms of the sample purity represented by coarse grains and consequently the slow crystallization of the granular aggregates (poor chondrules) compared with the lower intensity registered for the good chondrule types. Also, the degree of recrystallization results in minor chemical and mineralogical changes which can influence unique luminescent response. For example, the Blithfield specimen lacks chondritic structure, and the recrystallization is clearly indicated by red luminescent rings corresponding to areas depleted in impurities by the recrystallization process. The enstatite achondrites represent an even higher degree of reduction than the chondrites, and the achondrite pyroxene is essentially Fe-free. This purity is mirrored by the greater luminescence intensity shown by the enstatite achondrites, for both the range of 400-500 nm and 600-700 nm.

C. Applications

Electron luminescence studies of minerals or other

solid phases have important applications to problems in the study of natural and synthetic materials (Brindley and Hayami, 1965; Colby and Wise, 1964; Gallup, 1936; Hamiter, 1967; Long and Agrell, 1965; Sippel and Glover, 1965; Weber, 1963; Weber, et al., 1967; Weiblen, 1965). The low cost and flexibility of the three devices to produce and observe electron luminescence (the Tesla coil unit and the two monochromator-photomultiplier luminescence detection units) may encourage routine use of cathodoluminescence investigations.

Although the attachments have been used primarily in conjunction with the microprobe, they can, in principle, be used on any light microscope by preparing the appropriate microscope adapter. In this application the monochromator could facilitate measurements of index of refraction and dispersion as well as to help evaluate optical absorption and fluorescence spectra.

In other investigations, the cathodoluminescence pattern has been used as a "marker" to establish the original reaction interface in solid state reactions of oxide materials. The nondestructive analysis can be applied to soil samples, and is of particular interest when the quantity of specimens available for analysis is limited (Greer, et al., 1967a, 1968).

V. SUMMARY

The use of luminescence to characterize lunar surface materials was prompted by the observations of lunar luminescence reported by Kopal (1965) and Kopal and Rackham (1963, 1964). Cameron (1967), McCord (1967), Grainger and Ring (1967), Rackham (1967), and others (Operation Moon-Blink: Trident Engineering Associates Report, 1966) continue to report observations of transient luminescence phenomena occuring on the lunar surface. During the last two decades there has been over 450 sightings of these phenomena (Cameron, 1967). They occur at approximately 90 locations as summarized in Figure 19.

By demonstrating the influence and interrelations of such variables as crystal host, activator, purity and chemical composition, luminescence may eventually be used as a satisfactory remote sensing technique similar to the statistical air survey evaluations of various sand deposits accomplished by Romanova (1964), to the mid-infrared spectrum matching technique of Hunt and co-workers (1967), and to a variety of natural resources by Colwell (1968).

A basic laboratory study of the luminescence of minerals likely to occur on the moon has demonstrated the feasibility of obtaining correlations of mineral luminescent phenomena. A complex example is an explanation of the effect of increasing Ca concentration on optical fluorescence intensity. Intensity (at 686 nm) and Ca are inversely correlated at the one per cent level of significance for the chondrite enstatite specimens. Although the intensity and Mn correlation coefficient is positively (directly) correlated, it is not significant even at the 10 per cent level of significance. However, Mn and Ca are also correlated and the value of the sample

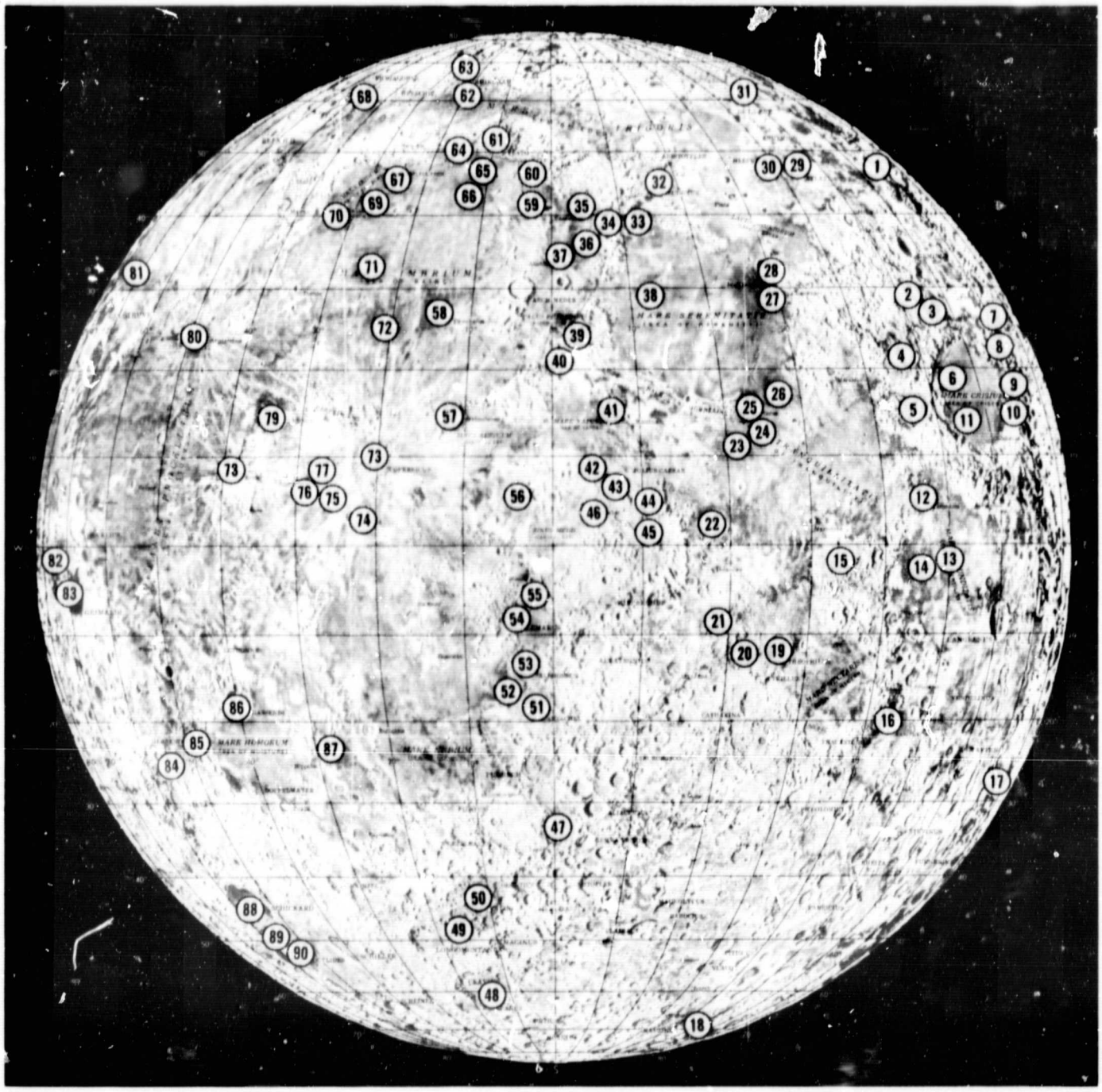

Figure 19. Locations of Lunar Transient Phenomena on the USAF Lunar Reference Mosaic. Areas of four or more reports of these phenomena include 11, 19, 30, 50, 53, 56, 57, 61, 65, 66, 73, 80, 85, 86, and 88.

correlation coefficient, $r_{Mn,Ca}$, is significant at the one per cent level. The partial sample correlation coefficient, $r_{Mn,I/Ca}$, which expresses the correlation of intensity and Mn independent of (rather than ignoring) the effect of Ca, is both positive and significant at one per cent, confirming an observed and presumed causal relationship between these variables. In addition, $r_{Mn,I/Ca,Fe}$, which expresses the correlation of intensity and Mn independent of both the effect of Ca and of Fe, is both positive and significant at an even higher level.

At higher impurity concentrations (about 0.5 weight %) the possibility of an impurity ion occupying an M_1 site adjacent to a Mn ion at an M_1 site in enstatite becomes sufficiently large and may result in a distortion of the oxygen octahedra at the Mn activator site which could possibly cause a detectable decrease of the luminescence output since more nonradiative transitions could occur at these sites even though the overall Mn concentration increased.

Quantitative optical fluorescence spectra and color pattern displays have application in the characterization of inorganic solids as demonstrated by newly developed, nondestructive analytical techniques. In most cases it is necessary to obtain point analyses for interpretation of color patterns since the X-ray detection level for point analyses is lower than the cation concentration displays. By conveniently utilizing the analytical capabilities of an electron microprobe X-ray analyzer and cathodoluminescence detection units, spectral data of micron size particles and of preselected micron size areas of larger mineral grains can be collected, and the variations in the fluorescence response of the specimens can be correlated with chemical composition and structure.

LITERATURE CITED

Atlas, L., (1952), "The Polymorphism of $MgSiO_3$ and Solid-State Equilibria in the System $MgSiO_3$ - $CaMgSi_2O_6$", J. Geol., 60, 125.

Ballhausen, C. J., (1962), Introduction to Ligand Field Theory, McGraw-Hill Book Co., N. Y.

Blair, I. M., and Edgington, J. A., (1968), "Luminescent Properties of Rocks, Meteorites and Natural Glasses under Proton Bombardment", Nature, 217, 157.

Boyd, F. R., England, J. L., and Davis, B. T. C., (1964a), "Effects of Pressure on the Melting and Polymorphism of Enstatite, $MgSiO_3$", J. Geophys. Res., 69, 2101.

Boyd, F. R., and Schairer, J. F., (1964b), "The System $MgSiO_3$ - $CaMgSi_2O_6$", J. Petrol., 5, 275.

Brindley, G. W., and Hayami, R., (1965), "Kinetics and Mechanism of Formation of Forsterite (Mg_2SiO_4) by Solid State Reaction of MgO and SiO_2", Phil. Mag., 12, 505.

Brown, G. M., (1960), "The Effect of Ion Substitution on the Unit Cell Dimensions of the Common Clinopyroxenes", Am. Mineral., 45, 15.

Buddhue, J. D., (1940), "Two New Constituents of Meteoritic Gases", Am. J. Sci., 238, 569.

Buddhue, J. D., (1941), "The Luminescence of Meteorites", Am. J. Sci., 239, 839.

Buddhue, J. D., (1942), "Ionoluminescence", The Min., 11, 11.

Burton, M., (1947), "Radiation Chemistry", J. Phys. Colloid Chem., 51, 611.

Cameron, W. S., (1967), "Observations of Changes on the Moon", Proc. Fifth Ann. Meet. of the Working Group on Extraterrestrial Resources, 47.

Cameron, W. S., and Gilheany, J. J., (1967), "Operation Moon Blink and Report of Observations of Lunar Transient Phenomena", ICARUS, 7, 29.

Campbell, W. J., Brown, J. D., and Thatcher, J. W., (1966), "X-ray Absorption and Emission", Anal. Chem., 38, 416R.

Colby, J. W., and Wise, W. N., (1964), "Cathodoluminescence as an Ancillary Technique to Microprobe Analysis", USAEC Report NLCO-920, 7.

Colwell, R. N., (1968), "Remote Sensing of Natural Resources", Sc. Amer., 218, 54.

Deer, W. A., Howie, R. A., and Zussman, J., (1965), Rock Forming Minerals, 2, Longmans, Green and Co., Ltd., London.

DeMent, J., (1945), Fluorochemistry, Chemical Publishing Co., N. Y.

Derham, C. J., and Gaeke, J. E., (1964a), "Luminescence of Meteorites", Nature, 201, 62.

Derham, C. J., Gaeke, J. E., and Walker, G., (1964b), "Luminescence of Enstatite Achondrite Meteorites", Nature, 203, 134.

Dixon, W. J., and Massey, F. J., Jr., (1957), Introduction to Statistical Analysis, McGraw-Hill Book Co., N. Y.

Ehrenberg, W., and King, D. E. N., (1963), "The Penetration of Electrons into Luminescent Materials", Proc. Phys. Soc., 81, 751.

Fonda, G. R., and Seitz, F., (1948), Preparation and Characteristics of Solid Luminescent Materials, John Wiley and Sons, N. Y..

Gaeke, J. E., and Walker, G., (1966), "The Luminescence Spectra of Meteorites", Geochim. Cosmochim. Acta, 30, 929.

Gaeke, J. E., and Walker, G., (1967), "Laboratory Investigations of Meteorite Luminescence", Proc. Roy. Soc. (London), A296, 337.

Gallup, J., (1936), "The Vacuum Cell Luminescence Microscope and Its Use in the Study of Luminescent Materials", J. O. S. A., 26, 213.

Garlick, G. F. J., (1949), Luminescent Materials, Oxford at the Clarendon Press.

Garlick, G. F. J., (1964), "Luminescence of Meteorites", Nature, 202, 171.

Grainger, J. F., and Ring, J., (1967), "Techniques of Observation of Lunar Luminescence", Proc. Roy. Soc. (London), A296, 330.

Greer, R. T., Staley, W. G., Jr., and Vand, V., (1967a), "Cathodoluminescence Device for Rapid Identification of Phase Assemblages", Am. Ceram. Soc. Bull., 46, 829.

Greer, R. T., and White, E. W., (1967b), "Microprobe Attachment for Quantitative Studies of Cathodoluminescence", Trans. Second Nat. Conf. on Electron Microprobe Analysis, paper 51.

Greer, R. T., Vand, V., and Weber, J. N., (1968), "Applications of Luminescence Techniques to the Study of the Lunar Surface", Symposium on the Interpretation of Lunar Probe Data. II., American Astronautical Society, Los Angeles.

Hamiter, L., (1967), "Infrared Techniques for the Reliability Enhancement of Microelectronics", S C P and Solid State Technology, 2, 41.

Hardy, A. E., (1947), "A Combination Phosphorometer and Spectroradiometer for Luminescent Materials", Trans. Electrochem. Soc., 91, 221.

Heinrich, K. F. J., (1962a), "Concentration Mapping Device for the Scanning Electron Probe Microanalyzer", Rev. Sci. Instr., 33, 884.

Heinrich, K. F. J., (1962b), "Oscilloscope Readout of Electron Microprobe Data", in Advances in X-ray Analysis, 3, Plenum Press, N. Y., 291.

Hunt, G. R., Salisbury, J. W., and Reed, J. W., (1967), "Rapid Remote Sensing by Spectrum Matching Technique. 2. Application in the Laboratory and in Lunar Observations", J. Geophys. Res., 72, 705.

Johnson, R. P., (1939), "Luminescence of Sulfide and Silicate Phosphors", J. O. S. A., 29, 387.

Keester, K. L., and White, W. B., (1968), "Crystal Field Spectra and Chemical Bonding in Manganese Minerals", Min. Mag., in press.

Keil, K., (1967a), "The Electron Microprobe X-ray Analyzer and Its Application in Mineralogy", Fortschr. Miner., 44, 4.

Keil, K., (1967b), "Chemical and Mineralogical Relationships among Enstatite Chondrites", G. S. A. Meeting, New Orleans, La.

Klick, C. C., (1955), "Divalent Manganese as a Luminescent Center", Brit. J. Appl. Phys., 4, S74.

Klick, C. C., and Schulman, J. H., (1957), "Luminescence in Solids", in Solid State Physics, 5, Academic Press, N. Y.

Kopal, Z., (1965), Photographic Atlas of the Moon, Academic Press, N. Y.

Kopal, Z., and Rackham, T. W., (1963), "The Excitation of Lunar Luminescence by Solar Activity", ICARUS, 2, 481.

Kopal, Z., and Rackham, T. W., (1964), "Excitation of Lunar Luminescence by Solar Flares", Nature, 201, 239.

Korda, E. J., Pruden, I. H., and Williams, J. P., (1967), "Scanning Electron Microscopy of a P-16 Phosphor. Cathodoluminescent and Secondary Electron Emission Modes", Appl. Phys. Let., 10, 205.

Kroger, F. A., (1948), Some Aspects of the Luminescence of Solids, Elsevier Publishing Co., N. Y.

Kyser, D. F., and Wittry, D. B., (1966), "Cathodoluminescence in Gallium Arsenide", in The Electron Microprobe, John Wiley and Sons, N. Y., 691.

Leverenz, H. W., (1940), "Cathodoluminescence as Applied in Television", RCA Rev., 5, 131.

Leverenz, H. W., (1950), Introduction to Luminescence of Solids, John Wiley and Sons, N. Y.

Larimer, J. W., (1967), "Chemical Fractionations in Meteorites. I. Condensation of the Elements", Geochim. Cosmochim. Acta, 31, 1215.

Larimer, J. W., and Anders, E., (1967), "Chemical Fractionations in Meteorites. II. Abundance Patterns and Their Interpretation", Geochim. Cosmochim. Acta, 31, 1239.

Lillicrap, S. C., (1967), "A Luminescence Spectrophotometer for Powders Excited by Pulsed Ionizing Radiation", J. Sci. Instr., 44, 584.

Long, J. V. P., (1963), "The Application of Electron-Probe Microanalyzer to Metallurgy and Mineralogy", in X-ray Optics and X-ray Microanalysis, Academic Press, N. Y. , 279.

Long, J. V. P., and Agrell, S. O., (1965), "Cathodoluminescence of Minerals in Thin Section", Min. Mag., 34, 318.

Mason, B., (1962), Meteorites, John Wiley and Sons, N. Y.

Mason, B., (1966), "The Enstatite Chondrites", Geochim. Cosmochim. Acta, 30, 23.

Mason, B., (1967), "Extraterrestrial Mineralogy", Am. Mineral., 52, 307.

Massey, H. S. W., and Burhop, E. H. S., (1952), Electronic and Ionic Impact Phenomena, Oxford University Press, London.

McClure, D. S., (1959), "Electronic Spectra of Molecules and Ions in Crystals. II. Spectra of Ions in Crystals", in Solid State Physics, 9, 399.

McCord, T. B., (1967), "Observational Study of Lunar Visible Emission", J. Geophys. Res., 72, 2087.

Meadows, A. J., (1967), "Meteorite Research in the United Kingdom", J. R. A. S., 8, 173.

Morimoto, N., Appleman, D. E., and Evans, H. T., (1960), "The Crystal Structures of Clinoenstatite and Pigeonite", Zeit. Krist., 114, 120.

Munsell, A. H., (1929), Munsell Book of Color, Munsell Color Co., Baltimore, Md.

Nash, D. B., (1966), "Proton Excited Luminescence of Silicates", J. Geophys. Res., 71, 2517.

NAS-NRC Pub. 1133, (1964), "Studies in Penetration of Charged Particles in Matter", Washington, D. C.

Pringsheim, P., and Vogel, M., (1943), Luminescence of Liquids and Solids and Its Practical Applications, Interscience Publishers, N. Y.

Pringsheim, P., (1949), Fluorescence and Phosphorescence, Interscience Publishers, N. Y.

Prizbram, K., (1956), Irradiation Colors and Luminescence, Pergamon Press Ltd., London.

Rackham, T. W., (1967), "Color on the Moon", ICARUS, 7, 297.

Reid, A. M., and Cohen, A. J., (1967), "Some Characteristics of Enstatite from Enstatite Achondrites", Geochim. Cosmochim. Acta, 31, 661.

Romanova, M. A., (1964), Air Survey of Sand Deposits by Spectral Luminance, Consultants Bureau, N. Y.

Saller, E. J., (1967), "Cathodoluminescence Detector for the Applied Research Laboratories Electron Microprobe", Rev. Sci. Instr., 38, 837.

Schutten, J., and van Dijk, T., (1966), "Luminescence Caused by Proton Impact with Special Reference to the Lunar Surface", Nature, 211, 470.

Sippel, R. F., and Glover, E. D., (1965), "Structures in Carbonate Rocks Made Visible by Luminescence Petrography", Science, 150, 1283.

Snedecor, G. W., and Cochran, W. G., (1962), Statistical Methods Applied to Experiments in Agriculture and Biology, The Iowa State University Press, Ames, Iowa.

Thornbury, W. D., (1954), Principles of Geomorphology, John Wiley and Sons, N. Y.

Trident Engineering Associates, (1966), "Project Moon-Blink", NASA CR-630.

Tyrrell, G. W., (1958), The Principles of Petrology, Methuen and Co., N. Y.

Urey, H. C., (1967), "Parent Bodies of the Meteorites and the Origin of Chondrules", ICARUS, 7, 350.

Van Schmus, W. R., and Wood, J. A., (1967), "A Chemical-Petrologic Classification for the Chondritic Meteorites", Geochim. Cosmochim. Acta, 31, 747.

Weber, B. C., (1963), "Luminescence Phenomena and Zirconia Research", Keram. Z., 15, 192.

Weber, J. N., Greer, R. T., and Vand, V., (1967), "Electron Excited Fluorescence of Serpentines", Planet. Space Sci., 15, 633.

Weiblen, P., (1965), "Investigations of Cathodo-Luminescence with the Petrographic Microscope", in Developments in Applied Spectroscopy, 4, Plenum Press, N. Y., 245.

White, E. W., (1967), Pittsburgh Probe Users Meeting, University Park, Pa., personal communication.

White, W. B., and Keester, K. L., (1966), "Optical Absorption Spectra of Iron in the Rock-Forming Silicates", Am. Mineral., 51, 776.

Wiik, H. B., (1956), "The Chemical Composition of Some Stony Meteorites", Geochim. Cosmochim. Acta, 9, 279.

Williams, F., (1966), "Theoretical Basis for Solid-State Luminescence of Inorganic Solids", in Luminescence of Inorganic Solids, Academic Press, N. Y., 1.

Wittry, D. B., and Kyser, D. F., (1964), "Use of Electron Probes in the Study of Recombination Radiation", J. Appl. Phys., 35, 2439.

Wittry, D. B., and Kyser, D. F., (1965), "Cathodoluminescence at p-n Junctions in GaAs", J. Appl. Phys., 36, 1387.

Wittry, D. B., (1966), "Cathodoluminescence and Impurity Variations in Te-Doped GaAs", Appl. Phys. Let., 8, 142.

Wyszecki, G., and Stiles, S. W., (1967), Color Science Concepts and Methods, Quantitative Data and Formulas, John Wiley and Sons, N. Y.

Young, J. R., (1953), "Deterioration of Luminescent Phosphors Under Positive Ion Bombardment", J. Appl. Phys., 26, 1302.